

Climatic controls on nonmarine depositional sequences in the Albuquerque Basin, Rio Grande rift, north-central New Mexico

Sean D. Connell^{*†}

New Mexico Bureau of Geology and Mineral Resources—Albuquerque Office, New Mexico Institute of Mining and Technology, 2808 Central Ave. SE, Albuquerque, New Mexico 87106, USA, and Department of Earth and Planetary Sciences, MSC03 2040, University of New Mexico, Albuquerque, New Mexico 87131, USA

Gary A. Smith[†]

Department of Earth and Planetary Sciences, MSC03 2040, University of New Mexico, Albuquerque, New Mexico 87131, USA

John W. Geissman[†]

Department of Geosciences, University of Texas at Dallas, 800 West Campbell Road, Richardson, Texas 75080, USA

William C. McIntosh[†]

New Mexico Bureau of Geology and Mineral Resources, New Mexico Institute of Mining and Technology, 801 Leroy Place, Socorro, New Mexico 87801, USA

ABSTRACT

We investigated a Plio-Pleistocene alluvial succession in the Albuquerque Basin of the Rio Grande rift in New Mexico using geomorphic, stratigraphic, sedimentologic, geochronologic, and magnetostratigraphic data. New $^{40}\text{Ar}/^{39}\text{Ar}$ age determinations and magnetic-polarity stratigraphy refine the ages of the synrift Santa Fe Group. The Pliocene Ceja Formation lies on the distal hanging-wall ramp across much of the Albuquerque Basin. The Ceja onlapped and buried a widespread, Upper Miocene erosional paleosurface by 3.0 Ma. Sediment accumulation rates in the Ceja Formation decreased after 3.0 Ma and the Ceja formed broad sheets of amalgamated channel deposits that prograded into the basin after ca. 2.6 Ma. Ceja deposition ceased shortly after 1.8 Ma, forming the Llano de Albuquerque surface. Deposition of the Sierra Ladrones Formation by the ancestral Rio Grande was focused near the eastern master fault system before piedmont deposits (Sierra Ladrones Formation) began prograding away from the border faults between 1.8 and 1.6 Ma. Widespread basin filling ceased when the Rio Grande began cutting its valley, shortly after 0.78 Ma. Although the Albuquerque Basin is tectonically active, the development of through-going drainage of the ancestral Rio Grande, burial of Miocene unconformities, and coarsening of upper Santa Fe Group synrift basin fill were likely driven by

^{*}Current address: Chevron Energy Technology Company, 6001 Bollinger Canyon Road, San Ramon, California 94583-2324, USA.

[†]E-mails: SeanConnell@Chevron.com; gsmith@umn.edu; geissman@utdallas.edu; mcintosh@nmt.edu.

Connell, S.D., Smith, G.A., Geissman, J.W., and McIntosh, W.C., 2013, Climatic controls on nonmarine depositional sequences in the Albuquerque Basin, Rio Grande rift, north-central New Mexico, in Hudson, M.R., and Grauch, V.J.S., eds., *New Perspectives on Rio Grande Rift Basins: From Tectonics to Groundwater*: Geological Society of America Special Paper 494, p. 383–425, doi:10.1130/2013.2494(15). For permission to copy, contact editing@geosociety.org. © 2013 The Geological Society of America. All rights reserved.

climatic changes. Valley incision was approximately coeval with increased northern-hemisphere climatic cyclicity and magnitude and was also likely related to climatic changes. Asynchronous progradation of coarse-grained, margin-sourced detritus may be a consequence of basin shape, where the basinward tilting of the hanging wall promoted extensive sediment bypass of coarse-grained, margin-sourced sediment across the basin.

INTRODUCTION

Rift basins are important tectonic elements within continental regions subjected to crustal extension. The stratigraphic architecture of intracontinental rift basins is defined by three depositional belts associated with the basin floor and two sets of flanking tributaries from the footwall uplift and on the hanging-wall ramp (Fig. 1). The distributions of these depositional belts are sensitive to several factors, including basin geometry, subsidence and sediment delivery rate, effective moisture, catchment morphology, and rock type (e.g., Fraser and DeCelles, 1992; Leeder and Jackson, 1993; Gawthorpe and Leeder, 2000; Paola, 2000).

Most studies of half-graben sedimentation focused on (footwall-derived) piedmont-slope and basin-floor successions that were deposited near the master fault system (Bridge and Leeder, 1979; Leeder and Gawthorpe, 1987; Blair and Bilodeau, 1988; Frostick and Reid, 1989; Mack and Seager, 1990; Heller and Paola, 1992; Paola et al., 1992; Bridge and Mackey, 1993; Leeder et al., 1996; Peakall, 1998; Peakall et al., 2000; Marr et al., 2000; Leeder and Mack, 2001; Smith et al., 2001). Quantitative models of fault development and basin filling describe first-order patterns in the stratigraphic architecture of rift basins

(Schlische, 1991; Travis and Nunn, 1994; Contreras et al., 1997). Computational models suggest that sediments derived from the footwall block prograde into the basin as complementary tributary deposits retreat up the hanging-wall block during times of diminished subsidence (Paola et al., 1992; Marr et al., 2000).

Understanding sedimentation patterns in half-graben basins can be accomplished by examining the timing of progradation of transverse (tributary) deposits derived from facing structural margins. We demonstrate the utility of combined sequence-stratigraphic, sedimentologic, and geomorphologic approaches to interpreting alluvial sequences developed within fluvially dominated intracontinental rift basins, such as the Albuquerque Basin of the Rio Grande rift, north-central New Mexico. Our primary motivation is to develop a comprehensive understanding of why certain facies belts occupy different parts of a basin at different times, with an emphasis on deposits on the distal hanging-wall ramp. This depositional belt should be sensitive to the activity of the basin master fault because progressive basinward tilting (fore-tilting) of the hanging wall increases the fan-surface area and stream gradients, thereby promoting erosion of distal areas and progradation of sediment toward the master fault (Leeder and Gawthorpe, 1987). Deposits on the hanging-wall ramp also tend to be well exposed and occupy less structurally complicated

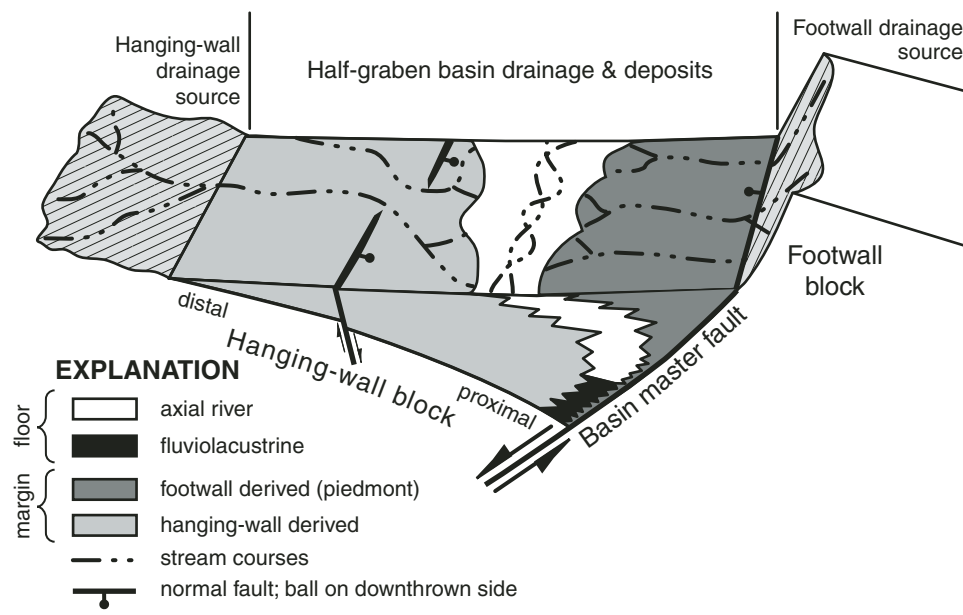


Figure 1. Three-dimensional diagram illustrating major depositional systems within a half-graben basin (modified from Mack and Seager, 1990, and Schlische, 1995). The basin axis contains sediments associated with internal surface drainage (fluviolacustrine) or through-going axial drainage (axial river) that are flanked by sets of tributary deposits originating from the footwall (piedmont slope) and distal hanging-wall ramp. The basin-floor/piedmont-slope boundary is sensitive to subsidence along the basin master fault (Leeder and Gawthorpe, 1987). Intrabasinal faults cut the hanging-wall ramp and allow steepening of the basement (rollover) toward the basin master fault (e.g., Xiao and Suppe, 1992). The asymmetric geometry of half-graben basins promotes the development of slightly angular (fore-tilted) unconformities on the hanging-wall ramp and strongly angular (back-tilted) unconformities next to the footwall cutoff.

areas relative to their depositional counterpart adjacent to the footwall block (e.g., Dart et al., 1995; Gawthorpe and Hurst, 1993). Nonmarine depositional sequences are well known from coastal settings, where changes in relative sea level dominate the stratigraphic architecture (e.g., Shanley and McCabe, 1994). Fluvial basins of the Rio Grande rift in New Mexico are more than 1500 km upstream of the coastline and are far from eustatic effects on base level. Thus, the upper limit of fluvial deposition is controlled by changes in discharge regimes, sediment supply, and tectonism (Blum and Törnqvist, 2000).

The Albuquerque Basin of north-central New Mexico (Fig. 2) is well suited for investigation because excellent exposures have permitted extensive geologic mapping and biostratigraphic, stratigraphic, and geochronologic studies (Bachman and Mehnert, 1978; Baldridge et al., 1980, 1987; Cole et al., 2007; Connell, 2004, 2008a, 2008b; Connell and Wells, 1999; Connell et al., 1998, 1999, 2000, 2001a, 2001b, 2001c, 2001d, 2002, 2005, 2007a, 2007b; Hawley, 1996; Hawley and Haase,

1992; Hawley et al., 1995; Lozinsky, 1994; Love and Connell, 2005; Love et al., 2001a, 2001b, 2001c; Lucas et al., 1993; Morgan and Lucas, 2003; Maldonado et al., 1999, 2006, 2007; Stone et al., 1998; Tedford and Barghoorn, 1999; Williams and Cole, 2007). New $^{40}\text{Ar}/^{39}\text{Ar}$ age determinations provide important temporal control for the development of a magnetic-polarity stratigraphy that refines the geochronology of the Plio-Pleistocene Ceja and Sierra Ladrones Formations. Previous studies of the magnetic properties of deposits in the Rio Grande rift show that alluvial sediments are suitable for the development of a robust polarity stratigraphy (Mack et al., 1993; Tedford and Barghoorn, 1999; Hudson et al., 2008). Rift basins in semiarid regions, such as in southwestern North America, provide an essential source of groundwater (Bartolino and Cole, 2002). As potable water becomes scarcer, more-robust models of extensional basin-fill architecture will aid in the management of these resources, as recently exemplified in the Rio Grande rift (McAda and Barroll, 2002).

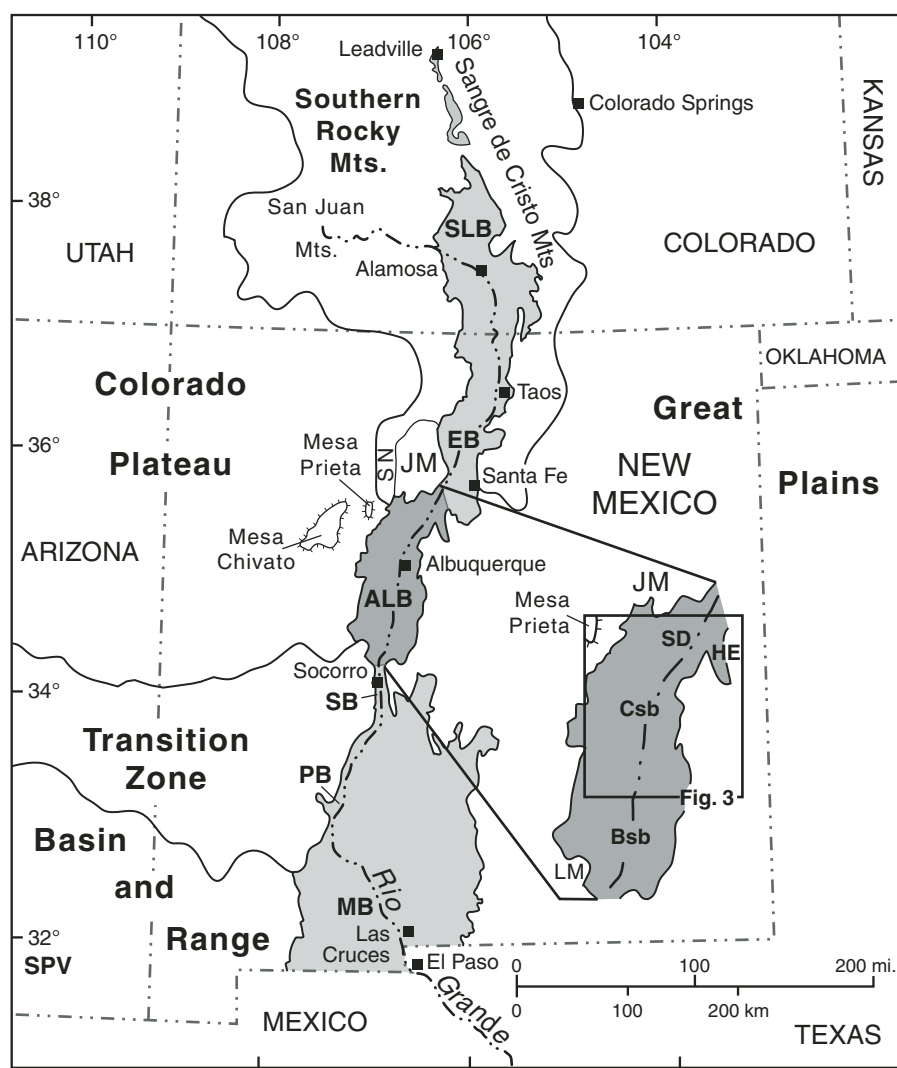


Figure 2. Basins of the Rio Grande rift in Colorado and New Mexico shaded in gray (modified from Thorn et al., 1993). Major basins include: San Luis Basin (SLB), Española Basin (EB), Albuquerque Basin (ALB), Socorro Basin (SB), Palomas Basin (PB), and Mesilla Basin (MB). The approximate location of the San Pedro Valley (SPV) of southeastern Arizona is also shown. Inset map denotes outline of the Albuquerque Basin and study area (Fig. 3), including the Hagan embayment (HE), Santo Domingo Basin (or sub-basin, SD), Calabacillas sub-basin (Csb), and Belen sub-basin (Bsb; modified from Grauch et al., 1999). Abbreviations denote physiographic features surrounding the Albuquerque Basin, including the Jemez Mountains (JM), Ladron Mountains (LM), and Sierra Nacimiento (SN).

Study Area

The Albuquerque Basin is part of the intracontinental Rio Grande rift, a chain of structurally and topographically linked extensional basins within a broader region of Neogene extension in the western United States and northern Mexico (Bryan, 1938; Kelley, 1952, 1979; Chapin, 1971; Chapin and Cather, 1994). The basin is flanked by the Colorado Plateau and Great Plains, and lies between the west-tilted Espanola and Socorro Basins (Fig. 2). The eastern flank abuts the rift-flank uplifts of the Sandia, Manzanita, and Manzano Mountains. The northwestern flank has little surface relief, but the rift-flanking uplifts of the Sierra Lucero and the Ladron Mountains define the southwestern margin of the basin.

The Albuquerque Basin resembles a single physiographic basin; however, the underlying geologic structure is complicated, and the basin has been segmented into at least three different sub-basins (cf. Russell and Snelson, 1994; Grauch et al., 1999), which are, from north to south: the Santo Domingo sub-basin (or basin, e.g., Smith et al., 2001), the Calabacillas sub-basin, and the Belen sub-basin. Most of the study area is within the Calabacillas sub-basin, but the study area extends into the southern part of the Santo Domingo sub-basin and the northern part of the Belen sub-basin (Fig. 2), where the basin fill generally dips eastward toward the Sandia, Manzanita, and Manzano Mountains.

The basin has relatively low topographic relief that is punctuated by two large, longitudinal river valleys and elongate tablelands (Fig. 3). The Ceja del Rio Puerco is a west-facing erosional escarpment that defines the eastern edge of the Rio Puerco valley (a southeastward-flowing tributary to the Rio Grande) and the western edge of the Llano de Albuquerque, which delineates the interfluve between the Rio Grande and Rio Puerco. La Ceja is a north-facing escarpment at the northern end of the Llano de Albuquerque. Other major landforms in the Albuquerque Basin include the Hubbell bench, a structural bench along the western flanks of the Manzanita and Manzano Mountains, and the Hagan embayment, a structural reentrant at the northeastern margin of the basin (Kelley, 1977). The central part of the study area (in the Calabacillas sub-basin) is a half graben cut by numerous intrabasinal faults (Fig. 4), many of which are tectonically active and have slip rates of 0.2–0.01 mm/a (Machette et al., 1998). The western flank of the study area forms a shallowly buried structural bench (Laguna bench of Russell and Snelson, 1994) that is defined by the San Ysidro and Cat Mesa fault zones and the western basin-border faults.

The sedimentary fill and interbedded volcanic deposits of Rio Grande rift basins are collectively known as the Santa Fe Group (Fig. 5). Regionally these strata accumulated between Late Oligocene and early Pleistocene time (Kelley, 1977; Hawley, 1978; Gile et al., 1981, 1995; Chapin and Cather, 1994). Deposition of the Santa Fe Group ceased as a result of incision of the present valleys (Spiegel and Baldwin, 1963). In the Albuquerque Basin, the Santa Fe Group is generally <1 km thick along the

western margin, but it thickens to nearly 5 km next to the eastern structural margin (Fig. 4; Lozinsky, 1994).

GEOCHRONOLOGY

The stratigraphic architecture of the Albuquerque Basin is examined through physical correlation of strata and bounding surfaces, $^{40}\text{Ar}/^{39}\text{Ar}$ age determinations, biostratigraphy, and magnetic-polarity stratigraphy. Neogene deposits of the Albuquerque Basin yielded a rich array of biostratigraphically useful vertebrate fossil remains that have been summarized by Morgan and Lucas (2003) and Tedford et al. (2004). The Arroyo Ojito, Cerro Conejo, Popotosa, and Zia Formations contain interbedded volcanic material and sparse age-diagnostic fossils of Miocene age (Lozinsky and Tedford, 1991; Tedford and Barghoorn, 1999; Connell, 2004). The Ceja Formation locally contains fossils indicative of late Pliocene age (3.5–2.2 Ma). The Sierra Ladrones Formation contains early Pleistocene fossils (Lucas et al., 1993) and Pliocene lava exposed in the adjacent Socorro Basin (Machette, 1978). Numerous isotopic age determinations and tephrochronologic correlations on ash and fluvially recycled pyroclastic rocks have been previously reported in the Albuquerque Basin and surrounding areas (Bachman and Mehnert, 1978; Baldridge et al., 1980; Connell, 2004, 2008b; Connell et al., 1999, 2002; Smith et al., 2001; Dunbar et al., 2001; Maldonado et al., 2006, 2007; Chamberlin and McIntosh, 2007).

$^{40}\text{Ar}/^{39}\text{Ar}$ Methods and Results

We use 20 previously reported $^{40}\text{Ar}/^{39}\text{Ar}$ and tephrochronologic age determinations (Table 1) and report 58 new $^{40}\text{Ar}/^{39}\text{Ar}$ age determinations to refine the ages of Upper Miocene through lower Pleistocene strata in the Albuquerque Basin (Figs. 6 and 7, Tables 2 and 3). Although some of the age determinations were informally reported on geologic maps and reports, details of the $^{40}\text{Ar}/^{39}\text{Ar}$ analyses are first presented herein (Cather and Connell, 1998; Connell, 2004, 2008a, 2008b; Connell et al., 1999, 2005; Koning and Personius, 2002; Maldonado et al., 1999, 2006; Williams and Cole, 2007). Samples were analyzed at the New Mexico Geochronological Research Laboratory at the New Mexico Institute of Mining and Technology in Socorro, New Mexico. Fish Canyon Tuff sanidine (28.02 Ma; Renne et al., 1998) was used as a monitor for reducing the analytical data. The previously reported age determinations in Table 1 have been adjusted to the revised standard of Renne et al. (1998). Complete analytical data, including age-spectra and age-probability distribution diagrams (Deino and Potts, 1992) are available in Appendix A (available on CD-ROM accompanying this volume and in the GSA Data Repository¹).

¹GSA Data Repository Item 2013132, Appendix A: Age determinations and Appendix B: Rock magnetic methods and results, is available at www.geosociety.org/pubs/ft2013.htm, or on request from editing@geosociety.org or Documents Secretary, GSA, P.O. Box 9140, Boulder, CO 80301-9140, USA.

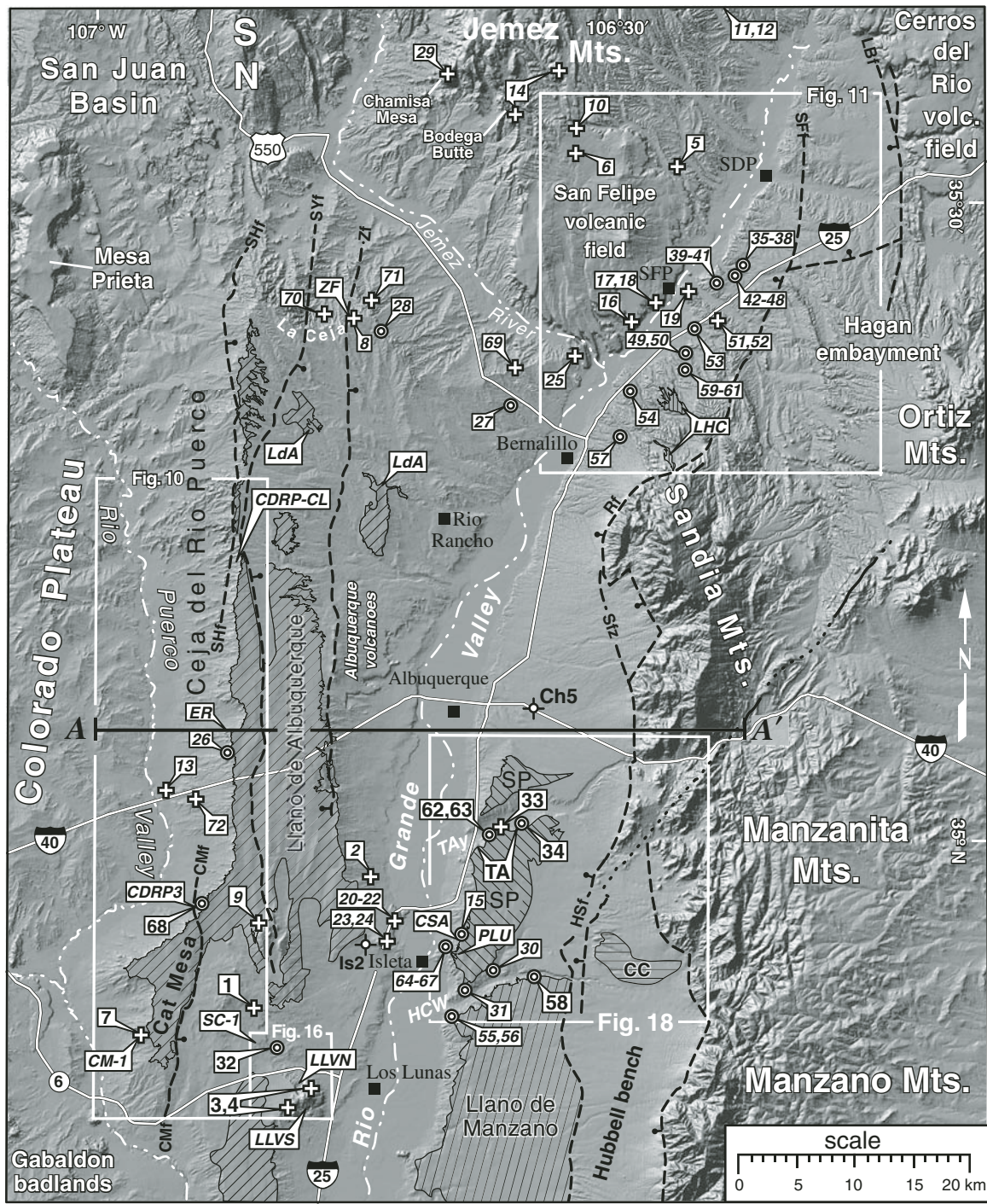


Figure 3. Shaded-relief map of the central and northern parts of the Albuquerque Basin, showing major physiographic features, towns, and study-area locations. Towns include Albuquerque, Bernalillo, Isleta Pueblo, Los Lunas, San Felipe Pueblo (SFP), and Santo Domingo Pueblo (SDP). Geomorphic surfaces (hatched areas) include the Cañada Colorada (CC), Las Huertas (LHC), Llano de Albuquerque (LdA), Llano de Manzano, and Sunport (SP). Selected major faults (thick dashed lines) include: La Bajada fault zone (LBf), Cat Mesa fault (CMf), Hubbell Spring fault zone (HSf), Rincon fault (Rf), Sand Hill fault (SHf), Sandia fault zone (Sfz), San Francisco fault (SFF), San Ysidro fault (SYf), and Zia and County Dump faults (Zf). Other features include the Sierra Nacimiento (SN), the mouths of Hell Canyon Wash (HCW) and Tijeras Arroyo (TAy), Hubbell bench, San Felipe volcanic field, Cerros del Rio volcanic field, La Ceja, and the Ceja del Rio Puerco. Cross section A-A' is shown on Figure 4. Wells include the Charles Wells well #5 (Ch5) and Shell Isleta #2 (Is2). Stratigraphic locations include CDRP3, CDRP-CL, CM-1, CSA-PLU, LLV, SC-1, TA, and ZF. The type section of the Ceja Formation is at El Rincón (ER; Connell, 2008a). White-bordered boxes denote locations of geologic maps (Figs. 10, 11, 16, and 18). Numbers denote geochronologic sample sites listed on Tables 1–3. The plus symbol denotes primary fallout, lava flows and intrusions that represent emplacement or depositional ages. The circle-in-circle symbol denotes fluvially recycled volcanic materials that represent maximum ages.

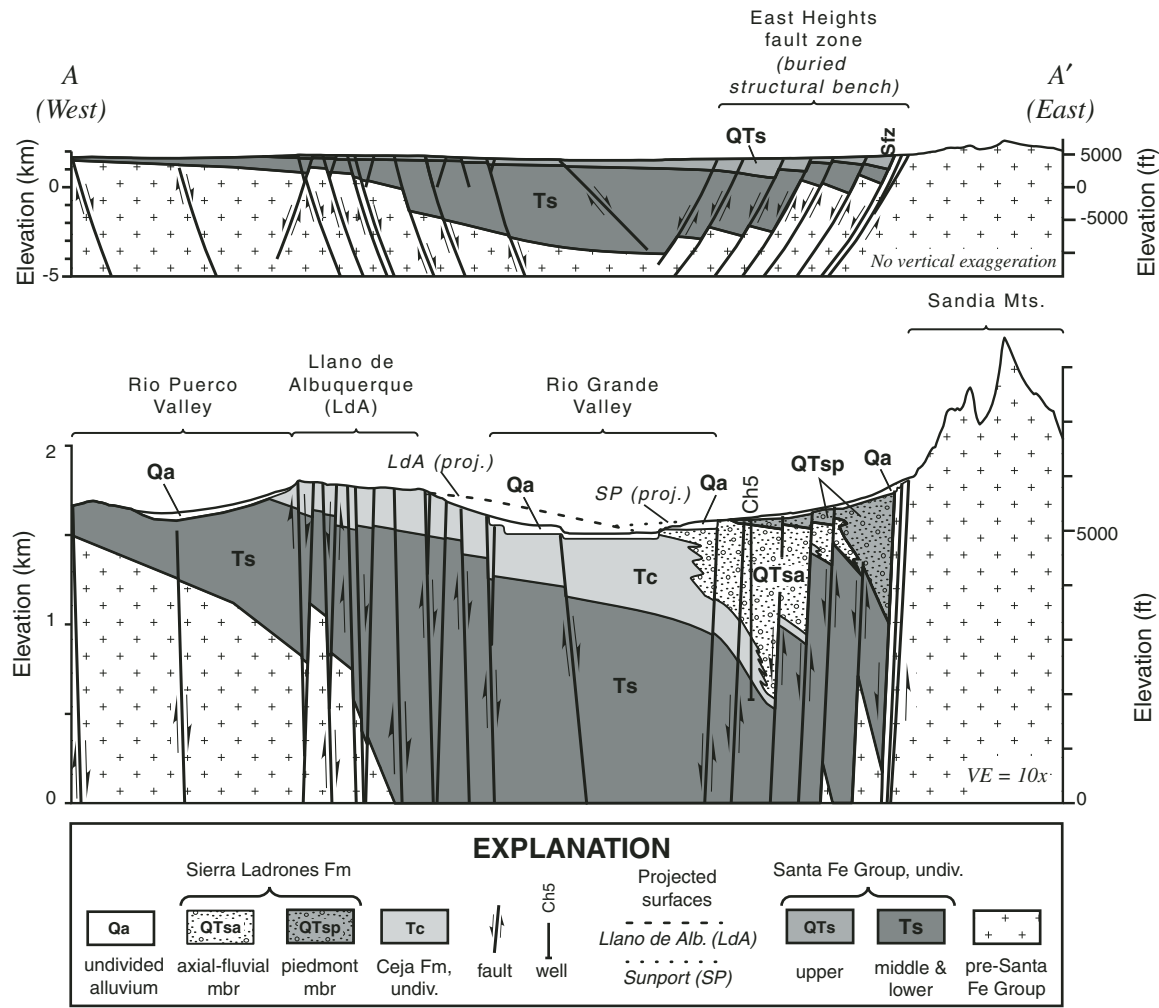


Figure 4. Simplified geologic cross section A–A' across the Albuquerque Basin (modified after Connell, 2008b). See Figure 3 for cross-section location. Top: Structure section with no vertical exaggeration (VE), illustrating the overall east-tilted character of the basin. Bottom: Vertically exaggerated cross section A–A' (VE = 10×), illustrating the Ceja Formation and the axial-fluvial and piedmont members of the Sierra Ladrones Formation. Surficial deposits are diagrammatically shown and faults are highly generalized. The basin master fault (Sandia fault zone, Sfz) is a zone of normal faults that lie along the eastern edge of the basin. Numerous intrabasinal faults cut the basin fill and probably control the position of the eastern part of the axial-fluvial member of the Sierra Ladrones Formation (QTsa). Projections of the Llano de Albuquerque and Sunport geomorphic surfaces denoted by dashed and dotted lines, respectively. The Charles Wells #5 well (Ch5) fully penetrates the axial-fluvial succession of the Sierra Ladrones Formation, above the Atrisco Member of Connell et al. (1998).

Volcanic rocks sampled for geochronology include tholeiitic basalt, trachyandesite, dacite, rhyodacite, and rhyolite associated with hydromagmatic tuff, fallout ash and lapilli, lava flows, and shallow intrusive rocks (Kelley and Kudo, 1978; Dunbar et al., 2001; Maldonado et al., 2006, 2007; Connell, 2008b). The ages of 15 samples were determined by resistance-furnace incremental heating (RFIH) of groundmass concentrate or hornblende (Table 2). The ages of 43 samples containing sanidine were dated by single-crystal laser-fusion (SCLF) methods (Table 3). One sample containing plagioclase was dated by SCLF methods. Age determinations for

18 samples (taken from volcanic fallout or lava flows) represent emplacement or depositional ages. The remaining samples taken from fluvially recycled pyroclastic material, ranging from pumiceous sand to pebbles and cobbles of pumice and welded tuff, represent maximum ages of deposition. Six samples of Miocene rocks provided maximum bounding ages for the overlying Plio-Pleistocene succession. Wherever possible the dense crystalline cores of mafic lava flows were sampled. Volcanic gravel was scraped clean of adhered sand grains at the time of collection, and interior parts of samples were collected for analysis.

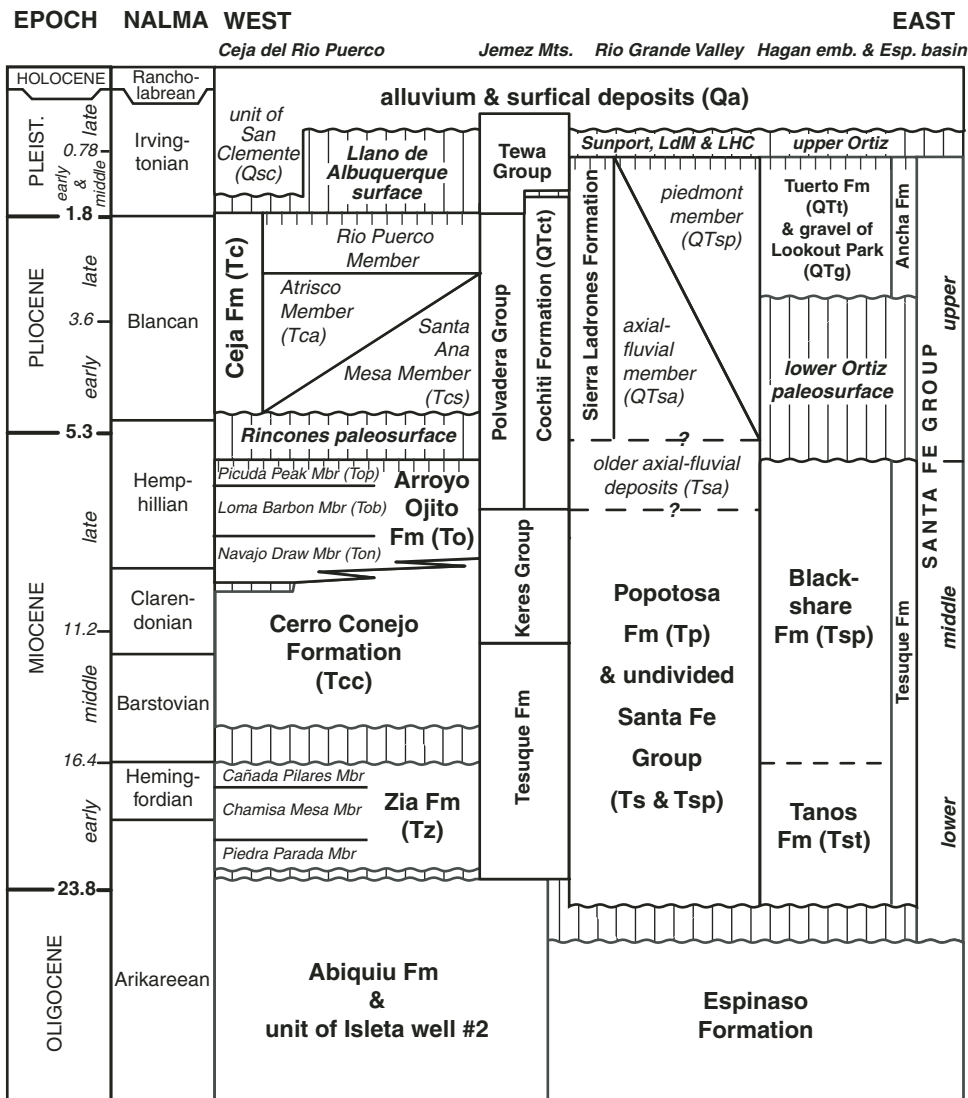


Figure 5. Age and correlation of stratigraphic units in the Albuquerque Basin (after Connell, 2004, 2008a; Connell et al., 2002; Koning et al., 2002), including geologic epoch and North American Land Mammal “Age” (NALMA; Bell et al., 2004; Tedford et al., 2004). The Rincones and lower Ortiz paleosurfaces define the base of the Ceja and Tuerto Formations, respectively. The Llano de Albuquerque, Sunport (SP), Llano de Manzano (LdM), Las Huertas (LHC), and upper Ortiz geomorphic surfaces represent local depositional tops of the Ceja, Sierra Ladrones, and Tuerto Formations. The Ancha and Tesuque Formations are in the Santa Fe embayment and Española Basin. emb.—embayment; Esp.—Española.

Figure 6 displays the stratigraphic assignments of age determinations for the Cerro Conejo, Arroyo Ojito, Cochiti, and Ceja Formations, and the unit of San Clemente (Maldonado et al., 2007), listed in increasing order of age. Four dacitic pumice pebbles in the Ceja Formation yielded late Pliocene dates that are similar to the age of the Pliocene Tschicoma volcanic field in the Jemez Mountains (Broxton et al., 2007). Three rhyolitic lapilli and ash beds in the Arroyo Ojito Formation yielded Late Miocene age determinations that correlate to the ca. 6.1–7.0 Ma Peralta Tuff Member of the Bearhead Rhyolite on the southeastern flanks of the Jemez Mountains (McIntosh and Quade, 1995; Juster and Spell, 2001; Smith, 2001; Smith et al., 2001; Chamberlin and McIntosh, 2007). Age determinations of 36 rhyolitic pumice and ash samples (Fig. 7, Table 3) are near the reported ages of early Pleistocene eruptions that formed the 1.9–0.6 Ma Tewa Group in the Jemez Mountains (Goff and Gardner, 2004), including the 1.85 ± 0.08 Ma tuff of San Diego Canyon (Spell et

al., 1990), 1.26 ± 0.01 Ma Tshirege (upper) and 1.61 ± 0.01 Ma Otowi (lower) Members of the Bandelier Tuff (Izett and Obrovich, 1994; Phillips et al., 2007), and the intracaldera 1.6–1.2 Ma Cerro Toledo Rhyolite (Spell et al., 1990, 1996). Three rhyolitic samples yielded dates that are slightly older than the tuff of San Diego Canyon (Table 3). Other tephra include the 0.639 ± 0.002 Ma Lava Creek B ash (Lanphere et al., 2002), and the ca. 3.28 Ma Nomlaki Tuff Member of the Tuscan and Tehama Formations of California (Sarna-Wojcicki et al., 1991; Connell et al., 1999).

Paleomagnetic Methods and Results

Oriented-block samples were collected from 171 paleomagnetic study sites across 425 m of stratigraphic thickness in Upper Miocene through Pleistocene alluvial strata. Descriptions of sampling methods, demagnetization results, and selected rock magnetic

TABLE 1. SUMMARY OF $^{40}\text{Ar}/^{39}\text{Ar}$ AGE DETERMINATIONS AND TEPHROCHRONOLOGY FROM PUBLISHED SOURCES

Map no.	Unit	Age $\pm 2\sigma$ (Ma)	Method	Sample no.	Comments
1	Qch	0.099 \pm 0.002	RFIH	³ CH-21-1	Youngest lava flow of Cat Hills volcanic field
2	Qrl	0.643 \pm 0.002	GCC	⁵ Gutierrez quarry	Lava Creek B ash; $^{40}\text{Ar}/^{39}\text{Ar}$ age from Lanphere <i>et al.</i> (2002)
3	Qlv	1.26 \pm 0.02	RFIH	^{2,4} S9a	Younger trachyandesite at El Cerro de los Lunas
4	Tlv	3.83 \pm 0.10	RFIH	^{2,4} S26	Younger trachyandesite at El Cerro de los Lunas
5	Tbs	2.43 \pm 0.03	RFIH	⁸ NMGRL 8364-1	NE flank of San Felipe vf
6	Tbs	2.46 \pm 0.22	RFIH	⁷ NMGRL 50139-1	NW flank of San Felipe vf
7	Tcm	3.02 \pm 0.10	RFIH	³ CM-01A	Cat Mesa lava flow
8	Tc	ca. 3.28	GCC	¹ SA-14	Nomlaki Tuff, fallout ash
9	Twm	4.04 \pm 0.16	RFIH	³ WM-01A	Wind Mesa basalt
SA	Tvsd	4.76 \pm 0.04	RFIH	⁶ San Acacia	Trachyandesite at San Acacia; not on map
10	QTct	6.29 \pm 0.04	SCLF	⁷ NMGRL 50523-1	Younger Peralta Tuff
11	QTct	6.23 \pm 0.06	SCLF	⁸ NMGRL 8353	Younger Peralta Tuff; north of study area
12	QTsa	6.86–6.92	SCLF	⁸ NMGRL 7870, 7160, 7165	Older Peralta Tuff (n = 3); north of study area
13	Tbm	8.16 \pm 0.05	RFIH	³ CH-13	Basaltic lava flow at La Mesita Negra.
14	Tcc	9.04–9.25	RFIH	⁷ NMGRL 9739, 50101, 50104, 50105	Basalt of Bodega Butte; overlies Cerro Conejo Fm. (n = 4)

Notes: Map number refers to numbers used in Figures 3, 6–8, 10–11, 13, and 15–20. Map units include: Cat Hills volcanic field (Qch), Lomas Negras Formation (Qrl) of Connell *et al.* (2007a), Los Lunas volcano (younger = Qlv, older = Tlv), Ceja Formation, undivided (Tc), San Felipe volcanic field (Tbs), basaltic lava at Cat Mesa (Tcm), Wind Mesa volcanic field (Twm), trachyandesite at San Acacia (Tvsd, not shown on maps), Cochiti Formation (QTct), axial-fluvial member of the Sierra Ladrones Formation (QTsa), basaltic lava at La Mesita Negra (Tbm), and Cerro Conejo Formation (Tcc). vf—volcanic field.

Methods include resistance-furnace incremental heating (RFIH), single-crystal laser fusion (SCLF), and geochemical correlation (GCC). $^{40}\text{Ar}/^{39}\text{Ar}$ age determinations recalculated to revised Fish Canyon Tuff sanidine standard (Renne *et al.*, 1998).

Sources include: ¹Connell *et al.* (1999); ²Dunbar *et al.* (2001); ³Maldonado *et al.* (2006); ⁴Maldonado *et al.* (2007); ⁵Connell *et al.* (2007a); ⁶Chamberlin *et al.* (2001); ⁷Chamberlin and McIntosh (2007); and ⁸Smith *et al.* (2001).

data and analysis are available in Appendix B (on CD-ROM; see footnote 1). A summary of the results is presented below.

Samples were collected following modifications to the approach of Lindsay *et al.* (1987). Eight sites were collected from the (Upper Miocene) Arroyo Ojito Formation and the (Pleistocene) unit of San Clemente. The sampling interval averaged ~2.3 m between sites, but varied from 0.2 m to 9.0 m in order to obtain suitable fine-grained sediments. Progressive, stepwise alternating-field and thermal demagnetization of 6 to 11 specimens per site were conducted at the University of New Mexico Paleomagnetism and Rock Magnetism Laboratory in Albuquerque, New Mexico.

Principal component analysis was used to determine the least-squares best-fit line of the characteristic component of magnetization for each specimen (Kirschvink, 1980). Specimen data were combined using Fisher (1953) statistics to determine mean site directions (Table 4). The assignment of normal polarities for specimens was more rigorously scrutinized than for reverse polarities because of the possibility of strong viscous overprinting or diagenetic modification during the 0.78-Ma-long Brunhes normal-polarity chron.

Sites were grouped into four classes following the approaches of Opdyke *et al.* (1977) and Johnson *et al.* (1982). Class I sites

have at least three statistically significant directions from three or more independent samples and have (α 95) confidence limits less than 20°. Class II sites have three or more statistically significant directions that are not significant at the 95% confidence level, but the polarity determination is not in doubt. Sites are class III if the confidence limit exceeded 35°. Class III sites have dispersed vectors and were only used to corroborate polarity from stratigraphically adjacent class I sites. Class IV sites are defined by only one accepted specimen and are also only used to corroborate polarity with stratigraphically adjacent class I sites. A fifth category (class V) involved sites that contained specimens of poor quality or yielded multiple polarity interpretations and were rejected. Site mean directions typically show interpretable magnetic polarity. Mean site declination (D), inclination (I), and virtual geomagnetic pole (VGP) values are reported for class I and II sites (Appendix B).

The tilt-corrected mean of all class I normal polarity sites (Table 4) is D = 2.8°, I = 45.0° (N = 58 sites), and of all class I reverse polarity sites is D = 180.2°, I = -41.7° (N = 50 sites). The combined mean values of all class I sites is D = 1.6°, I = 43.5° (N = 108 sites; Table 5), and is 19° shallower than the present-day field (D = 10.0°, I = 62.4°; NOAA Geophysical Data Center, 2005), and 8° shallower than the time-averaged

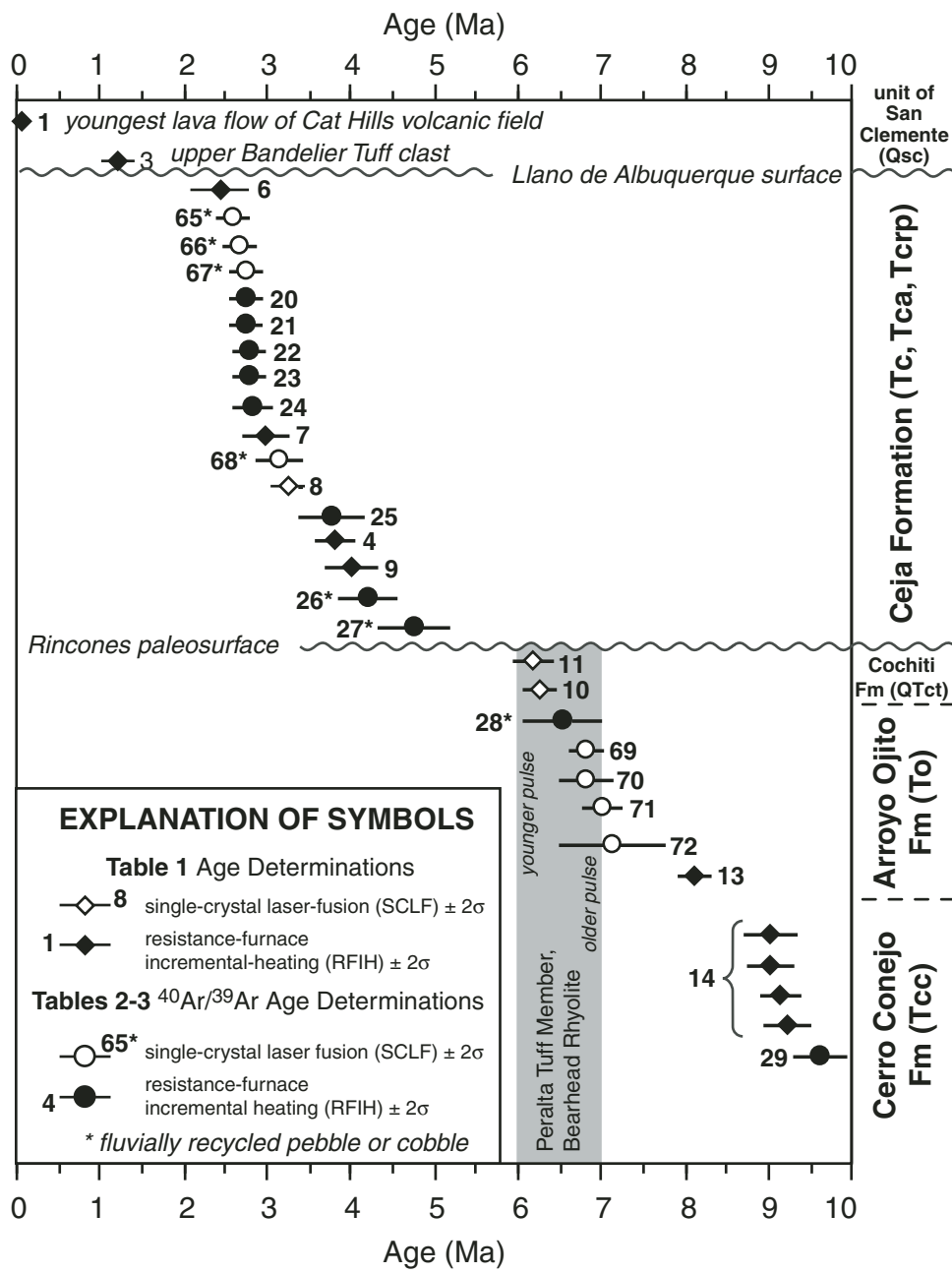


Figure 6. Summary of $^{40}\text{Ar}/^{39}\text{Ar}$ age determinations ($N = 32$) for the unit of San Clemente and the Ceja, Cochiti, Arroyo Ojito, and upper part of the Cerro Conejo Formations, showing mean sample ages and $\pm 2\sigma$ uncertainties, and sample number (Tables 1–3). Closed (black) symbols denote samples dated by resistance-furnace incremental-heating (RFIH) methods. Open (white) symbols denote samples dated by single-crystal laser-fusion (SCLF) methods. Major stratigraphic discontinuities include the Llano de Albuquerque and Rincones paleosurfaces. Asterisks denote fluvially recycled volcanic gravel that provides maximum ages of the deposits. Gray bar denotes range of the Peralta Tuff Member of the Bearhead Rhyolite (6.79–7.02 Ma). Plagioclase was analyzed in sample 72; hornblende was analyzed in sample 25.

inclination of the dipole field ($I = 54.5^\circ$). The tilt-corrected mean of all class I sites for the Sierra Ladrones Formation ($D = 0.8^\circ$, $I = 53.3^\circ$, $N = 15$ sites; Table 5) is similar to the time-averaged inclination of the dipole field and is $\sim 11^\circ$ steeper than the tilt-corrected mean inclination of the Ceja Formation ($D = 1.6^\circ$, $I = 42.5^\circ$, $N = 85$ sites; Table 5). The shallower inclination values for class I sites relative to the present-day and time-averaged dipole fields probably reflects a shallowing of inclination due to sediment compaction (e.g., Sun and Kodama, 1992). Combined mean inclinations (with reverse polarity directions inverted to north-seeking, positive-inclination values) in the Sierra Ladrones Formation are $\sim 21\%$ steeper than those in the

Ceja Formation, which may have been compacted by nearly one-fifth of its original thickness (see below).

STRATIGRAPHY

Measured stratigraphic sections and geochronologic data provide a robust framework for developing a magnetic-polarity reversal chronology in the Ceja and Sierra Ladrones Formations. Stratigraphic correlations were established using geologically mapped boundaries and dated volcanic material as datum planes (Fig. 8). Many stratigraphic surfaces possess strongly developed calcic paleosols (Machette, 1985; Connell, 2008b; Maldonado et

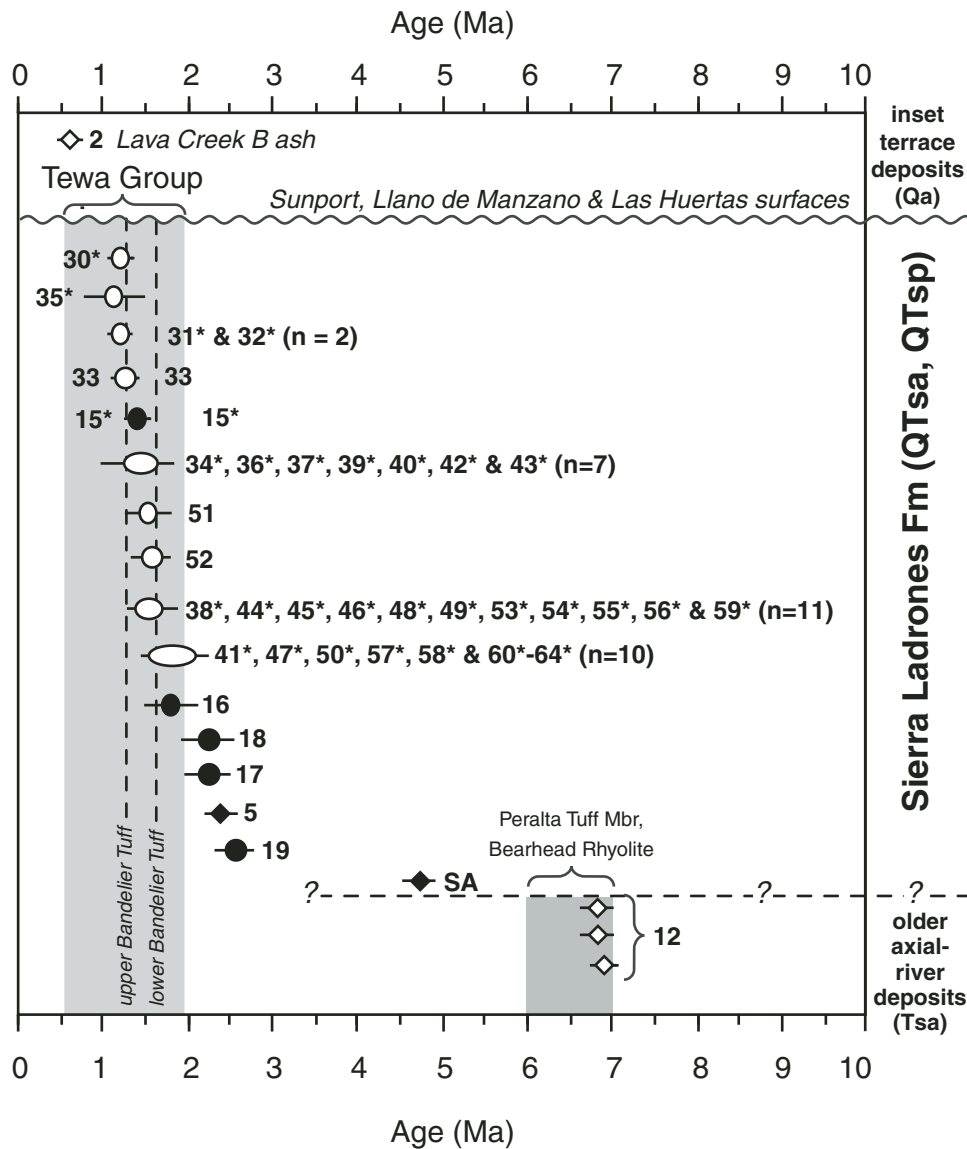


Figure 7. Summary of $^{40}\text{Ar}/^{39}\text{Ar}$ age determinations ($N = 46$) for the Lava Creek B ash in an inset terrace of the Rio Grande (Qr), the Sierra Ladrones Formation, and a Miocene axial-river deposit (Tsa), showing mean sample ages and $\pm 2\sigma$ uncertainties, and laboratory or sample numbers (Tables 1–3). Refer to Figure 6 for explanation of symbols. Gray bars denote age ranges of the Tewa Group and Peralta Tuff Member of the Bearhead Rhyolite. The trachyandesite at San Acacia (SA) lies near the boundary between the Socorro and Albuquerque Basins (Chamberlin et al., 2001). Fluvially recycled clasts are grouped into zones that are younger or older than the age ranges established for the upper and lower Bandelier Tuffs.

al., 2007) that were described using pedogenic carbonate morphologic stages (Birkeland, 1999).

The stratigraphic nomenclature for the Santa Fe Group in the Albuquerque Basin was summarized by Connell (2004). Later refinements by Connell et al. (2007a, 2007b) and Connell (2008a) are used in this study (Fig. 5). The Santa Fe Group is locally divided into three subgroups. The lower and middle subgroups include the Arroyo Ojito, Blackshare, Cerro Conejo, Popotosa, Tanos, and Zia Formations. These Upper Oligocene through Miocene units were deposited within internally drained basins, where streams flowed off emerging uplifts and terminated onto ephemeral and intermittent playa lakes (Chapin and Cather, 1994). The upper part of the Santa Fe Group was deposited after establishment of through-going axial drainage (by the ancestral Rio Grande) that linked adjacent basins (Machette, 1978; Gile et al., 1981; Chapin and Cather, 1994; Connell et al., 2005). These deposits include the Ceja, Cochiti, Sierra Ladrones, and Tuerto

Formations. The Ceja and Sierra Ladrones Formations contain fluvial deposits related to the development of the ancestral Rio Grande and its tributaries (Machette, 1978; Connell, 2008a). Widespread, but thin, conglomeratic sandstone commonly overlie widespread, basin-flanking unconformities (Connell, 2004, 2008a). Accumulations of alluvial, colluvial, and eolian sediment, such as the unit of San Clemente, are preserved in local structural depressions.

The geochronology of the Arroyo Ojito, Ceja, and Sierra Ladrones Formations was refined through correlation of the measured stratigraphic sections to the geomagnetic polarity time scale (GPTS; Gradstein et al., 2005) using dated temporal reference points that range from 9.7 to 0.1 Ma (Fig. 9, Tables 1–3). Twenty-three polarity intervals longer than 20 k.y. have been documented globally since the start of the Pliocene and are part of the GPTS. Nearly all of the major polarity chron (and subchrons) in the past 4 Ma were recorded in this study. The Llano de Albuquerque

TABLE 2. SUMMARY OF $^{40}\text{Ar}/^{39}\text{Ar}$ RESISTANCE FURNACE INCREMENTAL HEATING (RFIH) RESULTS.

Map no.	Sample	Map unit	Lat. ($^{\circ}\text{N}$)	Lon. ($^{\circ}\text{W}$)	Lab. no.	Method	Material	Irrad.	N	MSWD	Date	K/Ca $\pm 2\sigma$	Comment
15*	S14	QTsa	34.9233	-106.6552	53930	RFIH	Obsidian	NM162	7	4.87	1.44 ± 0.01	18.4 ± 0.8	Rabbit mountain obsidian pebble
16	SF-Bas3	Tb	35.4029	-106.4867	8928	RFIH	Groundmass	NM86	7	1.85 ± 0.16	0.2 ± 0.2	0.2 ± 0.2	San Felipe vf., SE mesa
17	SF-Bas2	Tb	35.4174	-106.4654	8927	RFIH	Groundmass	NM86	5	2.28 ± 0.09	0.2 ± 0.0	0.2 ± 0.0	San Felipe vf., boulder below SE flank
18	SF-bas1	QTsa	35.4176	-106.4653	8926	RFIH	Groundmass	NM86	4	2.34 ± 0.14	0.2 ± 0.1	0.2 ± 0.1	Same as no. 17
19	TQA-4	Tb	35.4283	-106.4255	51967	RFIH	Groundmass	NM33	7	6.67 ± 0.11	0.2 ± 0.2	0.2 ± 0.2	San Felipe vf., in QTsa
20	125NE	Tb	34.9419	-106.7055	8406	RFIH	Groundmass	NM78	6	3.63 ± 0.05	0.5 ± 0.6	0.5 ± 0.6	S17: Black Mesa flow, in Tcp
21	Iv1	Tb	34.9326	-106.7169	8387	RFIH	Groundmass	NM77	3	1.76 ± 0.03	0.8 ± 0.3	0.8 ± 0.3	S20: Isleta volcano, in Tcp
22	85	Tb	34.9202	-106.7058	8409	RFIH	Groundmass	NM78	5	5.27 ± 0.05	0.5 ± 0.2	0.5 ± 0.2	S18: Isleta volcano, in Tcp
23	225 block	Tb	34.9168	-106.7210	8407	RFIH	Groundmass	NM78	6	1.51 ± 0.03	0.3 ± 0.3	0.3 ± 0.3	S21: Isleta volcano, base surge
24	125S	Tb	34.9168	-106.7210	8404	RFIH	Groundmass	NM78	4	2.46 ± 0.07	0.2 ± 0.2	0.2 ± 0.2	S19: Isleta volcano, SA15: Spillway ash, 42 m below
25	022098-161-SANA	Tcs	35.3806	-106.5435	8977	RFIH	Hornblende	NM86	4	1.64 ± 0.23	0.1 ± 0.0	0.1 ± 0.0	Pliocene lavas
26*	030100-ER3a	Tcp	35.0659	-106.8742	51448	RFIH	Groundmass	NM127	5	1.86 ± 0.21	0.5 ± 0.4	0.5 ± 0.4	SA16: Basaltic cobble
27*	011598-31BERN	Tcs	35.3373	-106.6047	50483	RFIH	Hornblende	NM110	3	6.09 ± 0.26	0.1 ± 0.0	0.1 ± 0.0	SA18: Rhyodacite cobble
28*	8h-1	Top	35.4033	-106.7309	50485	RFIH	Hornblende	NM110	3	2.37 ± 0.33	0.3 ± 0.1	0.3 ± 0.1	SA19: 20 m below top
29	0903998-JP	Tcc	35.5955	-106.6643	52286	RFIH	Groundmass	NM137	3	1.64 ± 0.14	0.1 ± 0.1	0.1 ± 0.1	Chamisa Mesa

Notes: See Table 3 for details. Irrad. denotes irradiation batch. vf.—volcanic field.

TABLE 3. SUMMARY OF $^{40}\text{Ar}/^{39}\text{Ar}$ SINGLE CRYSTAL LASER FUSION (SCLF) RESULTS

Map no.	Sample	Map unit	Lat. ($^{\circ}\text{N}$)	Lon. ($^{\circ}\text{W}$)	Lab. no.	Method	Material	Irrad.	N	MSWD	Date $\pm 2\sigma$ (Ma)	$K/\text{Ca} \pm 2\sigma$	Comment
30*	ls10	QTsa	34.9006	-106.6219	6198	SCLF	Sanidine	NM45	11	1.42	1.23 ± 0.01	56.0 ± 7.5	Rhyolitic pumice S10
31*	ls4	QTsa	34.8870	-106.6486	6197	SCLF	Sanidine	NM45	15	2.25	1.24 ± 0.01	25.0 ± 10.0	Rhyolitic pumice S11
32*	99DS1	Qsc	34.8382	-106.8281	51932	SCLF	Sanidine	NM133	9	0.52	1.24 ± 0.02	52.9 ± 30.4	Upper Bandelier pumice
33	011700-ALE3	QTsa	35.0094	-106.6151	57256	SCLF	Sanidine	NM123	11	1.92	1.28 ± 0.02	41.6 ± 24.2	SA2; Tshirege ash
34*	102998-A-ALE	QTsa	35.0111	-106.5963	50256	SCLF	Sanidine	NM105	14	2.00	1.34 ± 0.04	2.4 ± 0.6	Rhyolitic pumice
35*	SF-ac522	QTsa	35.4462	-106.3828	9175	SCLF	Sanidine	NM89	23	0.20	1.18 ± 0.18	29.3 ± 25.3	Rhyolitic pumice
36*	SF-ac512	QTsa	35.4423	-106.3857	8933	SCLF	Sanidine	NM86	14	2.41	1.38 ± 0.03	37.4 ± 8.9	Rhyolitic pumice
37*	SF-ac511	QTsa	35.4423	-106.3857	8935	SCLF	Sanidine	NM86	8	4.79	1.46 ± 0.25	20.5 ± 26.5	Rhyolitic pumice
38*	SF-ac521	QTsa	35.4458	-106.3885	9174	SCLF	Sanidine	NM89	30	0.40	1.62 ± 0.09	52.4 ± 64.8	Rhyolitic pumice
39*	SF-18psm	QTsa	35.4326	-106.4016	9172	SCLF	Sanidine	NM89	9	0.37	1.45 ± 0.12	40.6 ± 38.4	Rhyolitic pumice
40*	SF-ac519	QTsa	35.4312	-106.4066	9176	SCLF	Sanidine	NM89	5	0.07	1.49 ± 0.06	18.5 ± 0.4	Rhyolitic pumice
41*	SF-ac517	QTsa	35.4329	-106.4082	9171	SCLF	Sanidine	NM89	30	1.15	1.70 ± 0.06	36.0 ± 31.4	Rhyolitic pumice
42*	SF-ac59	QTsa	35.4388	-106.3902	8920	SCLF	Sanidine	NM86	13	3.99	1.49 ± 0.03	39.3 ± 9.9	Rhyolitic pumice
43*	SF-ac58	QTsa	35.4388	-106.3902	8919	SCLF	Sanidine	NM86	6	0.48	1.41 ± 0.04	38.1 ± 6.8	Rhyolitic pumice
44*	SF-ac56	QTsa	35.4388	-106.3915	8917	SCLF	Sanidine	NM86	13	2.28	1.55 ± 0.01	29.5 ± 11.4	Rhyolitic pumice
45*	SF-ac54	QTsa	35.4388	-106.3915	8915	SCLF	Sanidine	NM86	12	0.41	1.61 ± 0.05	30.9 ± 15.7	Rhyolitic pumice
46*	SF-ac55	QTsa	35.4388	-106.3915	8916	SCLF	Sanidine	NM86	14	0.67	1.63 ± 0.04	36.6 ± 21.8	Rhyolitic pumice
47*	SF-ac57	QTsa	35.4388	-106.3915	8918	SCLF	Sanidine	NM86	14	2.08	1.66 ± 0.01	31.5 ± 4.3	Rhyolitic pumice
48*	SF-ac520	QTsa	35.4377	-106.3977	9173	SCLF	Sanidine	NM89	14	0.41	1.65 ± 0.09	35.4 ± 11.2	Rhyolitic pumice
49*	SF-ac52	QTsa	35.3972	-106.4293	8912	SCLF	Sanidine	NM86	12	0.67	1.54 ± 0.07	38.7 ± 12.8	Rhyolitic pumice
50*	SF-ac51	QTsa	35.3966	-106.4316	8911	SCLF	Sanidine	NM86	10	2.17	1.71 ± 0.04	30.9 ± 9.6	Rhyolitic pumice
51	Casino ash	QTsp	35.4107	-106.3995	9749	SCLF	Sanidine	NM105	14	1.67	1.57 ± 0.09	38.8 ± 30.7	SA3; 3 m above QTsa
52	12199728-SFP	QTsp	35.4031	-106.4089	8924	SCLF	Sanidine	NM86	15	8.49	1.60 ± 0.06	50.7 ± 8.3	Casino ash (SA3)
53*	PL-PS-1	QTsa	35.3651	-106.4382	8934	SCLF	Sanidine	NM86	11	6.13	1.60 ± 0.02	44.4 ± 19.7	Rhyolitic pumice
54*	QTsa	35.3488	-106.4907	7615	SCLF	Sanidine	NM63	12	4.14	1.62 ± 0.03	32.9 ± 18.0	Rhyolitic pumice	
55*	SS725 or LL3	QTsa	34.8658	-106.6637	51941	SCLF	Sanidine	NM133	2	1.18	1.56 ± 0.09	46.7 ± 3.8	S8; rhyolitic pumice
56*	99LLS1	QTsa	34.8659	-106.6677	51937	SCLF	Sanidine	NM133	7	1.94	1.64 ± 0.03	35.0 ± 11.8	Rhyolitic pumice
57*	PL-asc2	QTsa	35.3132	-106.5010	2340	SCLF	Sanidine	NM23	8	1.40	1.68 ± 0.02	33.7 ± 3.9	SA5; Rhyolitic pumice
58*	Hell Cyn	QTsa	34.8961	-106.5820	51223	SCLF	Sanidine	NM123	28	6.59	1.72 ± 0.04	33.2 ± 10.5	Rhyolitic pumice
59*	SF-ac516	QTsa	35.3780	-106.4379	8923	SCLF	Sanidine	NM86	14	7.92	1.65 ± 0.03	33.2 ± 10.5	Rhyolitic pumice
60*	SF-ac514	QTsa	35.3780	-106.4379	8921	SCLF	Sanidine	NM86	5	0.48	1.92 ± 0.09	31.6 ± 17.0	Rhyolitic pumice
61*	SF-ac515	QTsa	35.3780	-106.4379	8922	SCLF	Sanidine	NM123	22	2.98	1.92 ± 0.19	30.4 ± 16.1	Rhyolitic pumice
62*	011700-ALE2	QTsa	35.0065	-106.6219	51257	SCLF	Sanidine	NM123	13	4.43	1.68 ± 0.03	29.6 ± 11.9	Rhyolitic pumice
63*	011700-ALE1	QTsa	35.0069	-106.6237	51940	SCLF	Sanidine	NM133	7	1.28	2.00 ± 0.04	16.5 ± 9.7	Pumiceous sand
64*	99IS10	QTsa	34.9261	-106.6572	51936	SCLF	Sanidine	NM133	14	3.69	1.67 ± 0.04	31.4 ± 16.8	Rhyolitic pumice
65*	99IS3	Tca	34.9187	-106.6575	51933	SCLF	Sanidine	NM133	12	3.83	2.63 ± 0.05	18.5 ± 27.6	Dacitic pumice
66*	99IS6, 23Ay0	Tca	34.9139	-106.6737	51934	SCLF	Sanidine	NM133	11	1.69	2.70 ± 0.06	60.2 ± 212	Dacitic pumice

(Continued)

TABLE 3. SUMMARY OF $^{40}\text{Ar}/^{39}\text{Ar}$ SINGLE CRYSTAL LASER FUSION (SCLF) RESULTS (Continued)

Map no.	Sample	Map unit	Lat. (°N)	Lon. (°W)	Lab. no.	Method	Material	Irrad.	N	MSWD	Date $\pm 2\sigma$ (Ma)	K/Ca	Comment
67*	99/S8	Tca	34.9408	-106.6584	51935	SCLF	Sanidine	NM133	2	0.85	2.77 \pm 0.05	18.7 \pm 0.0	Dacitic pumice
68*	CH33A	Tca	34.9592	-106.8949	8144	SCLF	Sanidine	NM71	8	5.72	3.18 \pm 0.10	152.5 \pm 65.1	Dacitic pumice, 4 m above base of Tca
69	021798-130-BERN	Tob	35.3668	-106.6090	8925	SCLF	Sanidine	NM86	14	4.67	6.83 \pm 0.04	6.6 \pm 31.0	SA21; Peralta Tuff
70	090198-U12-SVNE	Tob	35.4076	-106.7760	9473	SCLF	Sanidine	NM93	14	0.89	6.85 \pm 0.13	49.4 \pm 7.0	100 m below top SA20; Peralta Tuff
71	11E	Tob	35.4196	-106.7318	50516	SCLF	Sanidine	NM110	5	0.67	7.06 \pm 0.06	58.8 \pm 35.1	SA22; Peralta Tuff
72	6F	Ton	35.0294	-106.9051	8945	SCLF	Plagioclase	NM86	6	0.14	7.16 \pm 0.47	37.7 \pm 65.2	Cerro Colorado dacite

Notes (Tables 2 and 3): See Appendix A (see text footnote 1) for detailed description and data tables. Map number refers to numbers used in Figures 3, 6–8, 10–11, 13, and 15–20. Asterisk (*) denotes fluvially recycled pyroclastic material, and represents a maximum age for the deposit. †Table 1 of Maldonado et al. (2007). In comments column, sample S denotes sample localities in Maldonado et al. (2007); sample SA denotes sample localities in Connell (2006, 2008b). Method is single-crystal laser fusion (SCLF) or resistance-furnace incremental heating (RFIH). Table 2: N is the number of individual crystals analyzed (SCLF), or the number of heating steps used to calculate weighted mean age (RFIH). Sample material is groundmass concentrate, hornblende, obsidian, plagioclase, or sanidine. K/Ca is the molar ratio calculated from K-derived ^{39}Ar and Ca-derived ^{37}Ar . MSWD denotes mean sum of weighted deviations. vf—volcanic field. Irrad. denotes irradiation batch.

Methods: Sample preparation: sanidine, plagioclase, biotite—crushing, LST (lithium polytungstate) heavy liquid separation, Franz magnetic separation, and HF (hydrofluoric acid etching); groundmass concentrate—crushing, picking. Irradiation: four separate *in vacuo* 7–14 hr irradiations (NM23, NM45, NM63, NM71, NM77, NM78, NM86, NM93, NM105, NM110, NM123, NM127, NM137, and NM162), D3 position, Nuclear Science Center, College Station, Texas. Neutron flux monitor inter-laboratory standard Fish Canyon Tuff sandine (FC-2) with an assigned age of 28.02 Ma (Renne et al., 1998); samples and monitors irradiated in alternating holes in machined aluminum discs.

Laboratory: New Mexico Geochronology Research Laboratory, Socorro, New Mexico. Instrumentation: Mass Analyzer Products on line with automated, all-metal extraction system. Heating: sanidine—SCLF, 10W continuous CO₂ laser; RFIH—25–45 mg aliquots in resistance furnace. Reactive gas cleanup: SAES GP-50 getters operated at 20 °C and ~450 °C; SCLF—9 minutes. Error calculation: all errors reported at $\pm 2\sigma$, mean ages calculated using inverse variance weighting of Samson and Alexander (1987). Decay constant and isotopic abundances: Steiger and Jäger (1977). Complete data set presented in the Data Repository (see text footnote 1).

Analytical parameters: Electron multiplier sensitivity = 1 to 3×10^{-17} moles/pA; typical system blanks were 470, 3, 0.6, 3, 3.0×10^{-18} moles (laser) and at 1730, 37, 2, 6, 9×10^{-18} moles (turnace) at masses 40, 39, 38, 37, 36 respectively; J-factors determined to a precision of $\pm 0.2\%$ using SCLF of 4 to 6 crystals from each of 4 to 6 radial positions around irradiation vessel. Correction factors for interfering nuclear reactions, determined using K-glass and CaF₂, are provided on the CD-ROM and in the GSA Data Repository.

Samples: Samples are listed in observed or inferred stratigraphic order and were collected by Steven M. Cather, Sean D. Connell, David W. Love, and Florian Maldonado. Sample 15* was geochemically correlated to a dated obsidian at Rabbit Mountain (lat 35.8282°, lon -106.4553°) in the Jemez Mountains (Nelia Dunbar, 2001, personal commun.). Table 1 of Maldonado et al. (2007). Map units include: Cerro Conejo Formation (Tcc); Navajo Draw (Ton), Loma Barbon (Tob), and Picuda Peak (Top) Members of the Arroyo Oltó Formation; axial-fluvial (QTs) and piedmont (QTsp) members of the Sierra Ladrones Formation; Rio Puerto (Tcp), Atrisco (Tca), and Santa Ana Mesa (Tcs) Members of the Ceja Formation; unit of San Clemente (Qsc); and basaltic lava (Tb).

TABLE 4. STATISTICAL PARAMETERS FOR CLASS I PALEOMAGNETIC STUDY SITES

Section		N	R	K	$\alpha 95$ ($^{\circ}$)	Dec. ($^{\circ}$)	Inc. ($^{\circ}$)
<u>All sites (N)</u>							
	Geo	58	53.5	12.76	5.4	3.5	47.1
	Strat	58	53.9	13.74	5.2	2.8	45.0
<u>All sites (R)</u>							
	Geo	50	45.4	10.64	6.5	181.9	-45.6
	Strat	50	45.4	10.69	6.5	180.2	-41.7
<u>All sites (R)*</u>							
	Geo	48	44.7	14.04	5.7	179.7	-47.1
	Strat	48	44.6	14.01	5.7	178.1	-43.2
<u>All Ceja Fm. (N)</u>							
	Geo	47	43.7	13.94	5.8	4.2	44.7
	Strat	47	44.1	15.73	5.4	2.9	42.3
<u>All Ceja Fm. (R)</u>							
	Geo	38	34.9	12.07	7.0	181.9	-47.0
	Strat	38	34.9	12.07	7.0	180.0	-42.6
<u>All Sierra Ladrones Fm. (N)</u>							
	Geo	7	6.6	14.83	16.2	14.9	60.3
	Strat	7	6.6	15.03	16.1	17.8	59.5
<u>All Sierra Ladrones Fm. (R)</u>							
	Geo	8	7.9	65.52	6.9	169.3	-46.7
	Strat	8	7.9	60.85	7.2	170.4	-46.6

Notes: N—number of sites averaged; R—Fisher statistic; K—precision parameter; $\alpha 95$ —cone of confidence; Dec.—declination; Inc.—inclination. Geographic (Geo) and tilt-corrected (Strat) declination and inclinations shown. (N)—normal sites; (R)—reversed sites. Asterisk (*) denotes removal of 2 outliers from the CDRP-CL section (CLS sites S11 and S25, Appendix B [see text footnote 1]) having a southward declination with positive inclination.

TABLE 5. STATISTICAL PARAMETERS FOR ROTATED CLASS I PALEOMAGNETIC STUDY SITES

Section		N	R	K	$\alpha 95$ ($^{\circ}$)	Dec. ($^{\circ}$)	Inc. ($^{\circ}$)
<u>All sites</u>							
	Geo	108	98.9	11.77	4.1	2.7	46.4
	Strat	108	99.2	12.18	4.1	1.6	43.5
<u>All reverse sites*</u>							
	Geo	48	47.9	15.73	5.4	0.7	47.9
	Strat	48	44.9	15.27	5.4	359.1	44.0
<u>Ceja Fm. sites</u>							
	Geo	85	78.6	13.15	4.4	3.2	45.8
	Strat	85	79.0	13.99	4.3	1.6	42.5
<u>Sierra Ladrones Fm. sites</u>							
	Geo	15	14.3	19.06	9.0	358.9	53.5
	Strat	15	14.3	18.73	9.1	0.8	53.3

Notes: Reverse polarity directions inverted to north-seeking, positive-inclination values; N—number of sites averaged; R—Fisher statistic; K—precision parameter; $\alpha 95$ —cone of confidence; Dec.—declination; Inc.—inclination. Geographic (Geo) and tilt-corrected (Strat) declination and inclinations shown. Asterisk (*) denotes removal of 2 outliers from the CDRP-CL section (CLS sites S11 and S25, Appendix B [see text footnote 1]) having a southward declination with positive inclination.

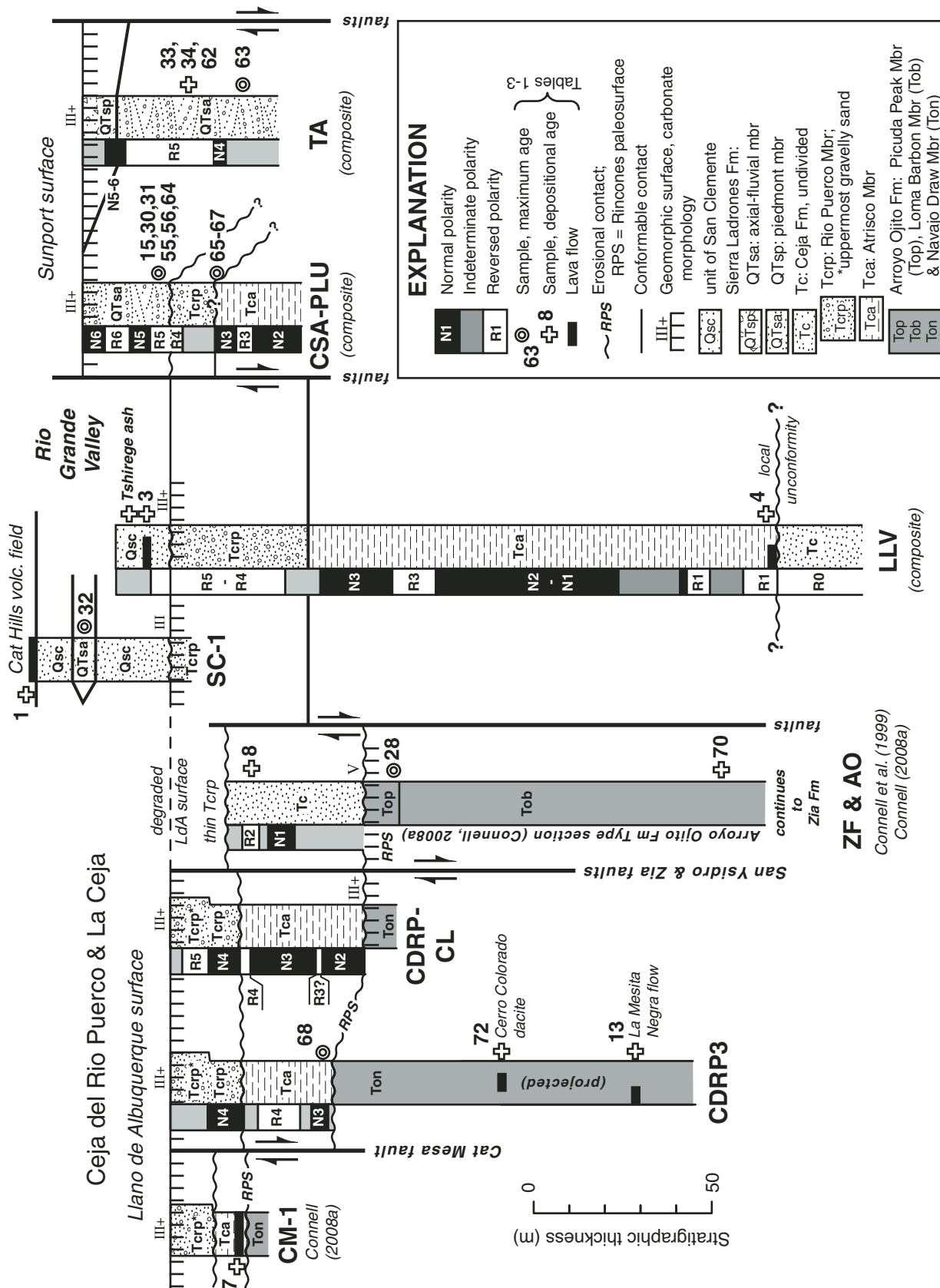


Figure 8. Stratigraphic fence diagram, illustrating correlations of measured stratigraphic sections (see Fig. 3 for locations). Measured sections were correlated using age determinations (Tables 1–3), the Rincones paleosurface, and the Llano de Albuquerque (LdA) and Sunport geomorphic surfaces as stratigraphic datum planes. The Arroyo Ojito (AO), Zia fault (ZF), Cat Mesa (CM-1), and San Clemente (SC-1) stratigraphic sections were modified from previous studies (Connell et al., 1999, 2001c; Connell, 2008a).

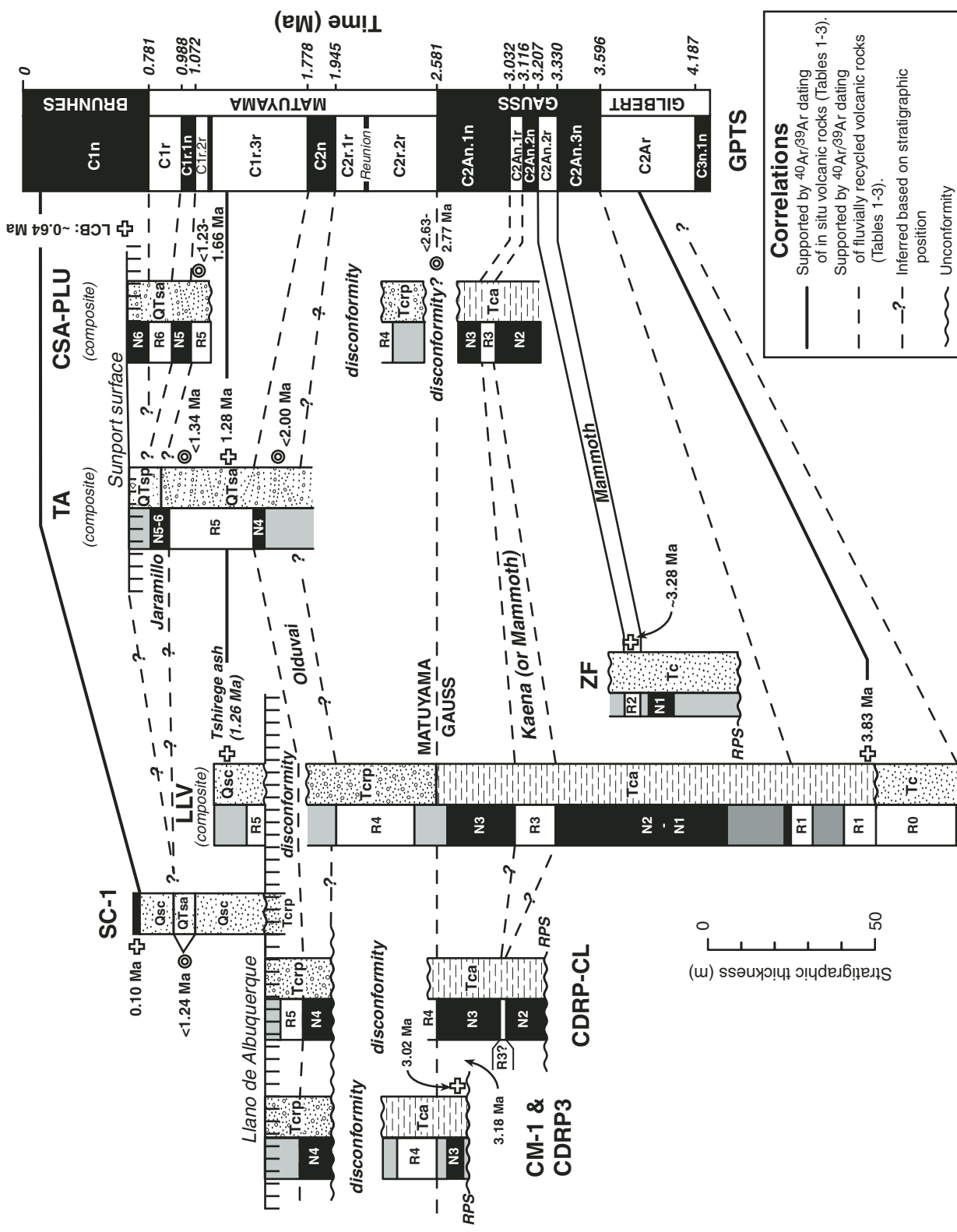


Figure 9. Stratigraphic fence diagram, illustrating correlations to the global geomagnetic polarity time scale (GPTS; Gradstein et al., 2005). Measured sections (see Fig. 3 for locations) were correlated using the Liano de Matuyama chron boundary, the Liano de Albuquerque and Sunport surfaces, and a 1.27 Ma ash correlated to the Tshirege Member of the Bandelier Tuff (Table 3). Stratigraphic sections are vertically separated across documented or inferred disconformities. The abbreviation LCB refers to the Lava Creek B tephra found within an inset terrace deposit of the Rio Grande (Connell et al., 2007a). See Figure 8 for explanation of geologic unit symbols.

and Sunport surfaces, the 2.581 Ma Gauss-Matuyama chron boundary, and an early Pleistocene volcanic ash (Bandelier Tuff, Tewa Group) provide important chronostratigraphic datum controls for intrabasinal correlation (Fig. 9). The Réunion and Cobb Mountain subchrons (<20 k.y.) were not recognized in this study. The preservation of such short-lived subchrons in an extensively channelized fluvial environment is probably low. The absence of these subchrons is supported by estimates of Plio-Pleistocene sediment accumulation, which ranged from 22 to 33 m/m.y. (Lozinsky, 1994). These sedimentation rates would require sampling intervals of 0.4–0.7 m to capture these subchrons. Thus, the average sampling interval (see above) was likely too coarse to capture these short-lived subchrons.

Miocene Deposits

Exposed Miocene sections in the Albuquerque Basin contain alluvial, eolian, and volcaniclastic deposits of the Arroyo Ojito, Blackshare, Cerro Conejo, Cochiti, Popotosa, Tanos, and Zia Formations (Fig. 5). The Tanos and Blackshare Formations (Connell et al., 2002) are well exposed along the northeastern flank of the basin and in the Hagan embayment. The Lower to Middle Miocene Zia Formation is exposed along the northwest flank of the basin (Connell, 2004). It consists of eolian and fluviatile sandstone and mudstone that represents deposition in a predominantly eolian setting with scattered interdune ponds and streams (Tedford and Barghoorn, 1999). Fluviolacustrine deposits of the Popotosa Formation are exposed in the southern part of the basin, and are also recognized in drill holes (Is2 on Fig. 3; Machette, 1978; Lozinsky, 1994; Cather et al., 1994; Connell et al., 2005; Maldonado et al., 1999, 2007). Popotosa mudstone has been reported in deep oil-test wells near Los Lunas and Isleta Pueblo (Lozinsky, 1994), but has not been recognized farther north in drill holes beneath Albuquerque (Hawley and Haase, 1992, section IV).

The Middle Miocene Cerro Conejo Formation is exposed along the northwestern flank of the Albuquerque Basin, where it contains eolian and fluvial sand and interbedded mudstone that was deposited between 14.5 and 9.5 Ma (Tedford and Barghoorn, 1999; Connell, 2008a). This unit represents a transition from the largely eolian Zia Formation to the predominantly fluviatile Arroyo Ojito Formation (see below). The Cochiti Formation is a Miocene through lower Pleistocene succession of volcanic-bearing sandstone and conglomerate exposed along the southern flank of the Jemez Mountains (Smith and Lavine, 1996).

The Arroyo Ojito Formation is exposed along the western flank of the Albuquerque Basin. It was deposited between 9.0 and 6.3 Ma by southeast-flowing streams that originated on the Colorado Plateau and nearby uplifts, such as the Sierra Nacimiento (Connell et al., 1999). A widespread erosion surface called the Rincones paleosurface marks the top of the Arroyo Ojito Formation (Connell, 2008a). The age of the lower part of the Arroyo Ojito Formation is determined by Upper Miocene basaltic lavas exposed near the top of the underlying Cerro Conejo Formation

(Pazzaglia et al., 1998; Smith et al., 2001; Chamberlin and McIntosh, 2007). Basaltic lava flows at Chamisa Mesa and Bodega Butte, along the southern flank of the Jemez Mountains (Fig. 3), yielded groundmass $^{40}\text{Ar}/^{39}\text{Ar}$ age determinations ranging between 9.67 and 9.04 Ma (Fig. 6, sample 14, Table 1; sample 29, Table 2).

Other age control for the Arroyo Ojito Formation comes from the Rio Puerco valley, where a basaltic lava flow at La Mesita Negra (Fig. 10) is interbedded with sandstone of the Navajo Draw Member. This flow yielded a $^{40}\text{Ar}/^{39}\text{Ar}$ age determination of 8.16 ± 0.05 Ma (Fig. 6, sample 13, Table 1; Maldonado et al., 2006). A dacitic volcanic vent at Cerro Colorado, ~3 km southeast of La Mesita Negra, yielded an age determination of 7.16 ± 0.47 Ma (Fig. 6, sample 72, Table 3). The basal edges of this feature rest on Navajo Draw sandstone, ~43–55 m below the Rincones paleosurface of Connell (2008a). The Loma Barbon Member of the Arroyo Ojito Formation contains ashes that range in age from 6.83 to 7.06 Ma (Fig. 6, samples 10–12, Table 1; samples 69–71, Table 3). These ashes correlate to the Peralta Tuff Member of the Bearhead Rhyolite (e.g., Smith, 2001), which interfingers with the Arroyo Ojito Formation and lower parts of the Cochiti Formation in the northern part of the Albuquerque Basin and southeastern flank of the Jemez Mountains.

The Arroyo Ojito Formation generally coarsens up-section of older (7.1–6.8 Ma) Peralta ashes (Connell, 2008b), culminating in deposition of the conglomeratic Picuda Peak Member by ca. 6.3 Ma. Lozinsky and Tedford (1991) reported an upward-coarsening trend in a 7–9 Ma section for piedmont deposits of the Popotosa Formation in the Gabaldon badlands, just southwest of the study area (Fig. 3). A maximum age of the top of the Arroyo Ojito Formation comes from a basaltic cobble ~20 m below the top of the Picuda Peak Member that yielded a groundmass $^{40}\text{Ar}/^{39}\text{Ar}$ age determination of 6.56 ± 0.33 Ma (Fig. 6, sample 28, Table 2).

An important age determination for the Miocene succession comes from a bed of rhyolitic pumice in the Cochiti Formation exposed along the northern flank of the San Felipe volcanic field (Fig. 11). This pumice yielded a $^{40}\text{Ar}/^{39}\text{Ar}$ age determination on sanidine of 6.29 ± 0.08 Ma (Fig. 6, sample 10, Table 1) that correlates to the Cerrito Yelo tephra of the Peralta Tuff (Chamberlin and McIntosh, 2007). It is ~20 m below the 2.46–2.43 Ma basaltic lavas of the San Felipe volcanic field (Figs. 6 and 7, samples 5 and 6, Table 1; samples 16–19, Table 2; Smith et al., 2001). The age of this tephra suggests the presence of an unconformity or condensed stratigraphic section between Upper Miocene and upper Pliocene rocks (Fig. 11). Geologic mapping north of the San Felipe volcanic field did not recognize any widespread unconformities within the Cochiti Formation (Smith et al., 2001); however, other workers reported multiple Miocene unconformities toward the western margin of the basin (Chamberlin and McIntosh, 2007). The earlier (basinward) mapping of Smith et al. (2001) took place before dating of the Cerrito Yelo tephra and recognition of the Rincones paleosurface (described below), so it is not clear if the Cochiti

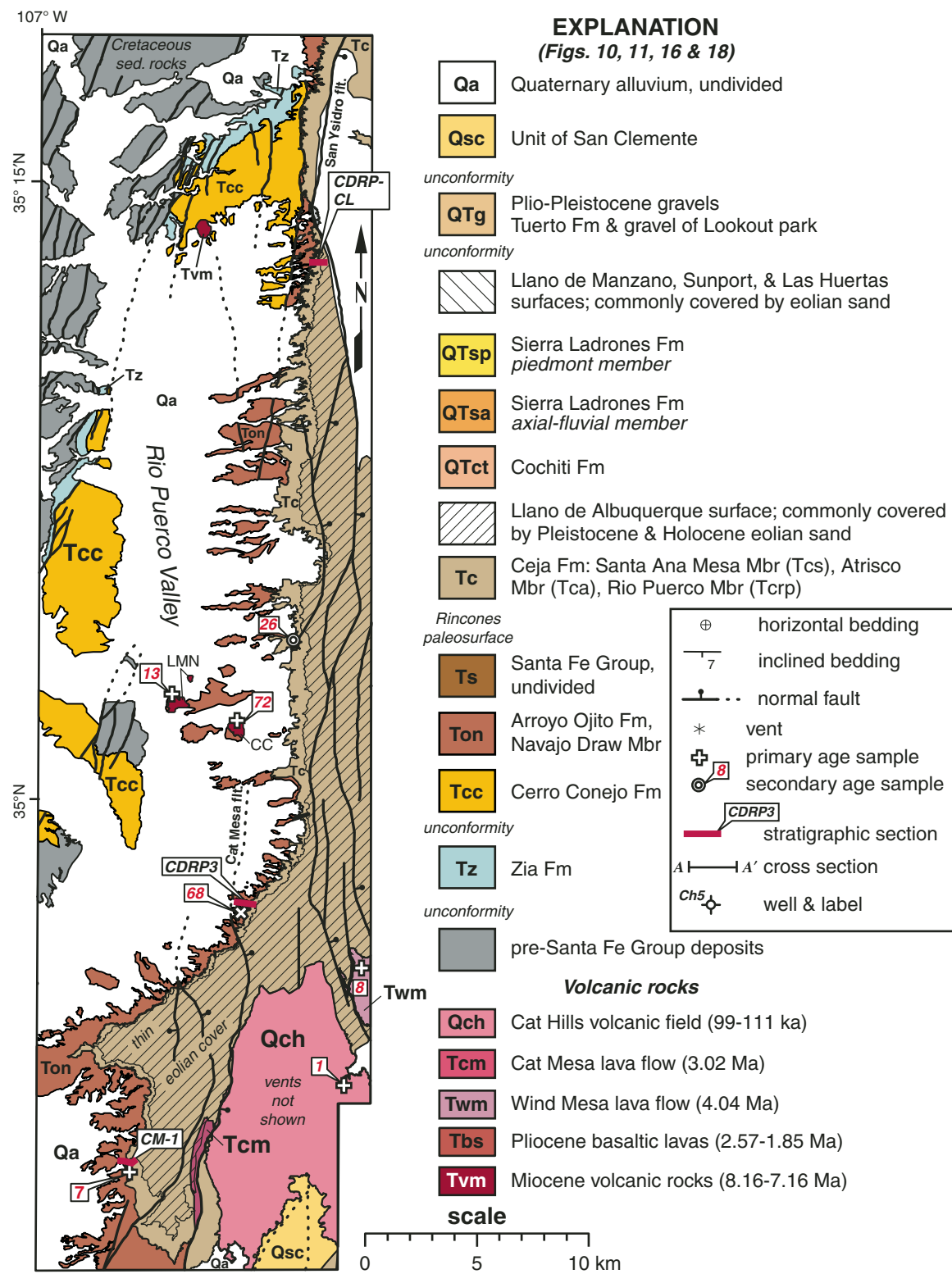


Figure 10. Simplified geologic map along part of the Ceja del Rio Puerco and western margin of the Albuquerque Basin, illustrating the locations of major faults, volcanic features (LMN—La Mesita Negra; CC—Cerro Colorado), age-determination sample sites (Tables 1–3), and measured stratigraphic sections (described in text). Primary sample (plus symbol) denotes age determinations of volcanic fallout tephra or lava flows that represent emplacement or depositional ages. Samples of fluvially recycled tephra (circle-in-circle symbol) represent maximum ages. The Ceja Formation disconformably overlies the lower part of the Arroyo Ojito Formation (i.e., Navajo Draw Member) and the Cerro Conejo Formation. The Cat Mesa lava flow and CM-1 section are on the footwall of the Cat Mesa fault; section CDRP3 is northeast of the hanging wall. CDRP-CL is on the footwall of the San Ysidro fault.

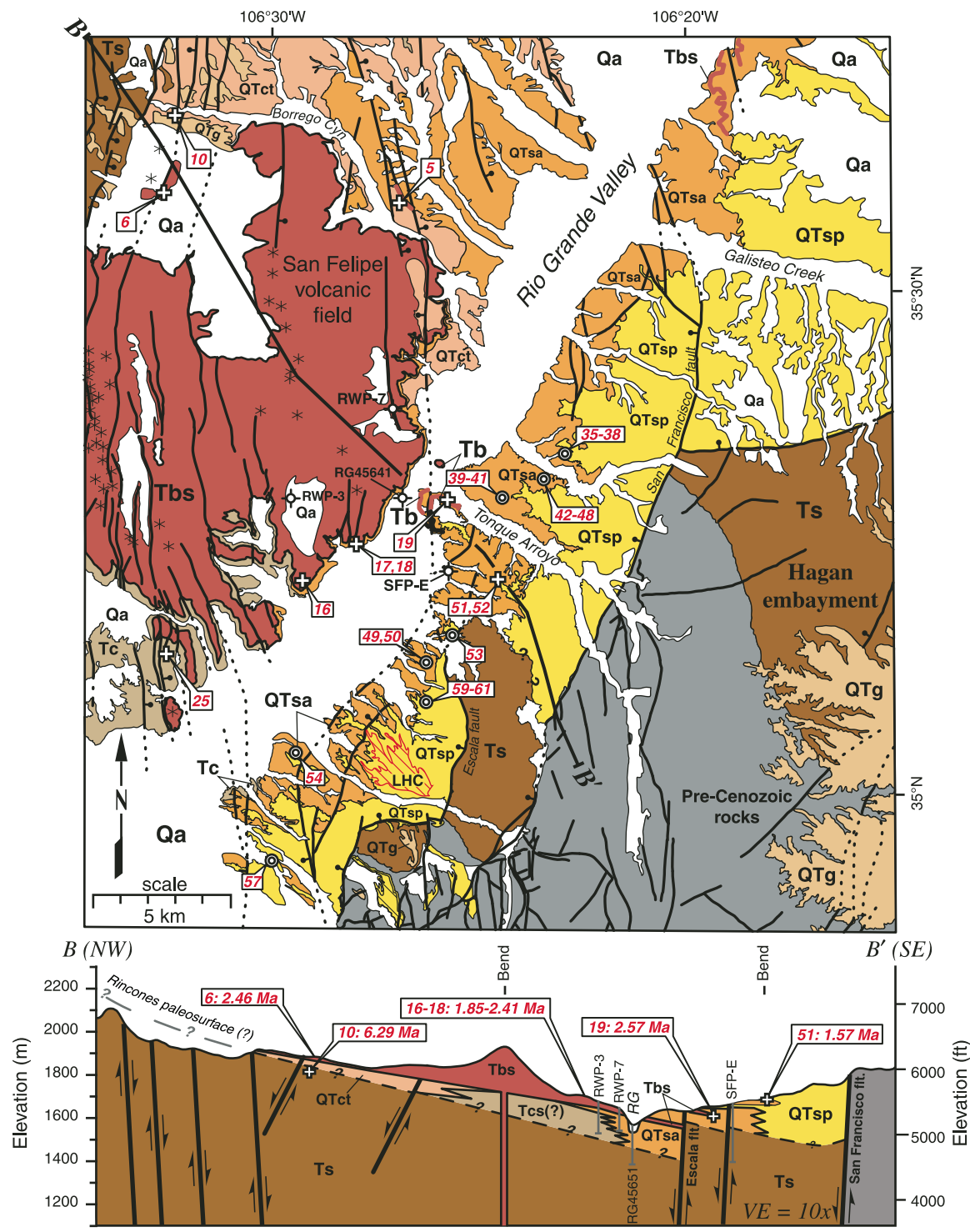


Figure 11. (Top) Simplified geologic map of the eastern part of the San Felipe volcanic field (Santa Ana Mesa) and eastern margin of the Albuquerque Basin (Santo Domingo sub-basin; modified from Smith et al., 2001; Connell, 2008b). Numeric labels denote $^{40}\text{Ar}/^{39}\text{Ar}$ age determination sites on Tables 1–3. Explanation of map units and symbols is on Figure 10; additional unit is the Santa Ana Mesa Member (Tcs) of the Ceja Formation. Las Huertas geomorphic surface (LHC, red diagonal lines) marks a local depositional top of the Sierra Ladrones Formation. (Bottom) Cross section B–B' (vertical exaggeration [VE] = 10 \times) based on previous geologic mapping (Chamberlin et al., 1999; Smith et al., 2001; Connell, 2008b); the cross-section location is on the top figure. Stratigraphic interpretations of wells used in cross section were taken from a digital database (Connell, 2006).

Formation contains a widespread and mappable unconformity, or if it is a condensed section.

Over 1 km of Miocene through lower Pleistocene conglomerate and sandstone is exposed across a faulted relay ramp that formed between the northern flank of the Sandia Mountains and the Hagan embayment (Fig. 3; Kelley, 1977, 1982; May et al., 1994; Russell and Snelson, 1994). These deposits form a generally conformable stratigraphic succession that records unroofing of the adjacent Sandia Mountains (Connell and Wells, 1999).

Ceja Formation

The Ceja Formation contains fluvial sandstone, conglomerate, and mudstone deposited by large southeast-flowing streams and fluvial fans that drained the southeastern Colorado Plateau, San Juan Basin, Sierra Nacimiento, and southern Jemez Mountains (Connell, 2008a). Streams of the Ceja Formation drained roughly the same region as those of the Arroyo Ojito Formation; however, the Ceja Formation contains a greater variety of rock types than the Arroyo Ojito Formation and represents deeper unroofing of the western flanks of the Albuquerque Basin (Connell et al., 1999). The Ceja Formation thickens to the east (from ~20 m to over 420 m) and is bounded by a basal erosional surface called Rincones paleosurface, and an upper relict depositional surface called the Llano de Albuquerque surface (see below).

The Ceja Formation is divided into the Santa Ana Mesa, Atrisco, and Rio Puerco Members (Fig. 5). The Atrisco and Santa Ana Mesa Members contain sandstone and mudstone with minor pebbly sandstone interbeds. The Atrisco Member contains thickly bedded, mottled and massive to well-sorted, fine-grained, eolian sand (Figs. 12A and 12D). The Santa Ana Mesa Member is generally redder in color and contains coarser gravel than the Atrisco Member. The Rio Puerco Member is dominated by coarse-grained, medium to very thickly bedded, pebbly to cobble sand with scattered cobbles and small boulders. The contact between the Atrisco and Rio Puerco Members is sharp and erosional along the Ceja del Rio Puerco. Gravelly beds in the Rio Puerco Member form overlapping, laterally and vertically stacked channels that commonly contain laminated to thinly bedded, low-angle, planar and locally trough cross-stratified sand and pebbly sand (Fig. 12B).

The Ceja Formation generally coarsens up-section, culminating in mesa-capping gravels of the Rio Puerco Member, and contains a nearly 2-m-thick accumulation of petrocalcic soils of the Llano de Albuquerque surface (Fig. 12A). Using borehole geophysical logs, Connell et al. (1998) interpreted an overall upward-coarsening trend in deposits overlying the Atrisco Member. This coarsening trend in the Ceja Formation was confirmed here by measuring the relative proportions of mud, sand, and gravel sizes along the Ceja del Rio Puerco and at El Cerro de los Lunas, or Los Lunas volcano (Fig. 3). Mudstone (12%–24% of the section) and sandstone (72%–81%) beds dominate the Atrisco Member along the Ceja del Rio Puerco, but gravels are a minor constituent (4%–7%). The overlying Rio Puerco Member

is dominated by gravel (35%–48%) and sand (49%–59%) with minor mud beds (3%–6%).

The upward-coarsening trend in the Ceja Formation is also reflected by gravel size. The lower part of the Atrisco Member contain medium pebbles (7 ± 3 cm, mean intermediate diameter of 5 ± 2 cm, $N = 67$ measurements), whereas the upper part contains medium to coarse pebbles (17 ± 4 cm, mean intermediate diameter of 11 ± 3 cm, $N = 26$). The Rio Puerco Member contains coarse pebbles (21 ± 9 cm, mean intermediate diameter of 15 ± 6 cm, $N = 42$). Very coarse pebbles and coarse cobbles (40–110 cm in maximum diameter) are scattered at the top of the Rio Puerco Member.

Geochronology

Lava flows and fluvially recycled volcanic gravel in the Ceja Formation demonstrate a Pliocene age of deposition (Connell, 2008a; Maldonado et al., 2007). The age of the Ceja Formation is refined by integrating isotopic and biostratigraphic age data into five composite stratigraphic sections that were sampled for magnetic polarity: CDRP3, CDRP-CL, CSA-PLU, LLV, and ZF (Figs. 13–15, 17, 19, and 20; locations shown in Fig. 3). The age of the base of the Atrisco Member increases into the basin across numerous intrabasinal normal faults (Fig. 9). The 3.02 Ma Cat Mesa lava flow marks the base of the Atrisco Member on Cat Mesa and along the Ceja del Rio Puerco (Fig. 6, sample 7, Table 1). A volcanic ash adjacent to the Zia fault at La Ceja in the ZF section (Fig. 15) was geochemically correlated to the ca. 3.28 Ma Nomlaki Tuff (sample 8, Table 1). This ash yielded a reverse-polarity magnetization that is consistent with polarity data for the Nomlaki Tuff (Reheis et al., 1991).

The Atrisco Member at CDRP3 and CDRP-CL contains normal- and reverse-polarity sites (Figs. 13 and 14) that indicate deposition during parts of the Gauss and Matuyama chrons (Fig. 9). The Santa Ana Mesa Member is locally capped by basaltic lavas of the San Felipe volcanic field (at Santa Ana Mesa), which yielded groundmass $^{40}\text{Ar}/^{39}\text{Ar}$ age determinations of 2.57 ± 0.11 Ma and 1.85 ± 0.10 Ma (Fig. 7, samples 19 and 16, Table 2). The Santa Ana Mesa Member contains an ash exposed in the spillway of the Jemez River dam that is ~42 m below these Pliocene basaltic lavas (Fig. 11). This spillway ash yielded a single-crystal $^{40}\text{Ar}/^{39}\text{Ar}$ age determination on hornblende of 3.81 ± 0.23 Ma (Fig. 6, sample 25, Table 2).

The thickest, most complete and accessible exposures of the Ceja Formation in the study area are along the flanks of El Cerro de los Lunas, also called Los Lunas volcano (Fig. 16; Kelley and Kudo, 1978; Love et al., 1998; Maldonado et al., 2007). A 210-m-thick composite stratigraphic section was assembled by correlating distinctive marker beds and an angular unconformity (Fig. 17). El Cerro de los Lunas contains two overlapping trachy-andesitic volcanoes that yielded groundmass $^{40}\text{Ar}/^{39}\text{Ar}$ age determinations of 3.83 ± 0.10 Ma and 1.26 ± 0.02 Ma (Fig. 6, samples 3 and 4, Table 1; Dunbar et al., 2001). The older event locally deformed a similarly aged bed of black lapilli tuff that was used to correlate the lower and upper parts of the LLV composite section

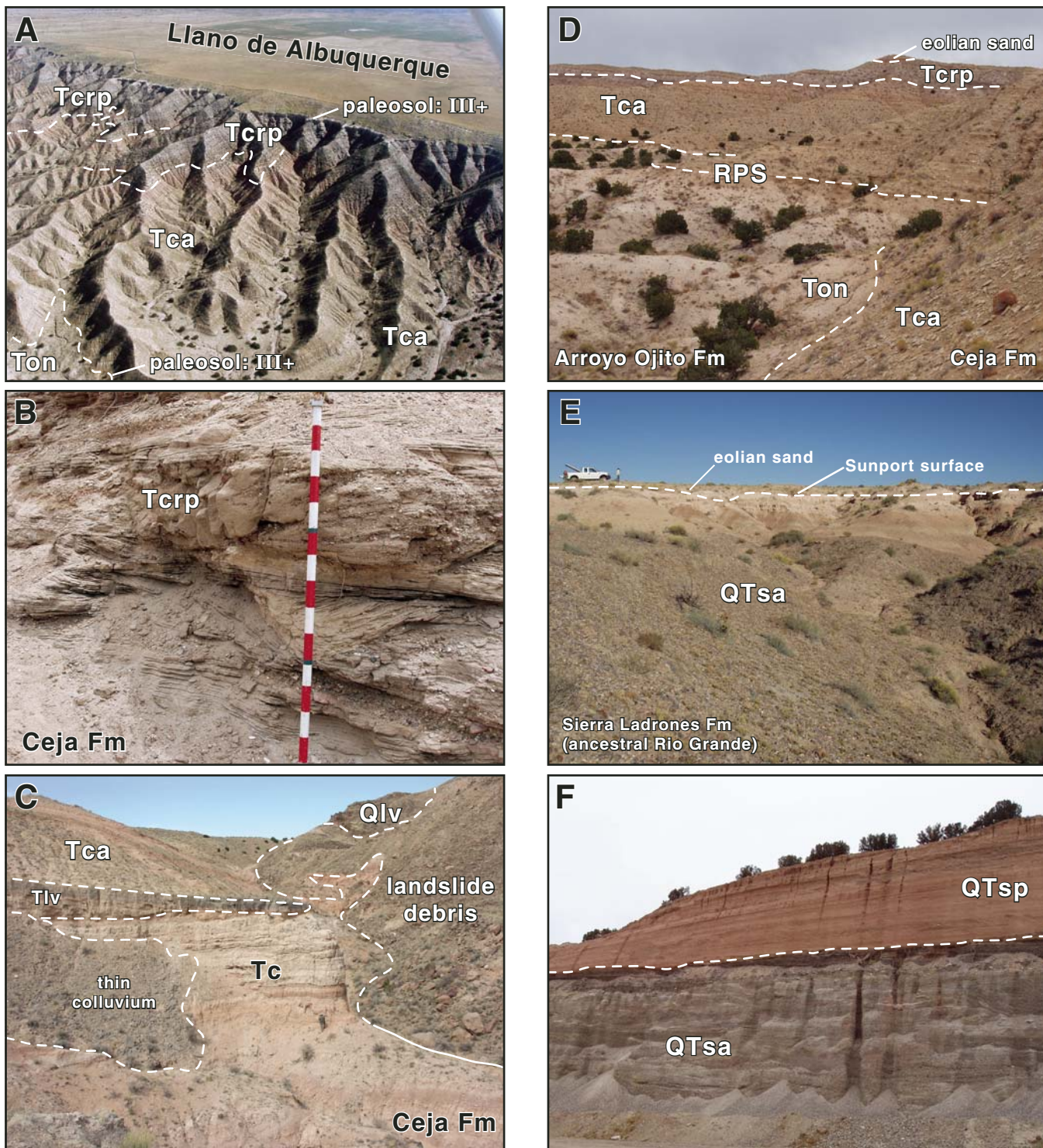


Figure 12. Photographs of deposits in the study area. Geologic contacts denoted by white lines. (A) View to north of the Ceja del Rio Puerco (near the CDRP-CL section), an ~55-m-high escarpment exposing Atrisco (Tca) and Rio Puerco (Tcrp) Members of the Ceja Formation that disconformably overlie Upper Miocene sandstone of the Navajo Draw Member (Ton) of the Arroyo Ojito Formation. (B) Cross-stratified pebbly sand in Rio Puerco Member (Tcrp) near the top of County Line section (CDRP-CL); 10 cm gradations on Jacob's staff. (C) View to north of black lapilli of the older Los Lunas tuff (Tlv) overlying the LLVS section, and underlying the Atrisco Member (Tca) of the Ceja Formation (Tc) and younger trachyandesitic flows (Qlv) at Los Lunas volcano; 1.9-m-tall person for scale. (D) View to north of white petrocalcic paleosols with stage III+ pedogenic carbonate morphology developed on the Rincones paleosurface (RPS) along the Ceja del Rio Puerco, near the CDRP-CL section; trees and shrubs are <3 m tall. (E) View to east of upper pumice-bearing, gravelly sand and mudstone of the axial-fluvial member (QTsa) of the Sierra Ladrones Formation in the PLU section and white petrocalcic soils of the Sunport surface (stage III+); truck is ~5 m long. (F) Sharp boundary of gravelly sand of axial-fluvial member (QTsa) and overlying muddy sand of piedmont member (QTsp) of Sierra Ladrones Formation, at a gravel quarry northeast of Bernalillo, New Mexico; exposures are ~15 m high.

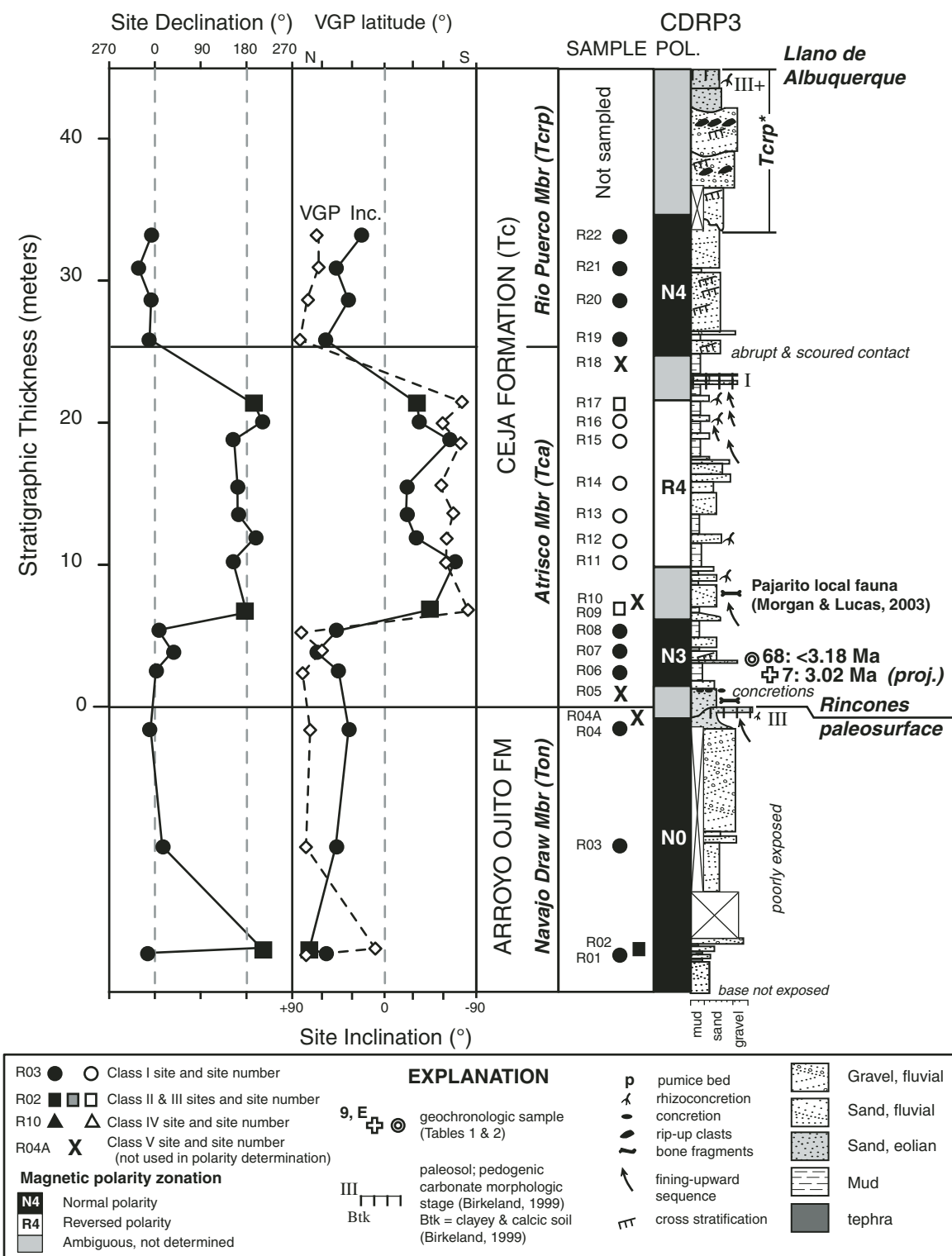


Figure 13. Lithostratigraphy and magnetic polarity stratigraphy of the CDRP3 stratigraphic section (see Fig. 10 for location), magnetostratigraphic composite section (VGP—virtual geomagnetic pole; Inc.—site inclination), and provisional magnetic polarity zonation. Lines connect stratigraphically consecutive sites. Age determination sites in Tables 1–3. Unit Tcrp* refers to the gravelly top of the Rio Puerco Member. Roman numerals denote pedogenic carbonate morphologic stages (Birkeland, 1999).

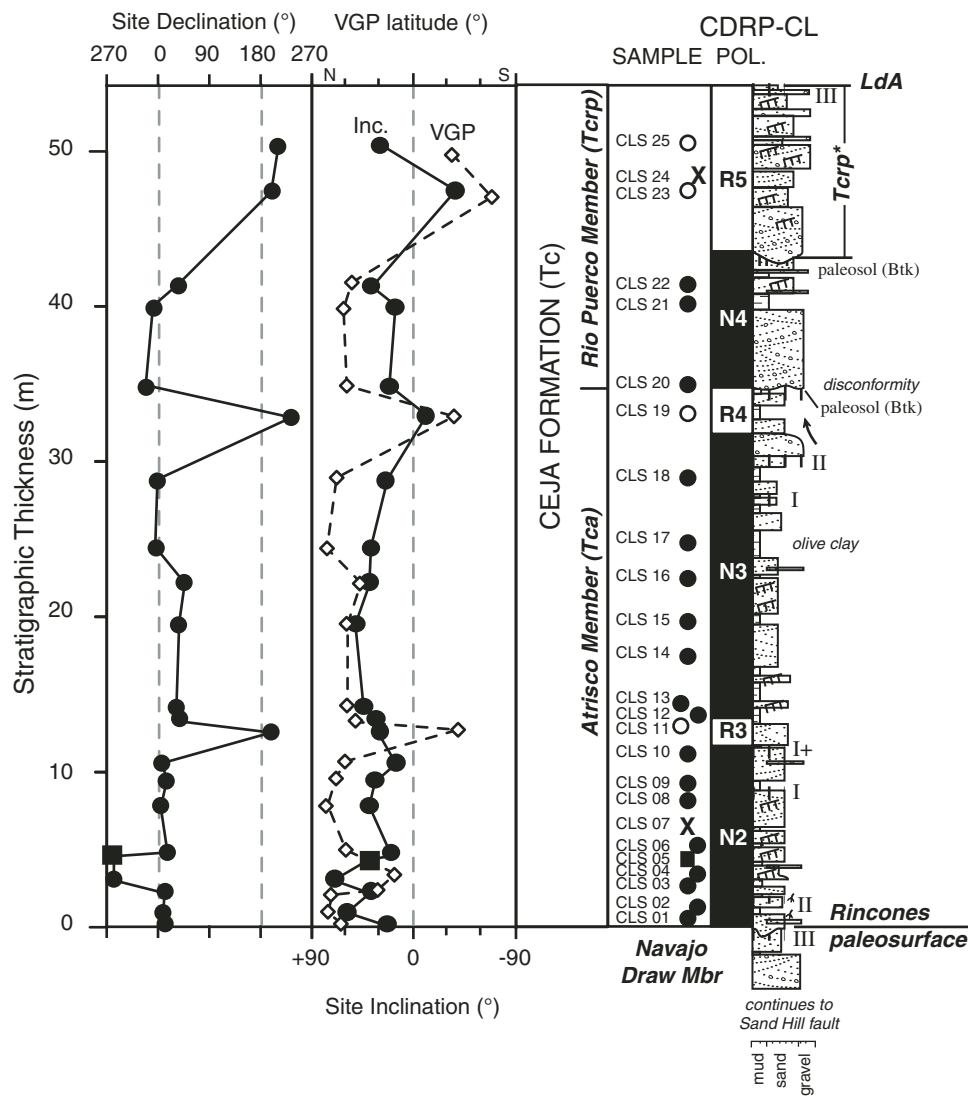


Figure 14. Lithostratigraphy and magnetic polarity stratigraphy of County Line (CDRP-CL) stratigraphic section (see Fig. 10 for location), magnetostratigraphic composite section (VGP—virtual geomagnetic pole; Inc.—site inclination), and correlation to a provisional magnetic polarity zonation. Lines connect stratigraphically consecutive sites. Refer to Figure 13 for explanation of symbols. Unit T_{crp}^* refers to the gravelly top of the Rio Puerco Member. Age determination sites in Tables 1–3. Roman numerals denote pedogenic carbonate morphologic stages; Btk refers to soil horizons in a buried paleosol with translocated clay and carbonate (Birkeland, 1999). LdA—Llano de Albuquerque surface.

(Figs. 12C and 16). This tuff overlies an unconformity having an angularity of up to 45° along the northern flank of the younger volcano. This boundary is subparallel to bedding where exposed at the southern flank. The abrupt change in the character of this stratal discontinuity and doming around the volcanoes suggest that this contact formed during emplacement of the older volcano, rather than representing a buried correlative of the Rincones paleosurface. Strata underlying the older lava flow yielded reverse polarity directions that are consistent with deposition during the later part of the Gilbert polarity chron, and after the normal polarity Cochiti subchron, at 4.187 Ma (Fig. 9). The top of the Ceja section contains a buried paleosol that is considered to be a buried correlative of the Llano de Albuquerque surface (Figs. 8 and 17). A bed of angular volcanic lapilli and blocks in the unit of San Clemente was deposited during the younger Los Lunas eruption.

The easternmost exposures of the Ceja Formation were examined in faulted blocks exposed along the flanks of the

Rio Grande valley (Fig. 18). Basaltic cinders from Perea Mesa (Isleta volcano, Kelley and Kudo, 1978) are exposed along the eastern edge of the Rio Grande valley (Fig. 6, samples 21–23, Table 2), ~4 km northwest of Isleta Pueblo (Fig. 3). These 2.8–2.9 Ma basaltic tephra are stratigraphically below the CSU-PLU measured sections (Figs. 18 and 19; Connell et al., 2001d, their figure 2-1). Gray dacitic pumice pebbles, scattered throughout much of the Ceja Formation, yielded $^{40}\text{Ar}/^{39}\text{Ar}$ age determinations of 2.63–2.77 Ma (Fig. 6, samples 65–67, Table 3). These maximum ages support correlation of the lower part of the CSA-PLU section to the upper Gauss and Matuyama chron (Fig. 9).

The Rio Puerco Member at CDRP3 and CDRP-CL contains a normal-polarity interval that is interpreted as part of the 1.945–1.778 Ma Olduvai subchron (Fig. 9). This interval is <10 m in thickness and probably did not record the geologically short (<10 k.y.) Réunion subchron. Assignment to the Réunion subchron would require deposition rates that would be two to five

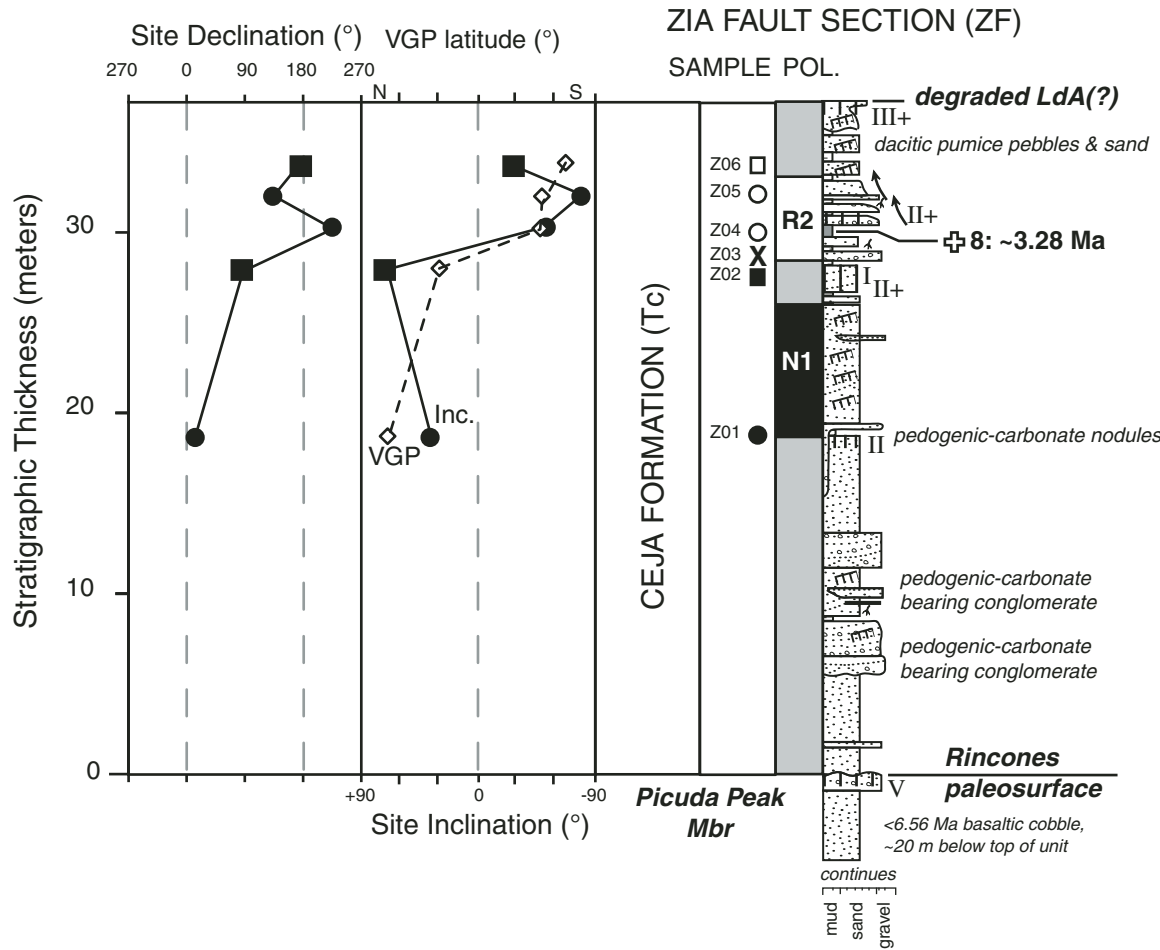


Figure 15. Lithostratigraphy and magnetic polarity stratigraphy of Zia Fault (ZF) stratigraphic section (see Fig. 3 for location), magnetostratigraphic composite section (VGP—virtual geomagnetic pole; Inc.—site inclination), and correlation to a provisional magnetic polarity zonation. Lines connect stratigraphically consecutive sites. The volcanic ash was geochemically correlated to the ca. 3.28 Ma Nomlaki Tuff. Refer to Figure 13 for explanation of symbols. Age determination sites in Tables 1–3. Roman numerals denote pedogenic carbonate morphologic stages (Birkeland, 1999). LdA—Llano de Albuquerque surface.

times greater than the highest known sedimentation rates estimated by Lozinsky (1994).

Assignment of thin, reverse-polarity intervals in the CDRP-CL, LLV, and CSA-PLU sections to GPTS subchrons are ambiguous because of a lack of adequate age control. Two thin (<4.5 m), reverse-polarity magnetozones at CDRP-CL may represent the Matuyama chron, or the Mammoth or Kaena subchrons. A 4.5-m-thick succession of sand and laminated silty sand in the Atrisco Member is disconformably overlain by the Rio Puerco Member at CDRP-CL. The estimated site mean direction ($D = 233^\circ$; $I = -11^\circ$; VGP latitude $= -33^\circ$) supports a reverse-polarity interpretation, and the stratigraphic position of this site (below the Rio Puerco Member) supports assignment to the lower part of the Matuyama chron. Thus, this stratigraphically lower reverse-polarity magnetozone (site 11) records either the Mammoth or Kaena subchrons. Assignment to the Kaena subchron is preferred because of the structurally higher position of the CDRP-CL sec-

tion (on the footwall of the San Ysidro fault) and similar stratigraphic position relative to the Cat Mesa flow (CM-1, Fig. 9). Assignment of a thin, reverse-polarity magnetozone in the LLV and CSA-PLU composite sections (Figs. 17 and 19) to the Kaena subchron is based on the presence of dacitic pumice pebbles. Although dacitic pebbles in the LLV section did not yield interpretable age determinations, similar volcanic pebbles in CDRP3 and CSA-PLU yielded age determinations that are younger than the 3.3–3.2 Ma Mammoth subchron.

Sierra Ladrones Formation

The Sierra Ladrones Formation, which is dominated by fluvial sandstone and conglomerate, represents a major change in basin drainage with the establishment of through-going axial drainage (i.e., the ancestral Rio Grande) into southern New Mexico. The base of the Sierra Ladrones Formation is unconformable

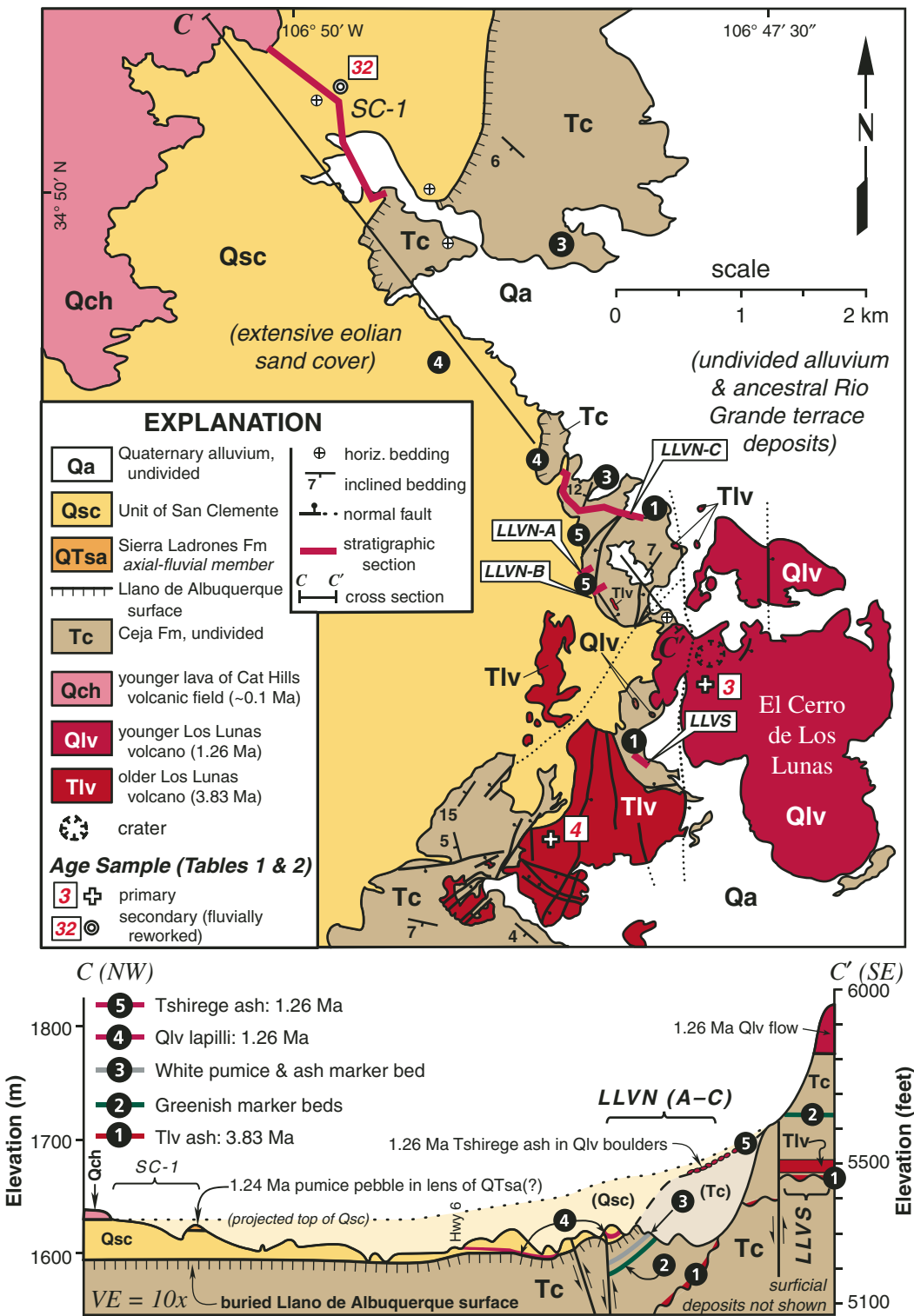


Figure 16. Geology of El Cerro de Los Lunas (Los Lunas volcano) and vicinity (modified from Love et al., 2001b). (Top) Geologic map. (Bottom) Geologic cross section C-C' (vertical exaggeration [VE] = 10×; simplified from Love et al., 2001c) illustrates stratigraphic relationships among the younger (Qlv) and older (Tlv) emplacement events at Los Lunas volcano, the Ceja Formation (Tc, including undivided Atrisco and Rio Puerco Members), unit of San Clemente (Qsc), and younger basaltic lava flows of the Cat Hills volcanic field (Qch). Hachured lines denote a buried Llano de Albuquerque surface. The interpreted extent of now eroded deposits of Qsc and Tc are shown in cross section by faint shading and parenthetical unit symbols. The San Clemente section (SC-1, Fig. 8) contains a 1.5–3 m lens of pumice-bearing pebbly sand, containing rounded pebbles of upper Bandelier Tuff, that is ~23 m stratigraphically above the Llano de Albuquerque surface. Refer to Figure 10 for explanation of other symbols and Tables 1–3 for age determinations.

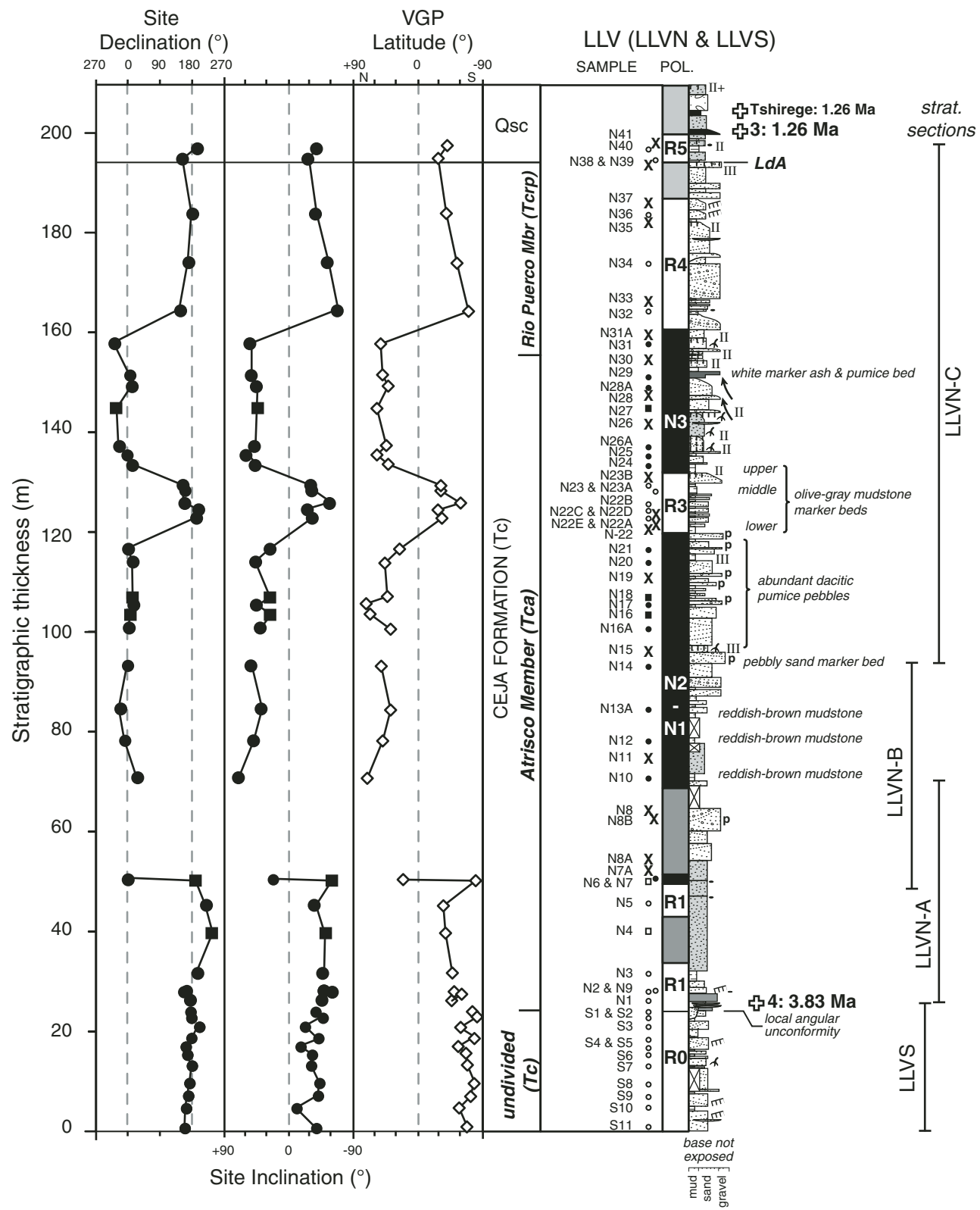


Figure 17. Lithostratigraphy and magnetic polarity stratigraphy of the Los Lunas volcano (LLV) composite section (see Fig. 16 for locations of individual sections), magnetostriatigraphic composite section (VGP—virtual geomagnetic pole), and correlation to a provisional magnetic polarity zonation. Lines connect stratigraphically consecutive sites. Individual sections were correlated using distinctive marker beds: LLVS and LLVN-A were correlated by a dark-gray andesitic fallout tephra that overlies an angular unconformity; LLVN-A and LLVN-B were correlated by comparing a similar succession of sandstone beds; LLVN-B and LLVN-C were correlated using a prominent pebbly sandstone marker bed. Refer to Figure 13 for explanation of symbols. Age determination sites in Tables 1–3. Roman numerals denote pedogenic carbonate morphologic stages (Birkeland, 1999). LdA—Llano de Albuquerque surface.

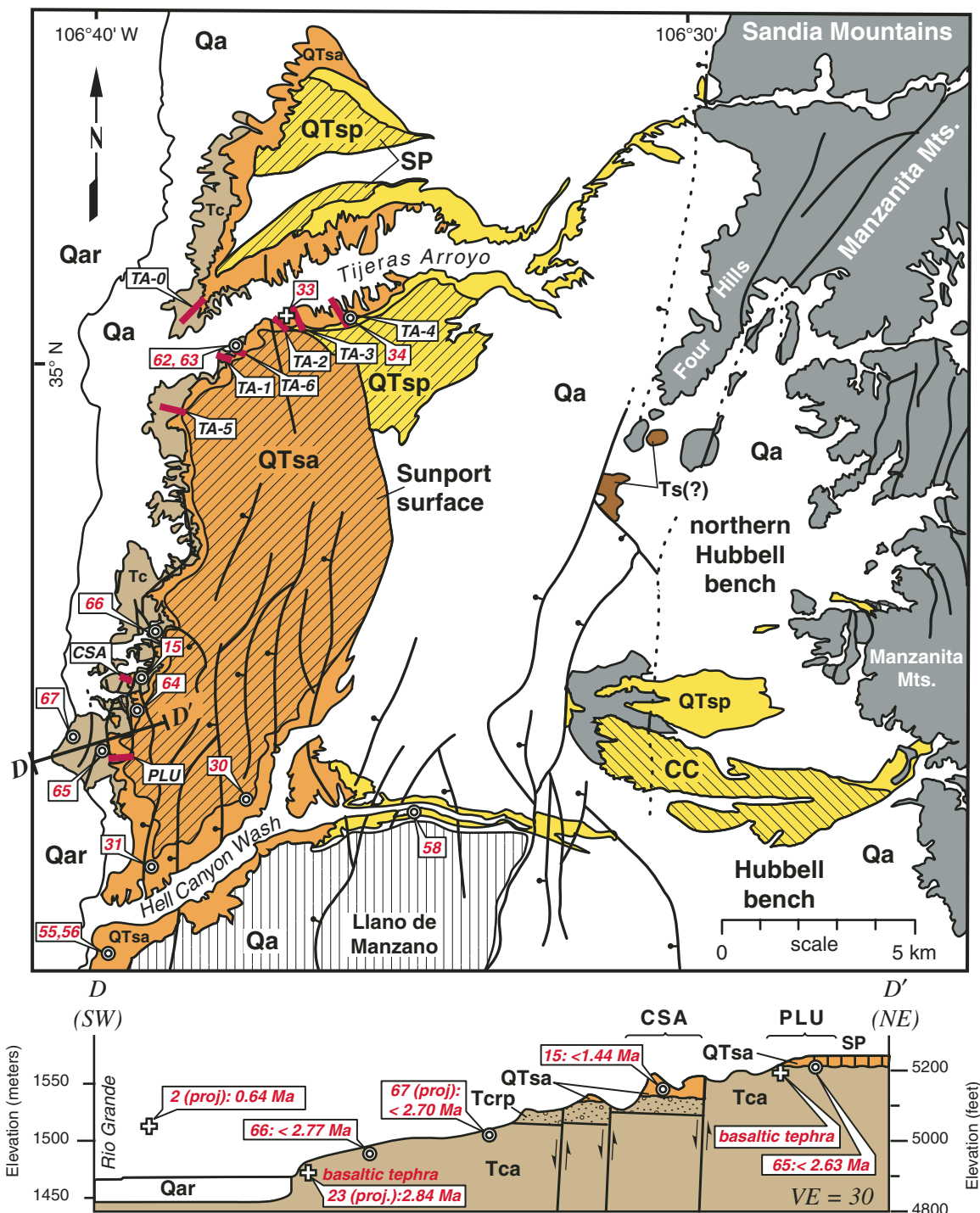


Figure 18. Geology of Tijeras Arroyo and Hell Canyon Wash. Top: Generalized geologic map, illustrating the locations of measured stratigraphic sections in Tijeras Arroyo (TA-0 through TA-6), and Isleta Powerline (PLU) and Casino (CSA). Unit Qar denotes alluvium of the Rio Grande valley and floodplain. Depositional tops of the Sierra Ladrones Formation (and younger alluvium) locally delineated by hachured lines and include the Cañada Colorada (CC), Sunport (SP), and Llano de Manzano geomorphic surfaces. Bottom: Geologic cross section D–D' (vertical exaggeration [VE] = 30×) across eastern margin of Rio Grande valley (modified from Connell et al., 2001c), illustrating projections of the CSA and PLU stratigraphic sections and dated pumice pebbles. Unit Qar refers to uppermost Pleistocene–Holocene alluvium of the Rio Grande valley. Explanation of other units on Figure 10, and age determination sites in Tables 1–3. Sample 15 refers to an obsidian pebble that was geochemically correlated by Nelia Dunbar (2001, personal commun.) to a dated sample (Table 3) taken from a vent at Rabbit Mountain in the Jemez Mountains.

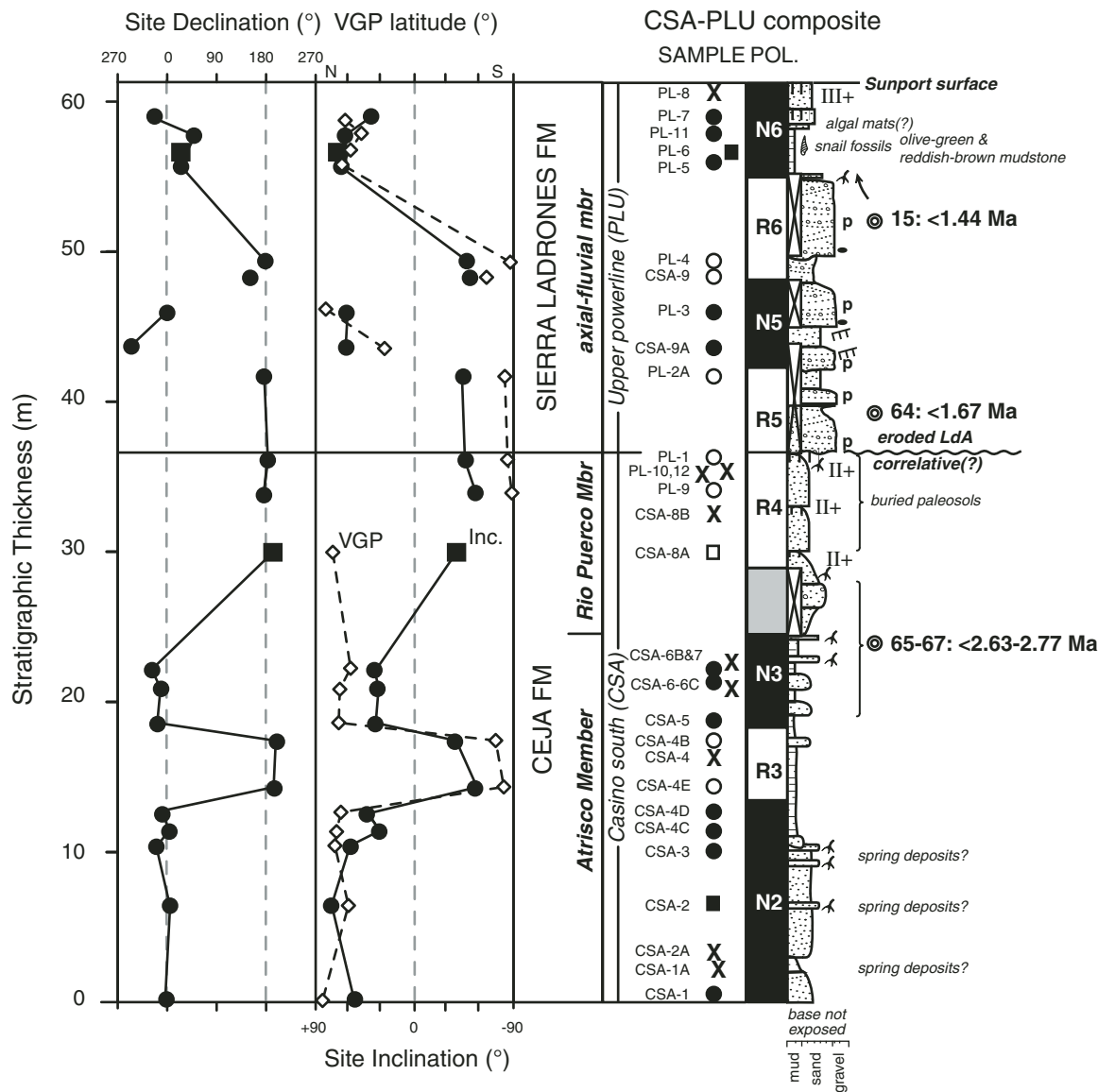


Figure 19. Lithostratigraphy and magnetic-polarity stratigraphy of CSA and PLU composite sections (see Fig. 18 for locations), magnetostratigraphic composite section (VGP—virtual geomagnetic pole; Inc.—site inclination), and correlation to a provisional magnetic polarity zonation. Lines connect stratigraphically consecutive sites. Refer to Figure 13 for explanation of symbols. Age determination sites in Tables 1–3. Roman numerals denote pedogenic carbonate morphologic stages (Birkeland, 1999). LdA—Llano de Albuquerque surface.

with older strata where exposed along the basin flanks (Machette, 1978; Lozinsky and Tedford, 1991; Cather et al., 1994). Much of the Sierra Ladrones Formation is poorly exposed in the study area, but it is as much as 580 m thick in wells beneath Albuquerque (Hawley et al., 1995; Connell et al., 1998).

The Sierra Ladrones Formation is informally divided into two interfingered members (Fig. 5; Machette, 1978): an axial-fluvial member (the ancestral Rio Grande), and a piedmont-slope member associated with tributary drainages from the rift-flanking uplifts. The axial-fluvial member contains trough cross-stratified sand and gravel with sparse muddy interbeds representing ances-

tral Rio Grande deposition (Fig. 12E). Sand and gravel typically form in a 5- to 14-km-wide depositional belt that, in the study area, lies almost entirely east of the present Rio Grande valley. The eastern edge of this depositional belt is 1–5 km west of the Hubbell bench and the basin-bordering Sandia Mountains (Connell, 2008b; Maldonado et al., 2007).

The top of the Sierra Ladrones Formation is marked by pedogenically modified depositional tops of the Cañada Colorada, Las Huertas, Llano de Manzano, and Sunport geomorphic surfaces (described below). The piedmont member forms a narrow belt of conglomerate and sandstone derived from the

basin-flanking uplifts of the Sandia, Manzanita, and Manzano Mountains (Figs. 11 and 18). The uppermost part of the piedmont-member forms a coarse-grained wedge of sediment that prograded (west) into the basin by 5–20 km, where it buried axial-fluvial deposits of the ancestral Rio Grande (Figs. 11, 12F, 18, and 20; Connell et al., 2001c, 2001d). Gravels of the axial-fluvial member coarsen stratigraphically above the lavas of the San Felipe volcanic field (Brandes, 2002). Water-supply wells in Albuquerque show a coarsening of the axial-fluvial member in the upper 317 m of the section (Ch5, Figs. 3 and 4; Hawley, 1996; Connell, 2006, 2008b). This coarsening also reflects the progradation of basin-margin alluvial fans and alluvial slopes over the axial-river deposits.

Geochronology

The Sierra Ladrones Formation is generally considered to range from Pliocene to early Pleistocene in age (4.7–0.8 Ma; Figs. 6 and 9); however, Late Miocene age determinations have been reported for axial-fluvial deposits in the northern part of the basin (Smith et al., 2001). Volcanic-bearing fluvial deposits of possible extrabasinal origin have been reported beneath the Atrisco Member of the Ceja Formation in water-supply wells beneath Albuquerque (Hawley and Haase, 1992, section IV). Pliocene lava flows of the San Felipe volcanic field are interbedded with axial-fluvial deposits (2.57 ± 0.11 Ma; Fig. 7, sample 19, Table 2). To the south, Pliocene-aged trachyandesitic lava lies above the projected base of the Sierra Ladrones Formation at San Acacia (Machette, 1978), ~60 km south of the study area. Chamberlin et al. (2001) reported a $^{40}\text{Ar}/^{39}\text{Ar}$ age determination of 4.76 ± 0.04 Ma for this volcanic feature (Fig. 7, sample SA, Table 1).

The top of the Sierra Ladrones Formation is well exposed at the mouth of Tijeras Arroyo (Figs. 18 and 20), where axial-fluvial deposits contain an early Pleistocene flora and vertebrate fauna that is older than ca. 0.8 Ma (Lucas et al., 1993; Morgan and Lucas, 2003; Bell et al., 2004). The axial-fluvial member contains abundant fluvially recycled, rhyolitic pumice and rounded obsidian pebbles and cobbles, some of which were dated or geochemically correlated to known eruptive sources (Fig. 7; Love et al., 2001a; Maldonado et al., 1999, 2007). These pumice-bearing beds were likely laid down by floods originating in the Jemez Mountains, where voluminous rhyolitic volcanism and river damming has occurred (e.g., Smith et al., 1970; Reneau and Dethier, 1996). Pumice-bearing Plio-Pleistocene flood deposits have also been reported in ancestral Rio Grande deposits nearly 300 km downstream of Tijeras Arroyo (Mack et al., 1996).

A bed of white volcanic ash (1.28 ± 0.2 Ma; Fig. 7, sample 33, Table 3) has been geochemically correlated with the Tshirege Member of the Bandelier Tuff (Nelia Dunbar, 2001, personal commun.). Beneath this ash lies a bed of nearly pure, medium-grained, gray and white, pumiceous sand that yielded a single-crystal $^{40}\text{Ar}/^{39}\text{Ar}$ age determination on sanidine of 2.00 ± 0.04 Ma (Fig. 7, sample 63, Table 3). This lower pumiceous interval lies within a normal-polarity magnetozone that is nearly 14 m stratigraphically below the Tshirege ash (Fig. 20) and is assigned to

part of the 1.945–1.778 Ma Olduvai subchron (Fig. 9). The presence of the Olduvai subchron demonstrates that deposition in the upper part of the Ceja Formation was contemporaneous with the axial-fluvial member of the Sierra Ladrones Formation, even though they are separated by a disconformity exposed along the flanks of the Rio Grande valley (Fig. 8).

The age of the top of the Sierra Ladrones Formation comes from the CSA-PLU composite section (Fig. 19), between Tijeras Arroyo and Hell Canyon Wash (Fig. 18). The upper part of this section contains $1.44\text{--}1.67$ Ma rhyolitic and pumiceous gravel (Fig. 7, e.g., samples 15 and 64, Tables 2 and 3). Deposits of the axial-fluvial member are exposed in Hell Canyon Wash (Fig. 18), where rhyolitic, pumice-bearing fluvial cobbles yielded an $^{40}\text{Ar}/^{39}\text{Ar}$ age determination on sanidine of 1.72 ± 0.04 Ma (Fig. 7, sample 58, Table 3).

An olive-green and reddish-brown sequence of mudstone, locally preserved against an intrabasinal fault, caps the Sierra Ladrones axial-fluvial succession at section PLU (Fig. 19). These mudstone beds contain a normal-polarity magnetozone that correlate to the early part of the Brunhes chron (0.781 Ma to present; Gradstein et al., 2005). A terrace deposit containing the 0.64 Ma Lava Creek B ash is inset (~60 m) below the top of the Sierra Ladrones Formation (Fig. 18; Connell et al., 2007a). Thus, deposition of the Sierra Ladrones Formation ended with the entrenchment of the Rio Grande valley, which occurred shortly after 0.78 Ma and was well under way by 0.64 Ma.

Few direct age determinations are available for the piedmont member of the Sierra Ladrones Formation. Just south of Tonque Arroyo (Fig. 11), a volcanic ash bed sits 3 m above the piedmont/axial-fluvial contact (Cather and Connell, 1998; Brandes, 2002). This ash yielded single-crystal $^{40}\text{Ar}/^{39}\text{Ar}$ age determinations on sanidine of 1.57 ± 0.09 Ma and 1.60 ± 0.06 Ma (Fig. 7, samples 51 and 52, Table 3). Piedmont-member deposits prograded by as much as 10 km toward the Rio Grande after 1.7–1.6 Ma and buried most of the axial-fluvial member deposits (Figs. 11 and 18).

Plio-Pleistocene Deposits

Gravelly deposits exposed along the faulted and structurally elevated flanks of the Albuquerque Basin are inset against Miocene basin fill and older parts of the Ceja and Sierra Ladrones Formations (e.g., Connell and Wells, 1999; Smith et al., 2001). The Tuerto Formation (Tuerto gravels of Stearns, 1953) is a thin and areally extensive, subhorizontally bedded succession of gravel and sand on the northern flank of the Sandia Mountains and in the Hagan embayment that overlies an angular unconformity marked by the lower Ortiz paleosurface (see below). The Tuerto Formation is dominated by amalgamated conglomeratic sandstone (Koning et al., 2001) that locally encloses basaltic lava flows of the Pliocene Cerros del Rio volcanic field near the boundary between the Albuquerque and Espanola Basins. Bachman and Mehnert (1978) reported a K-Ar age determination of 2.8 ± 0.1 Ma for a lava flow at the base of the Tuerto Formation.

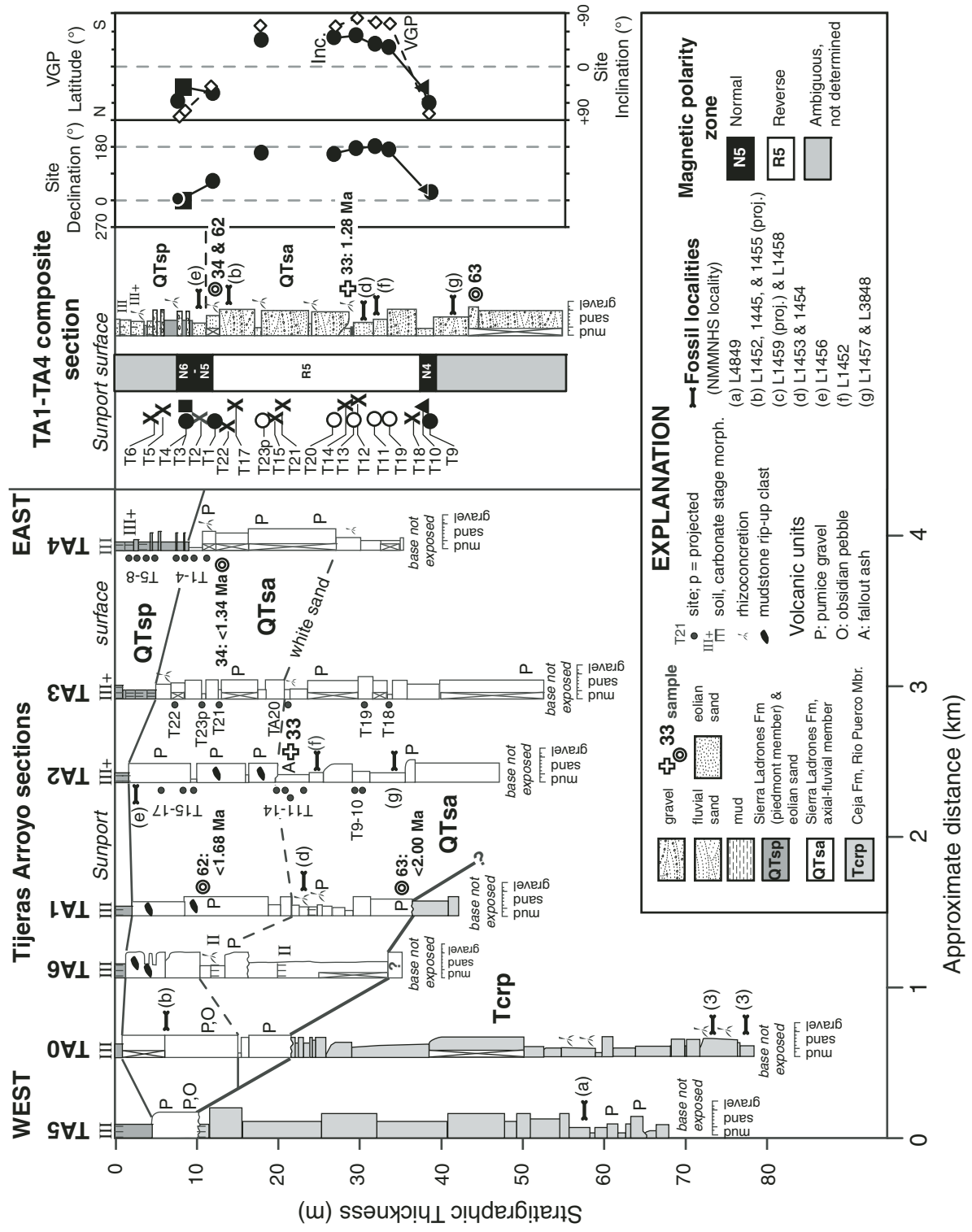


Figure 20. Stratigraphic fence diagram, illustrating physical correlations of stratigraphic sections in Tijeras Arroyo (see Fig. 18 for locations). Section TA was re-measured from previous studies (i.e., Lambert, 1968; Lucas et al., 1993). Vertebrate fossil localities of the New Mexico Museum of Natural History and Science (NMMNH; Lucas et al., 1993; Morgan and Lucas, 2003) are also shown. Site T23p is a volcanic ash projected ~3 km south into Tijeras Arroyo. Right side of figure portrays the generalized lithostratigraphy and magnetic polarity stratigraphy of TA composite section and correlation to a provisional magnetic polarity zonation (VGP—virtual geomagnetic pole; inc.—site inclination); lines connect stratigraphically consecutive sites. Age determination sites in Tables 1–3, Roman numerals denote pedogenic carbonate morphologic stages (Birkeland, 1999).

The unit of San Clemente was described by Love et al. (1998) for deposits of sand, mud, and gravel that overlie the Ceja Formation in structural depressions on the Llano de Albuquerque (Fig. 16). The unit of San Clemente is ~36 m thick and disconformably overlies the Llano de Albuquerque surface (Fig. 17; Connell et al., 2001c). The top of this section is marked by well-developed calcic paleosols that are locally capped by lava flows of the middle Pleistocene Cat Hills volcanic field (99–111 ka; Kelley and Kudo, 1978; Maldonado et al., 2006, 2007). Sparse gravel in this unit typically resembles that of the underlying Ceja Formation, except for a nearly 3-m-thick lens of cross-stratified, pumice-bearing pebbly sand ~22 m above the westward projection of the Llano de Albuquerque surface (Fig. 8 and Fig. 16 bottom). Rhyolitic pumice pebbles in this interval yielded a maxi-

mum age of 1.24 ± 0.02 Ma (Fig. 7, sample 32, Table 3) and are geochemically similar to the Tshirege Member of the Bandelier Tuff (N. Dunbar, 2001, personal commun.). The most likely source of this pumice-bearing bed was the ancestral Rio Grande.

Sediment-Accumulation Rates

Rates of sediment accumulation were estimated for parts of the Ceja and Sierra Ladrones succession using the measured stratigraphic sections, data from a deep water-supply well in Albuquerque (Ch5, Fig. 3), and available age control (Fig. 21). Plio-Pleistocene deposits are poorly consolidated and have undergone little diagenetic alteration beyond minor interstitial calcium-carbonate cementation and pedogenic alteration. Precise

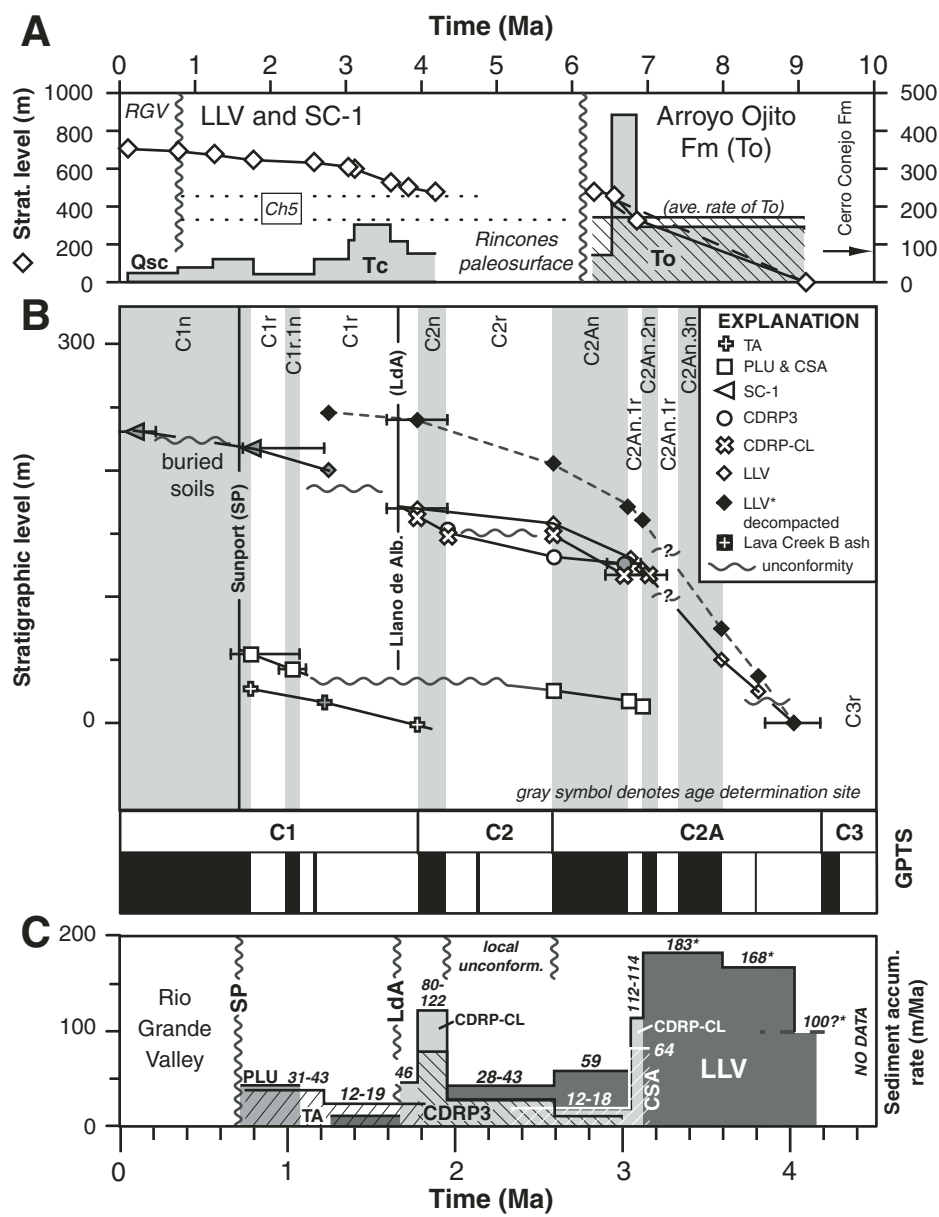


Figure 21. Sediment accumulation rates and major depositional events since Late Miocene time. (A) Plot of stratigraphic level and age (diamonds), and undecompressed sediment accumulation rates for the unit of San Clemente (Qsc), Arroyo Ojito (To), Ceja (Tc), and Sierra Ladrones (QTs) Formations. Black arrow denotes the mean accumulation rate estimated for the Cerro Conejo Formation (Tedford and Barghoorn, 1999). Two dotted lines denote decompactsed sediment accumulation rates for Charles Wells #5 well (Ch5) using different ages for the inferred base of the Ceja Formation. ave.—average. (B) Plot of deposit age against stratigraphic level (thickness) and the global polarity timescale (GPTS) for the Ceja and Sierra Ladrones Formations using stratigraphic sections CDRP3, CDRP-CL, CSA-PLU, LLV, SC-1, and TA. Alb.—Albuquerque. (C) Plot of sediment accumulation rates since 4.1 Ma; decompactsed rates are noted by an asterisk.

determinations of accumulation rates are difficult because of incomplete geochronologic control, exposure, and preservation. Truncation of magnetozones by disconformities would result in higher estimated rates. Accumulation rates for measured sections thinner than 60 m were adjusted for compaction using the approximation method of Van Hinte (1978) and porosity-depth relationships from Albuquerque area wells (Haneberg, 1995). The thicker section in the well was decompacted by applying an integral method described in Angevine et al. (1990) to the porosity-depth curves of Haneberg (1995).

On the basis of sparse age control, Lozinsky (1994) reported undecompressed sediment accumulation rates of 200–600 m/m.y. for Miocene strata, although his highest estimated rates are probably much lower than ours (Fig. 21A; Connell, 2004). The type section of the Arroyo Ojito Formation is 478 m thick (Connell et al., 1999) and accumulated between 9.0 and 6.3 Ma, yielding a long-term (undecompressed) accumulation rate of ~177 m/m.y. (478 m/2.7 m.y.). At the Arroyo Ojito type area, a 6.85 Ma ash is 328 m above the base, and ~150 m below the top (Connell et al., 1999; Connell, 2008a). This ash and the 9 Ma estimated age of the base of the Arroyo Ojito Formation yield an undecompressed rate of ~153 m/m.y. (328 m/2.15 m.y.). The stratigraphic interval between the Peralta ashes and the assumed 6.3 Ma upper estimate for the Arroyo Ojito Formation yields a higher undecompressed rate of ~252 m/m.y. (151 m/0.6 m.y.). A slower rate of accumulation for the Picuda Peak Member (20 m/0.31 m.y. = 65 m/m.y.) was estimated using the ages of the 6.6 Ma basaltic cobble in the Picuda Peak Member and the 6.3 Ma Cerro Yelo ash, which is interbedded within the Cochiti Formation.

Plio-Pleistocene accumulation rates were estimated using age determinations and magnetic-polarity stratigraphy (Figs. 21B–21C). Compaction errors in the Los Lunas volcano sections were negligible in the upper 60 m (post-3.0 Ma) of the LLV section. The lower part of this section was adjusted for compaction, yielding rates that were a factor of 1.2–1.4 higher than the undecompressed rates. An undecompressed rate between the older and younger Los Lunas eruptive products was ~32 m/m.y., which is similar to sedimentation rates determined by Lozinsky (1994) and to rates reported for comparably aged rift-basin fill in southern New Mexico (Mack et al., 1993).

The absence of a normal-polarity magnetozone in the Gilbert-aged part of the LLVS (Fig. 17) suggests that deposition occurred after the Cochiti subchron (C3n.1n, Fig. 9) at 4.187 Ma. This age constraint resulted in a decompact rate 100 m/m.y. (undecompressed rate of 66 m/m.y.). Decompressed accumulation rates ranged from 168 to 183 m/m.y. between 3.8 and 3.0 Ma (undecompressed rate of 114–155 m/m.y. for the same time interval). Accumulation rates in the Ceja Formation decreased by ~66% between 3.8 and 3.0 Ma, and by ~80% (59–12 m/m.y.) between 3.0 and 1.8 Ma (Fig. 21). Miscorrelation of the Kaena (or Mammoth) subchron would only result in decreasing accumulation rates after 3.3 Ma, rather than after 3.0 Ma.

Accumulation rates for the CDRP3, CDRP-CL, CSA-PLU, TA, and SC-1 sections demonstrate an overall decrease in

the rate of sediment accumulation by a factor of three or four since 3.0 Ma (12–59 m/m.y.) and are similar to the rates estimated for the Ceja Formation in the Los Lunas volcano sections (Figs. 21B–21C). This decrease in sedimentation rate occurred nearly 0.45 m.y. before the Ceja section became much coarser grained (in the Rio Puerco Member). Decreases in sedimentation rates after 3 Ma were punctuated by short intervals of relatively rapid accumulation in gravelly beds in CDRP3 and CDRP-CL. These faster rates may be the result of rapid deposition by river channels or they may merely be an artifact of shorter sampling and time intervals (Sadler, 1981). Accumulation rates estimated for the Sierra Ladrones Formation at the CSA-PLU and TA sections range from 12 to 43 m/m.y. (Fig. 21C) and are in general agreement with estimates by Lozinsky (1994).

The Charles Wells #5 well (Ch5) penetrated the base of the Atrisco Member (at 872 m below land surface; Connell et al., 1998) near its deepest known level in the basin. Although the top of the Sierra Ladrones Formation is not preserved in this well, the top of this well is <27 m below the projection of the Sunport surface (Connell, 2008b). Thus, Ch5 contains the thickest known accumulation of Sierra Ladrones deposits in the Albuquerque Basin. A decompactsed sediment thickness for this entire succession is 917 m, and yields an average sediment accumulation rate of 167 or 229 m/m.y. (Fig. 21A), depending on the ages selected for the base (i.e., 6.3–0.8 Ma or 4.8–0.8 Ma); undecompressed rates are 158 or 218 m/m.y. Higher accumulation rates would result if the Sierra Ladrones succession was younger than 4.8 Ma near the well. These long-term rates are greater than those determined for the measured sections, which are 12–30 km away from the master fault. The lower rates estimated toward the western basin margin may be a result of reduced accommodation up the hanging-wall ramp in this part of the basin.

PALEOSURFACES

The Plio-Pleistocene alluvial succession in the Albuquerque Basin is defined by a set of bounding surfaces (Fig. 22). The lower boundary is defined by the Rincones and lower Ortiz paleosurfaces. The upper boundaries are locally defined by a set of depositional (constructional) geomorphic surfaces developed on the Ceja, Sierra Ladrones, and Tuerto Formations. The Rincones paleosurface was named by for a disconformity between Miocene and Pliocene deposits in the western part of the Albuquerque Basin (Connell, 2008a). This discontinuity is exposed beneath the Ceja Formation, along the western and northern flanks of the Llano de Albuquerque and La Ceja, where as much of 450 m of the subjacent Miocene strata is missing. It is commonly disconformable (but forms angular unconformities near major intrabasinal faults), and locally contains strongly developed petrocyclic paleosols that exhibit stage III+ and V pedogenic carbonate morphology, depending on structural position. Elsewhere this boundary is marked by a pinkish, mottled, and bioturbated sand with scattered pebbles (e.g., Fig. 13).

The Ortiz paleosurface is an angular unconformity between Miocene and Pliocene strata in the Albuquerque and Española Basins (Bryan, 1938; Bryan and McCann, 1938). Bryan and co-workers (Bryan and McCann, 1938; Wright, 1946; Stearns, 1979) considered the Ortiz paleosurface to represent a regional surface of erosion that divided moderately deformed Miocene strata from less-deformed Plio-Pleistocene strata. The subjacent Miocene strata were tilted by as much as 32° and were subjected to several hundred meters of erosion before being buried by subhorizontally bedded Plio-Pleistocene fluvial deposits of the Tuerto and Ancha Formations (Stearns, 1953; Koning et al., 2002; Connell et al., 2002). The Ortiz paleosurface was extended across the Albuquerque Basin and onto the eastern flank of the Colorado Plateau and was correlated to the Llano de Albuquerque surface (Bryan and McCann, 1938; Wright, 1946; Kelley, 1977; Stearns, 1979).

Bachman and Mehnert (1978) recognized the compound (and allostratigraphic) character of the Ortiz paleosurface, but

restricted it to the upper aggradational surface on the Tuerto Formation in the Hagan embayment (Koning et al., 2001), and on the Ancha Formation in the adjacent Española Basin (Koning et al., 2002). This division was challenged by Stearns (1979) who considered the lower surface to be more useful as a boundary between tilted Miocene rocks and the overlying subhorizontally bedded Plio-Pleistocene sediment. We also consider the erosional aspect of the lower paleosurface to have regional importance and correlate it to the Rincones paleosurface; however, we assign the relict depositional top of the Ceja Formation to the younger Llano de Albuquerque surface (see below).

The Rincones and lower Ortiz paleosurfaces are recognized along the flanks of the Albuquerque Basin, and represent essentially the same lacuna (Fig. 22). The character of these paleosurfaces in depocentral areas is not clear. Drill-hole data indicate that the stratigraphic correlatives to the Rincones paleosurface in depocentral areas form a rather sharp boundary (Connell et al., 1998; Stone et al., 1998). This boundary in the drill holes supports an

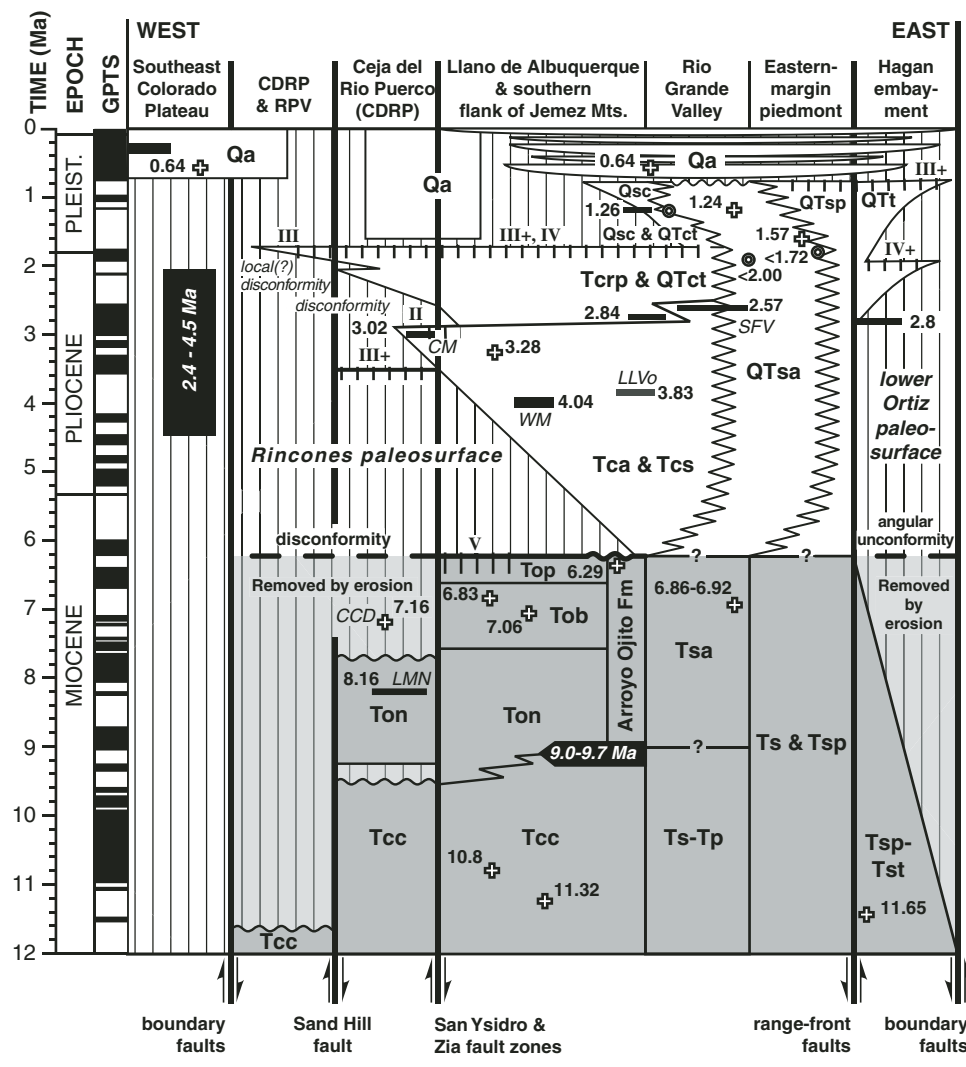


Figure 22. Chronostratigraphic diagram depicting major stratigraphic units, bounding surfaces, and fault zones across the southeastern margin of the Colorado Plateau, Albuquerque Basin, and Hagan embayment, including the Ceja del Rio Puerco (CDRP), Rio Puerco valley (RPV), and Rio Grande valley. The global polarity timescale (GPTS) is shown for reference. Thick vertical lines schematically denote major fault zones, and vertical hachures denote stratigraphic lacunae. Short-hachured lines denote petrocalcic paleosols developed on bounding surfaces; Roman numerals denote maximum pedogenic carbonate morphologic stage. Unit symbols defined on Figure 5. Italicized abbreviations refer to volcanic units: Cat Mesa flow (CM), Cerro Colorado dacite (CCD), La Mesita Negra flow (LMN), older Los Lunas volcano (LLVo), a lava from San Felipe volcanic field (SFV), and Wind Mesa volcano (WM). Younger deposits (Qa) include a suite of terraces of the Rio Grande (chronology from Connell et al., 2007a), and alluvial, colluvial, and eolian deposits. Miocene units are shaded gray; light gray shading denotes eroded deposits. Black rectangles denote lava flows. The plus and circle-in-circle symbols denote primary and recycled volcanic materials, respectively. Numbers refer to age determinations (in Ma) from Tables 1–3 and other studies (Bachman and Mehnert, 1978; Izett and Wilcox, 1982; Drake et al., 1991; Hallett et al., 1997; Connell et al., 1999, 2002; Connell, 2008a, 2008b; Maldonado et al., 2006, 2007).

abrupt change in environmental conditions or a disconformity; however, major stratigraphic discontinuities were not recognized in the exposed piedmont succession along the eastern margin of the basin (Fig. 16; Kelley, 1982; Cather and Connell, 1998; Connell, 2008b), suggesting that deposition may have continued with little or no interruption within the deepest parts of the basin.

The Llano de Albuquerque surface represents the depositional top of the Ceja Formation (Machette, 1985). The Llano de Albuquerque landform is a 106-km-long, south-sloping tableland between the Rio Grande and Rio Puerco valleys that is 110–494 m above the Rio Grande. Petrocalcic paleosols developed on this relict depositional surface commonly possess stage III+ to IV pedogenic carbonate morphology and are thicker than those developed on the Sierra Ladrones Formation (Machette, 1985; Connell, 2008a; Connell and Wells, 1999). The sharp contact between the Sierra Ladrones and Ceja Formations exposed along the eastern flank of the Rio Grande valley likely represents an eroded remnant of this surface (Fig. 18).

The Cañada Colorada, Las Huertas, Sunport, and Llano de Manzano geomorphic surfaces define local tops of the Sierra Ladrones Formation and parts of the younger piedmont alluvium (Lambert, 1968; Machette, 1985; Maldonado et al., 1999; Connell and Wells, 1999; Connell, 2004). The Cañada Colorada surface developed on a faulted block on the northern Hubbell bench (Maldonado et al., 1999). The other surfaces are 95–120 m above the Rio Grande and serve as useful stratigraphic datum planes to correlate depositional tops of the Sierra Ladrones Formation. Petrocalcic paleosols on the Cañada Colorada surface (stage III+ to V; Connell et al., 2001c) are more strongly developed than those on the Las Huertas, Llano de Manzano, and Sunport surfaces (stage III+; Machette, 1985; Connell and Wells, 1999), suggesting that it may be much older than these other surfaces. Isolated, high-level, relict surfaces are preserved on remnants of locally derived alluvium on the northern flank of the Sandia Mountains (Connell and Wells, 1999; Connell, 2008b). These surfaces have erosionally modified petrocalcic soils (stage IV+ pedogenic carbonate morphology) and may represent older surfaces of the Tuerto Formation.

ALLUVIAL SEQUENCES

The Ceja and Sierra Ladrones Formations form a basin-wide, nonmarine depositional sequence that is defined by distinct sets of bounding surfaces (Fig. 22). The lower bounding surface, defined by the Rincones and lower Ortiz paleosurfaces, contains strongly developed paleosols that indicate that large parts of the basin were subjected to prolonged periods of landscape stability (10^5 – 10^6 years; Machette, 1985) before being buried by the Ceja Formation. Although these paleosurfaces are really extensive, the lack of an obvious unconformable boundary in the piedmont succession near the basin master fault (along the northern flank of the Sandia Mountains) suggests that sedimentation continued essentially uninterrupted in the deeper parts of the basin.

The upper boundaries of this alluvial sequence are defined by a suite of relict depositional surfaces (i.e., Cañada Colorada, Llano de Albuquerque, Las Huertas, Sunport, and Llano de Manzano) that contain strongly developed paleosols. Depositional onlap and intrabasinal faulting increased the duration of stratigraphic lacunae toward the basin margins (Fig. 22). Deep incision by younger alluvium associated with episodic cutting by the Rio Grande (and major tributaries) also defines the upper boundary of this sequence.

Miocene Sedimentation

Middle to Upper Miocene strata exposed in the northern part of the Albuquerque Basin are dominated by fluvial and eolian deposits of the Cerro Conejo Formation (Fig. 23A). The eastward (basinward) slope of the Rincones paleosurface, generally consistent eastward to southeastward stratal tilt directions, eastward thickening of the basin fill, southeast-directed paleoflow directions, and western-margin (i.e., Colorado Plateau–Sierra Nacimiento) gravel provenance (Brandes, 2002; Connell, 2004; Connell, 2008a, 2008b) all indicate that the study area has been dominated by generally eastward basin subsidence, and has not been subjected to any major changes in the direction of basin tilting since Early Miocene time (cf. Ingersoll, 2001).

Movement along the basin-master fault system increased after ca. 9 Ma, resulting in continued eastward tilting and thickening of the Arroyo Ojito Formation (Fig. 23B). The northern part of the Albuquerque Basin received extrabasinal sediments as early 7 Ma, but the southern part of the basin was dominated by internal surface drainage until early Pliocene time (Figs. 23B–23C). Deposition of the Arroyo Ojito Formation ceased shortly after ca. 6.3 Ma with the development of the Rincones paleosurface (Fig. 23B). During Late Miocene time, the underlying fluvialite succession was subjected to ~0.5 km of erosion across the western (up-dip) margin of the basin (Figs. 23B–23C).

Workers in the adjacent Socorro and Española Basins reported an overall reduction in the rate of deformation after ca. 10 Ma (Cather et al., 1994; Koning et al., this volume). Geochronologically calibrated deformational indicators (e.g., stratal-tilt data) are not well established in the Albuquerque Basin, but they also suggest a slight decrease in stratal tilt across the Rincones paleosurface (Connell, 2008b). The slight change in tilts of the underlying Miocene strata suggest that the Rincones and lower Ortiz paleosurfaces were cut following major deformation and support a reduction in tectonism after ca. 6 Ma.

Plio-Pleistocene Sedimentation and Axial-Drainage Development

The relatively long Miocene phase of internal surface drainage gave way to through-going drainage of the ancestral Rio Grande into southern New Mexico by early Pliocene time (Figs. 23B–23C; Leeder et al., 1996; Mack et al., 2002, 2006). Interbasinal integration of surface drainage may have occurred

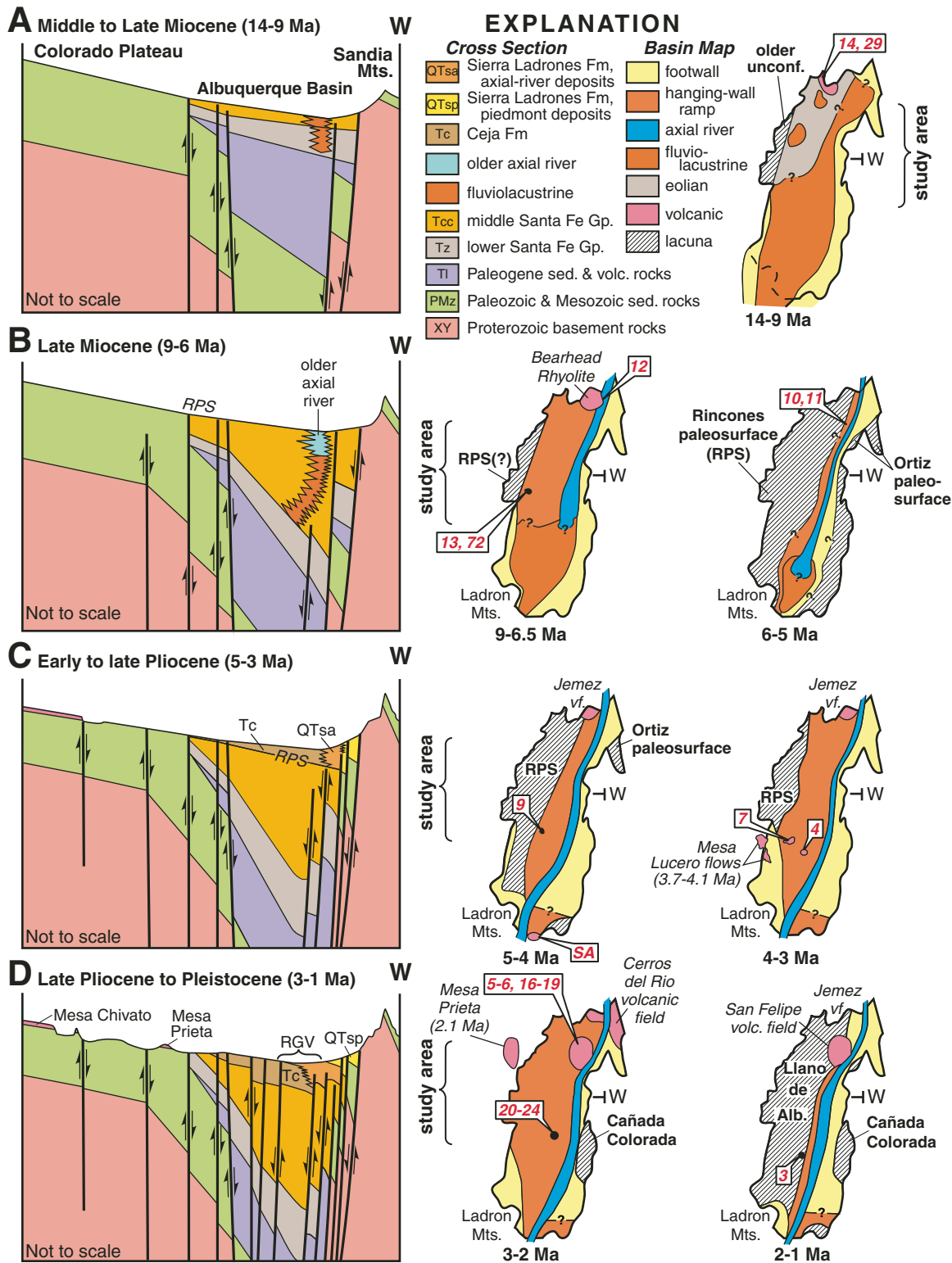


Figure 23. Schematic cross sections (left) and paleogeographic diagrams (right) illustrating the history of subsidence and sedimentation in the Albuquerque Basin since Middle Miocene time (14–1 Ma): (A) Middle to Late Miocene, (B) Late Miocene, (C) early to late Pliocene, and (D) late Pliocene to early Pleistocene. RPS—Rincons paleosurface; vf.—volcanic field; Alb.—Albuquerque. Red numbers denote age determinations (Tables 1–3). Other K-Ar and $^{40}\text{Ar}/^{39}\text{Ar}$ age determinations for lava flows on Mesa Lucero and Mesa Prieta are from Baldridge et al. (1980, 1987) and Hallett et al. (1997), respectively.

through the burial of low-lying structural zones (Jackson and Leeder, 1994) between the Albuquerque and Socorro Basins. The integration of ancestral Rio Grande drainage into southern New Mexico could have been a consequence of progressive onlap of Pliocene sediments over low-lying structural culminations between these basins (Cather et al., 1994).

The Rincones and lower Ortiz paleosurfaces became progressively buried by the Ceja, Sierra Ladrones, and Tuerto Formations after ca. 3.0 Ma (Figs. 22 and 23C). The Ceja succession began to coarsen slightly in the Los Lunas section (LLV) after 3.6 Ma, but did not become dominated by coarse-grained detritus until after ca. 2.6 Ma. Coarsening of the Ceja Formation culminated with the deposition of areally extensive sheets of pebble- to boulder-bearing sand that extended across much of the basin and east of the present Rio Grande valley after ca. 1.8 Ma.

The overall lack of mud and clay in the upper part of the Ceja Formation indicates that most of the finer-grained sediment was transported out of the basin during this time. This coarsening of the Ceja Formation occurred after integration of the ancestral Rio Grande into southern New Mexico and western Texas (Connell et al., 2005) and was not directly related to base-level lowering of the axial river by drainage capture. Coarsening of the Ceja Formation ended with the development of the Llano de Albuquerque surface during (or shortly after) the 1.9–1.8 Ma Olduvai subchron (Figs. 22 and 23D).

After 1.8 Ma, sedimentation was largely restricted to the eastern part of the basin, where the course of the ancestral Rio Grande (Sierra Ladrones Formation) was within 5 km of the basin-boundary fault system. Also after 1.8 Ma, the Sierra Ladrones Formation lapped westward onto the abandoned top of the Ceja Formation and graded toward the Llano de Albuquerque surface. The presence of the Olduvai subchron in the Ceja and Sierra Ladrones Formations demonstrates contemporaneous sedimentation for these units and precludes incision of an earlier paleovalley of the ancestral Rio Grande (cf. Cole et al., 2001, 2007). Like the Ceja Formation, gravel in the axial-fluvial member of the Sierra Ladrones Formation increased in size and abundance after 2.6 Ma, but the piedmont member deposits prograded away from the master fault after ca. 1.8–1.6 Ma (Figs. 21C and 23C). Deposition of the Sierra Ladrones Formation continued for another 1 m.y. until entrenchment of the Rio Grande valley began shortly after 0.8 Ma.

Depositional Patterns

The stratigraphy of the Albuquerque Basin generally follows a progression of drainage development and sedimentation patterns that is similar to other continental rifts (e.g., Lambiase and Bosworth, 1995; Contreras et al., 1997; Olsen, 1997). The basins initially become dominated by internal surface drainage as subsidence exceeds sedimentation. This results in an under-filled condition that persists until sediment discharge exceeds the volume of basin formed by subsidence. The basin then becomes overfilled, leading to the topographic and hydrologic connec-

tion with adjoining, lower-lying basins. At higher rates of strain, topographic closure of the basin would be maintained, even with increasing contributions of sediment (e.g., Contreras et al., 1997). It is possible that the stratigraphic progression in the Albuquerque Basin may reflect an evolutionary phase in the development of rift-basin alluvial sequences, where climatically induced increases in sediment delivery, rather than tectonism, dominate the Plio-Pleistocene stratigraphic architecture (see below).

The asynchronous progradation of fluvial deposits derived from opposing basin flanks, and the development of diachronous relict (depositional) tops on the Plio-Pleistocene alluvial succession, may be a geometric consequence of asymmetrical basin subsidence where basinward tilting of the hanging-wall ramp promotes extensive sediment bypass near the basin flanks (Figs. 22 and 23; Connell et al., 2001a; Smith et al., 2001). The distal hanging-wall ramp has a fore-tilted basin geometry that allows potential accommodation to increase down the structural dip toward the master fault. Back-tilted stratal geometry dominates near the structural footwall cutoff, where accommodation decreases away from the master fault. Because of this fore-tilted geometry, drainages would be more sensitive to changes in subsidence than near the (back-tilted) footwall block. Thus, decreases in basin subsidence could drive the progradation (offlap) of coarse-grained sediment off of the distal hanging-wall ramp, which would promote sediment bypass and the eventual cessation of deposition as accommodation decreased marginward. Intrabasinal (normal) faulting of the hanging-wall ramp would accentuate erosion and sediment bypass on the upthrown block.

The asynchronous depositional pattern in the study area seems to support numerical models of basin filling that suggest progradation of these opposing marginal wedges could be driven by changes in subsidence rate (e.g., Paola et al., 1992; Travis and Nunn, 1994). This progradational couplet is not likely attributable to changing subsidence rates because it would require an unreasonably short pulse in tectonism (after 2.6 Ma), followed by a rapid decrease after 1.8 Ma. Long-term (average) sediment accumulation rates for the Ch5 well are slightly higher than those determined for the Gauss-aged part of the Atrisco Member that is exposed near the basin flanks (Fig. 21A). The higher average accumulation rate for the Ch5 well suggests that basin subsidence did not significantly diminish in depocentral areas. Thus, the overall decrease in sediment accumulation in the measured sections may be the result of decreased accommodation toward the basin margins.

Synchronous progradation of basin-flanking deposits would be expected if sediment flux increased in similarly sized tributary catchments; however, hanging-wall catchments are typically much larger than those on the footwall (e.g., Leeder and Jackson, 1993). Larger hanging-wall catchments should respond to climatic changes with greater magnitude than the smaller footwall catchments. For example, the present Rio Puerco drainage basin (a major tributary to the Rio Grande) covers nearly 19,000 km² of the southeastern Colorado Plateau and northwestern Albuquerque Basin (Love and Connell, 2005) and is more

than 12 times larger than the combined drainage area of the eastern mountain fronts south of the Hagan embayment (1573 km^2 in Anderholm, 2001).

The coarsening of the uppermost Ceja succession and formation of the Llano de Albuquerque geomorphic surface, before the onset of regional fluvial entrenchment, suggests that incision of the paleo-Rio Puerco drainage system may have begun earlier along the structurally higher western flank of the basin. It is not clear whether the remnants of an early paleovalley existed, but such a paleovalley could have graded into a conformable stratigraphic succession toward the southern end of the basin where basin tilting shifted to the west (Russell and Snelson, 1994). If this were the case, the southward course of the present Rio Puerco drainage would be antecedent and controlled by sediment bypass during the final stages of deposition of the Rio Puerco Member. It is also possible that the depositional top of the Ceja Formation remained active as a thin, transport-dominated surface until the Rio Grande began to incise during early Pleistocene time. This is unlikely because the thickness and degree of pedogenic development on the Llano de Albuquerque surface supports a greater age of formation than for the younger geomorphic surfaces on the Sierra Ladrones Formation.

Climatic Implications

Rates of sediment accumulation, reported from numerous globally distributed settings, increased by a factor of two to ten over the last 4 m.y. (e.g., Zhang et al., 2001). This globally recognized increase in sediment flux is thought to represent a depositional response to increased climatic variability and magnitude (Molnar, 2004). The Late Miocene was a period of extreme aridity that was followed by periods of increased discharge and greater seasonal climate variability (e.g., Axelrod, 1981; Smith, 1994; Webb and Opdyke, 1995; Chapin, 2008).

Alluvial successions in the semiarid southwestern regions of North America may record the effects of Pliocene and Pleistocene climatic change on both tectonically active and quiescent basins. Studies of Plio-Pleistocene fluviacustrine and fluvial deposits (St. David Formation) in the tectonically quiescent San Pedro Valley of southeastern Arizona (Fig. 2) indicate an increase in sheet channels and sand-to-mud ratios and a reduction in sediment accumulation rates after the Gauss-Matuyama chron boundary at 2.58 Ma (Smith, 1994). These sedimentologic changes coincided with climate changes inferred from the stable-isotopic composition of pedogenic carbonate in paleosols (Smith et al., 1993). A similar correspondence between basin sedimentation and climate was also reported for Plio-Pleistocene fluvial deposits of the Palomas and Camp Rice Formations in the tectonically active Rio Grande rift in southern New Mexico (Mack et al., 1993, 1994).

The Plio-Pleistocene alluvial succession in the Albuquerque Basin is interpreted to reflect the effects of long-term aggradation within a basin that has been subjected to either constant or decreasing rates of tectonic subsidence since Miocene time. Dur-

ing Late Miocene through early Pliocene time, subsidence would continue to deform the basin flanks as discharges diminished to a level where basin depocenters would receive less sediment. Later increases in discharge would strip the uplifted basin flanks and surrounding upland regions and provide more sediment for the basin. Although subsidence controls cannot be completely ruled out, the overall upward coarsening of this alluvial succession and increase in gravel size supports augmentation of discharge in the sediment delivery system, rather than solely due to a reduction in tectonic subsidence.

Changes in sedimentation may have been driven by expansion of hinterland drainage area (Fraser and DeCelles, 1992), late Cenozoic climatic variability (Zhang et al., 2001; Chapin, 2008), or diminished basin subsidence (e.g., Mack and Seager, 1990). The present limits of the major western tributaries to the Albuquerque Basin were probably established by late Pliocene time (Love and Connell, 2005). Studies of the Arroyo Ojito and Ceja Formations indicate that crystalline basement rock was probably exposed by Late Miocene time (Connell et al., 1999), so durable basement rocks would have been exposed in hinterland catchment regions before the Ceja streams transported coarse-grained deposits.

Amalgamated coarse-grained channel deposits in the Ceja, Sierra Ladrones, and Tuerto Formations occurred after sediment-accumulation rates decreased on the distal hanging-wall ramp (Fig. 21B and 21C), suggesting that the basin may have filled to a level that promoted extensive sediment bypass through the basin. Although a decrease in sedimentation rate and overall coarsening of the Ceja section during late Pliocene time may suggest a decrease in subsidence rate, it seems unlikely that diminished subsidence can solely account for the relatively sudden introduction of coarse-grained clastic detritus into the basin following a decrease in sediment-accumulation rate. The approximately coeval depositional responses in the Albuquerque Basin and the tectonically quiescent San Pedro Valley of Arizona (Smith, 1994) suggest that climate may play an important role in the development of sedimentary sequences in slowly subsiding basins.

The 0.8 Ma onset of valley cutting coincides with the start of eccentricity-driven climate cycles (e.g., Zachos et al., 2001) and is within the chronological resolution reported for the cutting of the Rio Grande valley in southern New Mexico (Mack et al., 2006) and in southeastern Arizona (Smith, 1994). The transition from basin filling to valley cutting also agrees with other studies that document the onset of major regional incision before 0.6 Ma (e.g., Dethier, 2001). The timing of onset of incision and the approximate number (and age) of inset terrace deposits support the importance of regional climatic controls, rather than tectonic changes, to base level (Gile et al., 1981; Connell et al., 2007a; Leeder and Mack, 2007).

Valley incision in central and southern New Mexico may be slightly older than the 0.43 Ma age of overflow that Machette et al. (2007, this volume) postulated for their Lake Alamosa in the Rio Grande headwaters region, ~240 km north of Albuquerque and near the Colorado-New Mexico state line (Fig. 2). If this

age of upper-basin drainage integration is correct, then a nearly 0.3 m.y. lag exists between the initial cutting of the Rio Grande valley in the Albuquerque Basin and integration of the headwaters in southern Colorado. Such a lag would not support capture of the upper Rio Grande as the principal driver of downstream valley incision in central and southern New Mexico (Wells et al., 1987). It is possible that Pleistocene integration of the upper Rio Grande drainage might have been promoted by filling of the southern San Luis Basin by sediment in response to climatically induced increases in discharge.

SUMMARY AND CONCLUSIONS

We utilized combined geochronologic, sequence-stratigraphic, sedimentologic, and geomorphologic approaches to interpreting the development of a Plio-Pleistocene alluvial sequence in the Albuquerque Basin of the Rio Grande rift in north-central New Mexico. Seventy-eight new and previously published age determinations refine the ages of Miocene through lower Pleistocene basin fill of the synrift Santa Fe Group. These geochronologic data permitted the development of a robust magnetic-polarity stratigraphy for the Plio-Pleistocene part of the basin-fill succession.

The Ceja and Sierra Ladrones Formations form a nonmarine depositional sequence that is bounded by distinct sets of erosional and depositional surfaces. Deposition of Upper Miocene strata in the Albuquerque Basin ceased shortly after 6.3 Ma and is marked by widespread erosion of the basin flanks and development of the Rincones and lower Ortiz paleosurfaces. The upper boundaries of this alluvial sequence are defined by a suite of relict depositional surfaces that include the Cañada Colorada, Llano de Albuquerque, Las Huertas, Sunport, and Llano de Manzano surfaces.

Integration of axial-river drainage (by the ancestral Rio Grande) through the Albuquerque Basin occurred by 4.8 Ma, probably as a result of increased sedimentation that began to bury these areally extensive Upper Miocene unconformities, eventually burying low-lying structural culminations that divided the southern Albuquerque and Socorro Basins. Progressive, marginward onlap of the Ceja and Tuerto Formations eventually buried the Rincones and lower Ortiz paleosurfaces between 2.8 and 2.6 Ma. Later stages of paleosurface burial corresponded to a coarsening of the Ceja succession, and culminated with the development of the Llano de Albuquerque surface shortly after 1.8 Ma. Deposition of the Sierra Ladrones Formation continued for another million years until cutting of the Rio Grande valley initiated shortly after 0.8 Ma. Progradation of Sierra Ladrones piedmont deposits away from the master fault began after ca. 1.8–1.6 Ma. Cutting of the Rio Grande valley (south of the Española Basin) coincided with increased global climatic variability, and may have occurred before entrenchment of the headwaters region of the Rio Grande in southern Colorado.

The asynchronous progradation of margin-sourced deposits in this stratigraphic succession probably reflects a geometric response to decreasing accommodation up the hanging-wall ramp.

The fore-tilted geometry of the hanging wall promoted progradation of amalgamated channels that formed broad sheets across the distal hanging-wall ramp as sediment bypassed the basin margins. Reduced sediment accumulation rates after 3.0 Ma may represent extensive sediment bypass. Although active tectonism is clearly of first-order importance in the formation of sedimentary successions, the development of an Plio-Pleistocene alluvial sequence in the Albuquerque Basin may reflect the importance of climate on basin filling in slowly subsiding basins.

ACKNOWLEDGMENTS

This contribution was supported by the National Science Foundation (EAR-0344146) and the New Mexico Bureau of Geology and Mineral Resources. The $^{40}\text{Ar}/^{39}\text{Ar}$ dating and geologic mapping were supported by the New Mexico STATEMAP Program component of the National Cooperative Geologic Mapping Act of 1992. The Pueblos of Cochiti, Isleta, Jemez, Sandia, San Felipe, Santo Domingo, and Zia graciously provided access to tribal lands. Ivan Benavidez, Westland Corporation, and the King Brothers Ranch kindly provided access to much of the land along the Ceja del Rio Puerco. The New Mexico State Land Office also kindly provided rights of access to parts of Tijeras Arroyo. Teresa and Kathleen Connell, Holly Buehler, Linda Donohoo-Hurley, Dan Koning, Travis Naibert, Scott Muggleton, Mitchell Reese, and Kate Zeigler assisted with the acquisition, preparation, and analysis of more than 1400 paleomagnetic specimens. Steve Cather, Richard Chamberlin, Nelia Dunbar, and Dave Love kindly provided some of the geochronologic data presented here. This paper benefited from conversations with Steve Cather, Richard Chamberlin, John Hawley, Dan Koning, and Dave Love. Reviews by Brian Horton, Mark Hudson, and Mike Leeder improved the paper and are gratefully acknowledged.

REFERENCES CITED

- Anderholm, S.K., 2001, Mountain-Front Recharge along the East Side of the Albuquerque Basin, Central New Mexico (revised): U.S. Geological Survey Water-Resources Investigations Report 00-4010, 36 p.
- Angevine, C.L., Heller, P.L., and Paola, C., 1990, Quantitative Sedimentary Basin Modeling: American Association of Petroleum Geologists Continuing Education Course Note Series 32, 247 p.
- Axelrod, D.L., 1981, Role of Volcanism in Climate and Evolution: Geological Society of America Special Paper 185, 59 p.
- Bachman, G.O., and Mehnert, H.H., 1978, New K-Ar dates and the late Pliocene to Holocene geomorphic history of the central Rio Grande region, New Mexico: Geological Society of America Bulletin, v. 89, p. 283–292, doi:10.1130/0016-7606(1978)89<283:NKDATL>2.0.CO;2.
- Baldridge, W.S., Damon, P.E., Shafiqullah, M., and Bridwell, R.J., 1980, Evolution of the central Rio Grande rift, New Mexico: New potassium-argon ages: Earth and Planetary Science Letters, v. 51, p. 309–321, doi:10.1016/0012-821X(80)90213-7.
- Baldridge, W.S., Perry, F.V., and Shafiqullah, M., 1987, Late Cenozoic volcanism of the southeastern Colorado Plateau: I. Volcanic geology of the Lucero area, New Mexico: Geological Society of America Bulletin, v. 99, p. 463–470, doi:10.1130/0016-7606(1987)99<463:LCVOTS>2.0.CO;2.
- Bartolino, D.P., and Cole, J.C., 2002, Ground-Water Resources of the Middle Rio Grande Basin, New Mexico: U.S. Geological Survey Circular 1222, 132 p.

- Bell, C.J., Lundelius, E.L., Jr., Barnosky, A.D., Graham, R.W., Lindsay, E.H., Ruez, D.R., Semken, H.A., Jr., Webb, S.D., and Zakrzewski, R.J., 2004, The Blanca, Irvingtonian, and Rancholabrean Mammal Ages, in Woodburne, M.O., ed., Late Cretaceous and Cenozoic Mammals of North America: Biostratigraphy and Geochronology: New York, Columbia University Press, p. 232–314.
- Birkeland, P.W., 1999, Soils and Geomorphology (3rd edition): New York, Oxford University Press, 430 p.
- Blair, T.C., and Bilodeau, W.L., 1988, Development of tectonic cycloths in rift, pull-aparts, and foreland basins: Sedimentary response to episodic tectonism: *Geology*, v. 16, p. 517–520, doi:10.1130/0091-7613(1988)016<0517:DOTCIR>2.3.CO;2.
- Blum, M.D., and Törnqvist, T.E., 2000, Fluvial responses to climate and sea-level change: A review and look forward: *Sedimentology*, v. 47, suppl. 1, p. 2–48, doi:10.1046/j.1365-3091.2000.00008.x.
- Brandes, N.N., 2002, Lithostratigraphy and Petrography of Upper Santa Fe Group Deposits in the Northern Albuquerque Basin, New Mexico [M.S. thesis]: Socorro, New Mexico Institute of Mining and Technology, 208 p.
- Bridge, J.S., and Leeder, M.R., 1979, A simulation model of alluvial stratigraphy: *Sedimentology*, v. 26, p. 617–644, doi:10.1111/j.1365-3091.1979.tb00935.x.
- Bridge, J.S., and Mackey, S.D., 1993, A revised alluvial stratigraphy model, in Marzo, M., and Puigdefábregas, C., eds., Alluvial Sedimentation: International Association of Sedimentologists Special Publication 17, p. 319–336.
- Broxton, D., WoldeGabriel, G., Peters, L., Budahn, J., and Luedemann, G., 2007, Pleistocene volcanic rocks of the Tschicoma Formation, east-central Jemez volcanic field: Chemistry, petrography, and age constraints, in Kues, B.S., Kelley, S.A., and Lueth, V.W., eds., *Geology of the Jemez Region II*: New Mexico Geological Society Guidebook 58, p. 284–295.
- Bryan, K., 1938, Geology and ground-water conditions of the Rio Grande depression in Colorado and New Mexico: Washington, D.C., Natural Resources Committee, Regional Planning, Part 6, Upper Rio Grande Basin, v. 1, p. 2, sec. 1, p. 197–225.
- Bryan, K., and McCann, F.T., 1938, The Ceja del Rio Puerco: A border feature of the Basin and Range province in New Mexico, part II, geomorphology: *The Journal of Geology*, v. 46, p. 1–16, doi:10.1086/624618.
- Cather, S.M., and Connell, S.D., 1998, Geology of the San Felipe Pueblo 7.5-Minute Quadrangle, Sandoval County, New Mexico: New Mexico Bureau of Mines and Mineral Resources Open-File Geologic Map 19, scale 1:24,000.
- Cather, S.M., Chamberlin, R.M., Chapin, C.E., and McIntosh, W.C., 1994, Stratigraphic consequences of episodic extension in the Lemitar Mountains, central Rio Grande rift, in Keller, G.R., and Cather, S.M., eds., *Basins of the Rio Grande Rift: Structure, Stratigraphy, and Tectonic Setting*: Geological Society of America Special Paper 291, p. 157–170.
- Chamberlin, R.M., and McIntosh, W.C., 2007, Geochronology and structural control of late Cenozoic volcanism in the Loma Creston quadrangle, southern Jemez Mountains, New Mexico, in Kues, B.S., Kelley, S.A., and Lueth, V.W., eds., *Geology of the Jemez Mountains Region II*: New Mexico Geological Society Guidebook 58, p. 248–261.
- Chamberlin, R.M., Pazzaglia, F.J., Wegmann, K.W., and Smith, G.A., 1999 (revised 2007), Preliminary Geologic Map of the Loma Creston Quadrangle, Sandoval County, New Mexico: New Mexico Bureau of Mines and Mineral Resources Open-File Geologic Map 25, scale 1:24,000.
- Chamberlin, R.M., Cather, S.M., Nyman, M.W., and McLemore, V.T., 2001, Preliminary Geologic Map of the Lemitar 7.5-Minute Quadrangle, Socorro County, New Mexico: New Mexico Bureau of Mines and Mineral Resources Open-File Geologic Map 38, scale 1:24,000, 29 p.
- Chapin, C.E., 1971, The Rio Grande rift, part 1: Modifications and additions, in James, H.L., ed., *Guidebook of the San Luis Basin, Colorado*: New Mexico Geological Society Guidebook 22, p. 191–201.
- Chapin, C.E., 2008, Interplay of oceanographic and paleoclimate events with tectonism during middle to late Miocene sedimentation across the southwestern USA: *Geosphere*, v. 4, p. 976–991, doi:10.1130/GES00171.1.
- Chapin, C.E., and Cather, S.M., 1994, Tectonic setting of the axial basins of the northern and central Rio Grande rift, in Keller, G.R., and Cather, S.M., eds., *Basins of the Rio Grande Rift: Structure, Stratigraphy, and Tectonic Setting*: Geological Society of America Special Paper 291, p. 5–25.
- Cole, J.C., Stone, B.D., Shroba, R.R., and Dethier, D.P., 2001, Pliocene incision of the Rio Grande in northern New Mexico: Geological Society of America Abstracts with Programs, v. 33, no. 5, p. A-48.
- Cole, J.C., Mahan, S.A., Stone, B.D., and Shroba, R.R., 2007, Ages of Quaternary Rio Grande terrace-fill deposits, Albuquerque area, New Mexico: *New Mexico Geology*, v. 29, p. 123–132.
- Connell, S.D., 2004, Geology of the Albuquerque Basin and tectonic development of the Rio Grande rift in north-central New Mexico, in Mack, G.H., and Giles, K.A., eds., *The Geology of New Mexico: A Geologic History*: New Mexico Geological Society Special Publication 11, p. 359–388.
- Connell, S.D., 2006, Preliminary Geologic Map of the Albuquerque–Rio Rancho Metropolitan Area, Bernalillo and Sandoval County, New Mexico: New Mexico Bureau of Geology and Mineral Resources Open-File Report 496, version 2.0, scale 1:50,000.
- Connell, S.D., 2008a, Refinements to the stratigraphic nomenclature of the Santa Fe Group, northwestern Albuquerque Basin, New Mexico: *New Mexico Geology*, v. 30, p. 14–35.
- Connell, S.D., 2008b, Geologic Map of the Albuquerque–Rio Rancho Metropolitan Area, Bernalillo and Sandoval County, New Mexico: New Mexico Bureau of Geology and Mineral Resources Geologic Map GM-78, scale 1:50,000, 2 plates.
- Connell, S.D., and Wells, S.G., 1999, Pliocene and Quaternary stratigraphy, soils, and tectonic geomorphology of the northern flank of the Sandia Mountains, New Mexico: Implications for the tectonic evolution of the Albuquerque Basin, in Pazzaglia, F.J., and Lucas, S.G., eds., *Albuquerque Geology*: New Mexico Geological Society Guidebook 50, p. 379–391.
- Connell, S.D., Allen, B.D., and Hawley, J.W., 1998, Subsurface stratigraphy of the Santa Fe Group from borehole geophysical logs, Albuquerque area, New Mexico: *New Mexico Geology*, v. 20, p. 2–7.
- Connell, S.D., Koning, D.J., and Cather, S.M., 1999, Revisions to the stratigraphic nomenclature of the Santa Fe Group, northwestern Albuquerque Basin, New Mexico, in Pazzaglia, F.J., and Lucas, S.G., eds., *Albuquerque Geology*: New Mexico Geological Society Guidebook 50, p. 337–353.
- Connell, S.D., Love, D.W., Maldonado, F., Jackson, P.B., McIntosh, W.C., and Eppes, M.C., 2000, Is the top of the Santa Fe Group diachronous in the Albuquerque Basin? [abstract]: U.S. Geological Survey Open-File Report 00-488, p. 18–20.
- Connell, S.D., Love, D.W., Cather, S.M., Smith, G.A., and Lucas, S.G., 2001a, Tectonics, climate, and the transition from aggradation to incision of the upper Santa Fe Group, Albuquerque Basin, central New Mexico: Geological Society of America Abstracts with Programs, v. 33, no. 5, p. A-48.
- Connell, S.D., Lucas, S.G., Koning, D.J., Maynard, S.R., and Derrick, N.N., 2001b, First-day, Santo Domingo sub-basin: Hagan Embayment and northern flank of the Sandia Mountains, in Connell, S.D., Love, D.W., Lucas, S.G., Koning, D.J., Derrick, N.N., Maynard, S.R., Morgan, G.S., Jackson-Paul, P.B., and Chamberlin, R., trip leaders., *Stratigraphy and Tectonic Development of the Albuquerque Basin, Central Rio Grande Rift*, Field Trip Guidebook: Albuquerque, New Mexico, Geological Society of America, Rocky Mountain–South Central Section Meeting: New Mexico Bureau of Geology and Mineral Resources Open-File Report 454A, p. 1–15.
- Connell, S.D., Love, D.W., and Sorrell, J.D., 2001c, Geology of the Isleta Reservation, First-day road log, October 12, 2001, in Connell, S.D., Love, D.W., Sorrell, J.D., and Harrison, J.B.J., trip leaders., *Plio-Pleistocene Stratigraphy and Geomorphology of the Central Part of the Albuquerque Basin*: Friends of the Pleistocene, Rocky Mountain Cell, Field-Trip Guidebook: New Mexico Bureau of Geology and Mineral Resources Open-File Report 454C, p. 1–1–28.
- Connell, S.D., Love, D.W., and Sorrell, J.D., 2001d, Geology of southern Albuquerque and Tijeras Arroyo, Second-day road log, October 13, 2001, in Connell, S.D., Love, D.W., Sorrell, J.D., and Harrison, J.B.J., trip leaders., *Plio-Pleistocene Stratigraphy and Geomorphology of the Central Part of the Albuquerque Basin*: Friends of the Pleistocene, Rocky Mountain Cell, Field-Trip Guidebook: New Mexico Bureau of Geology and Mineral Resources Open-File Report 454C, p. 2-1–2-23.
- Connell, S.D., Cather, S.M., Dunbar, N., McIntosh, W.C., and Peters, L., 2002, Stratigraphy of the Tanos and Blackshare Formations (lower Santa Fe Group), Hagan embayment, Rio Grande rift, New Mexico: *New Mexico Geology*, v. 24, p. 107–119.
- Connell, S.D., Hawley, J.W., and Love, D.W., 2005, Late Cenozoic drainage development in the southeastern Basin and Range of New Mexico, southeasternmost Arizona, and western Texas, in Lucas, S.G., Morgan, G.S., and Ziegler, K.E., eds., *New Mexico's Ice Ages*: New Mexico Museum of Natural History and Science Bulletin 28, p. 125–150.

- Connell, S.D., Love, D.W., and Dunbar, N.W., 2007a, Geomorphology and stratigraphy of inset fluvial deposits along the Rio Grande valley in the central Albuquerque Basin, New Mexico: *New Mexico Geology*, v. 29, p. 13–31.
- Connell, S.D., Koning, D.J., Kelley, S.A., and Brandes, N.N., 2007b, Oligocene–Miocene sedimentation in the southwestern Jemez Mountains and northwestern Albuquerque basin, New Mexico, in Kues, B.S., Kelley, S.A., and Lueth, V.W., eds., *Geology of the Jemez Region II: New Mexico Geological Society Guidebook* 58, p. 195–208.
- Contreras, J., Scholz, C.H., and King, G.C.P., 1997, A model of rift basin evolution constrained by first-order stratigraphic observations: *Journal of Geophysical Research*, v. 102, p. 7673–7690, doi:10.1029/96JB03832.
- Dart, C., Cohen, H.A., Akyuz, H.S., and Barka, A., 1995, Basinward migration of rift-border faults: Implications for facies distribution and preservation potential: *Geology*, v. 23, p. 69–72, doi:10.1130/0091-7613(1995)023<0069:BMORBF>2.3.CO;2.
- Deino, A., and Potts, R., 1992, Age-probability spectra from examination of single-crystal $^{40}\text{Ar}/^{39}\text{Ar}$ dating results: Examples from Olorgesailie, Southern Kenya Rift: *Quaternary International*, v. 13/14, p. 47–53, doi:10.1016/1040-6182(92)90009-Q.
- Dethier, D.P., 2001, Pleistocene incision rates in the western United States calibrated using Lava Creek B tephra: *Geology*, v. 29, p. 783–786, doi:10.1130/0091-7613(2001)029<0783:PIRITW>2.0.CO;2.
- Drake, P.G., Harrington, C.D., Wells, S.G., Perry, F.V., and Laughlin, A.W., 1991, Late Cenozoic geomorphic and tectonic evolution of the Rio San Jose and tributary drainages within the Basin and Range/Colorado Plateau transition zone in west-central New Mexico, in Julian B., and Zidek, J., eds., *Field Guide to Geologic Excursions in New Mexico and Adjacent Areas of Texas and Colorado: New Mexico Bureau of Mines and Mineral Resources Bulletin* 137, p. 149–157.
- Dunbar, N.W., McIntosh, W.C., and Love, D.W., 2001, Dating basalts using the $^{40}\text{Ar}/^{39}\text{Ar}$ method: Improvements based on electron microprobe evaluation of samples: *Eos (Transactions, American Geophysical Union)*, v. 82, p. F1321.
- Fisher, R.A., 1953, Dispersion on a sphere: *Proceedings of the Royal Society of London*, v. A217, p. 295–305.
- Fraser, G.S., and DeCelles, P.G., 1992, Geomorphic controls on sediment accumulation at margins of foreland basins: *Basin Research*, v. 4, p. 233–252, doi:10.1111/j.1365-2117.1992.tb00047.x.
- Frostick, L.E., and Reid, I., 1989, Is structure the main control of river drainage and sedimentation in rifts?: *Journal of African Earth Sciences*, v. 8, p. 165–182, doi:10.1016/S0899-5362(89)80022-3.
- Gawthorpe, R.L., and Hurst, J.M., 1993, Transfer zones in extensional basins: Their structural style and influence on drainage development and stratigraphy: *Journal of the Geological Society of London*, v. 150, p. 1137–1152, doi:10.1144/gsjgs.150.6.1137.
- Gawthorpe, R.L., and Leeder, M.R., 2000, Tectono-sedimentary evolution of active extensional basins: *Basin Research*, v. 12, p. 195–218.
- Gile, L.H., Hawley, J.W., and Grossman, R.B., 1981, Soils and Geomorphology in the Basin and Range Area of Southern New Mexico: *Guidebook to the Desert Project: New Mexico Bureau of Mines and Mineral Resources Memoir* 39, 222 p.
- Gile, L.H., Hawley, J.W., Grossman, R.B., Monger, H.C., Montoya, C.E., and Mack, G.H., 1995, Supplement to the Desert Project Guidebook, with Emphasis on Soil Micromorphology: *New Mexico Bureau of Mines and Mineral Resources Bulletin* 142, 96 p.
- Goff, F., and Gardner, J., 2004, Late Cenozoic geochronology of volcanism and mineralization in the Jemez Mountains and Valles caldera, north central New Mexico, in Mack, G.H., and Giles, K.A., eds., *The Geology of New Mexico: A Geologic History: New Mexico Geological Society Special Publication* 11, p. 295–312.
- Gradstein, F., Ogg, J., and Smith, A., 2005, *A Geologic Time Scale 2005*: Cambridge, UK, Cambridge University Press, 589 p.
- Grauch, V.J.S., Keller, G.R., and Gillespie, C.L., 1999, Discussion of new gravity maps for the Albuquerque Basin area, in Pazzaglia, F.J., and Lucas, S.G., eds., *Albuquerque Geology: New Mexico Geological Society Guidebook* 50, p. 119–124.
- Hallett, R.B., Kyle, P.R., and McIntosh, W.C., 1997, Paleomagnetic and $^{40}\text{Ar}/^{39}\text{Ar}$ age constraints on the chronologic evolution of the Rio Puerco volcanic necks and Mesa Prieta, west-central New Mexico: Implications for transition zone magmatism: *Geological Society of America Bulletin*, v. 109, p. 95–106, doi:10.1130/0016-7606(1997)109<0095:PAAAAC>2.3.CO;2.
- Haneberg, W.C., 1995, Depth-porosity relationships and virgin specific storage estimates for the upper Santa Fe Group aquifer system, central Albuquerque basin, New Mexico: *New Mexico Geology*, v. 17, p. 62–71.
- Hawley, J.W., ed., 1978, *Guidebook to Rio Grande rift in New Mexico and Colorado: New Mexico Bureau of Mines and Mineral Resources Circular* 163, 241 p.
- Hawley, J.W., 1996, Hydrogeologic framework of potential recharge areas in the Albuquerque Basin, central New Mexico, in Hawley, J.W., and Whitworth, T.M., compilers, *Hydrogeology of Potential Recharge Areas for the Basin- and Valley-Fill Aquifer Systems, and Hydrogeochemical Modeling of Proposed Aquifer Recharge of the Upper Santa Fe Aquifer, Northern Albuquerque Basin, New Mexico: New Mexico Bureau of Mines and Mineral Resources Open-File Report* 402D, Chapter 1, 68 p.
- Hawley, J.W., and Haase, C.S., compilers, 1992, *Hydrogeologic Framework of the Northern Albuquerque Basin: New Mexico Bureau of Mines and Mineral Resources Open-File Report* 387, 165 p., 7 plates.
- Hawley, J.W., Haase, C.S., and Lozinsky, R.P., 1995, An underground view of the Albuquerque Basin, in Ortega-Klett, C.T., ed., *The Water Future of Albuquerque and Middle Rio Grande Basin: Proceedings of the 39th Annual New Mexico Water Conference, Nov. 3–4, 1994, Albuquerque, New Mexico: New Mexico Water Resources Research Institute Report* 290, p. 27–55.
- Heller, P.L., and Paola, C., 1992, The large-scale dynamics of grain-size variation in alluvial basins, 2: Application to syntectonic conglomerate: *Basin Research*, v. 4, p. 91–102, doi:10.1111/j.1365-2117.1992.tb00146.x.
- Hudson, M.R., Grauch, V.J.S., and Minor, S.A., 2008, Rock magnetic characterization of faulted sediments with associated magnetic anomalies in the Albuquerque Basin, Rio Grande rift, New Mexico: *Geological Society of America Bulletin*, v. 120, p. 641–658, doi:10.1130/B26213.1.
- Ingersoll, R.V., 2001, Structural and stratigraphic evolution of the Rio Grande rift, northern New Mexico and southern Colorado: *International Geology Review*, v. 43, p. 867–891, doi:10.1080/00206810109465053.
- Izett, G.A., and Obradovich, J.D., 1994, $^{40}\text{Ar}/^{39}\text{Ar}$ age constraints for the Jaramillo normal subchron and the Matuyama-Brunhes geomagnetic boundary: *Journal of Geophysical Research*, v. 99, p. 2925–2934, doi:10.1029/93JB03085.
- Izett, G.A., and Wilcox, R.E., 1982, Map Showing Localities and Inferred Distributions of the Huckleberry Ridge, Mesa Falls, and Lava Creek Ash Beds (Pearlette Family Ash Beds) of Pliocene and Pleistocene Age in the Western United States and Southern Canada: U.S. Geological Survey Miscellaneous Investigation Series Map I-1325, scale 1:4,000,000.
- Jackson, J.A., and Leeder, M.R., 1994, Drainage systems and the development of normal faults: An example from Pleasant Valley, Nevada: *Journal of Structural Geology*, v. 16, p. 1041–1059, doi:10.1016/0191-8141(94)90051-5.
- Johnson, N.M., Opdyke, N.D., Woodward, G.D., Lindsay, E.H., and Tehirkhelhi, R.A.K., 1982, Magnetic polarity stratigraphy and ages of Siwalik Group rocks of the Potwar Plateau, Pakistan: *Palaeogeography, Palaeoclimatology, Palaeoecology*, v. 37, p. 17–42, doi:10.1016/0031-0182(82)90056-6.
- Justet, L., and Spell, T.L., 2001, Effusive eruptions from a large silicic magma chamber: The Bearhead Rhyolite, Jemez volcanic field, NM: *Journal of Volcanology and Geothermal Research*, v. 107, p. 241–264, doi:10.1016/S0377-0273(00)00296-1.
- Kelley, V.C., 1952, Tectonics of the Rio Grande depression of central New Mexico, in Johnson, R.B., and Read, C.B., eds., *Rio Grande Country: New Mexico Geological Society Guidebook* 3, p. 93–105.
- Kelley, V.C., 1977, Geology of the Albuquerque Basin, New Mexico: *New Mexico Bureau of Mines and Mineral Resources Memoir* 33, 60 p.
- Kelley, V.C., 1979, Tectonics, middle Rio Grande rift, New Mexico, in Riecker, R.E., ed., *Rio Grande Rift: Tectonics and Magmatism*: Washington, D.C., American Geophysical Union, p. 57–70.
- Kelley, V.C., 1982, The right-relayed Rio Grande rift, Taos to Hatch, New Mexico, in Wells, S.G., Grambling, J.A., and Callender, J., eds., *Albuquerque Country II: New Mexico Geological Society Guidebook* 33, p. 147–151.
- Kelley, V.C., and Kudo, A.M., 1978, Volcanoes and Related Basaltic Rocks of the Albuquerque-Belen Basin, New Mexico: *New Mexico Bureau of Mines and Mineral Resources Circular* 156, 30 p.
- Kirschvink, J.L., 1980, The least squares line and plane and the analysis of paleomagnetic data: *Geophysical Journal of the Royal Astronomical Society*, v. 62, p. 699–718, doi:10.1111/j.1365-246X.1980.tb02601.x.
- Koning, D.J., and Personius, S.F., 2002, Preliminary Geologic Map of the Bernallillo NW Quadrangle, Sandoval County: U.S. Geological Survey Miscellaneous Field Investigations Map MF-2404, scale 1:24,000.

- Koning, D.J., Connell, S.D., Pazzaglia, F.J., and McIntosh, W.C., 2001, Stratigraphy of the Tueru and Ancha formations (upper Santa Fe Group), Hagan and Santa Fe embayments, north-central New Mexico, in Connell, S.D., Lucas, S.G., and Love, D.W., eds., Stratigraphy and Tectonic Development of the Albuquerque Basin, Central Rio Grande Rift, Mini-Papers for Field Trip Guidebook: Albuquerque, New Mexico, Geological Society of America, Rocky Mountain–South-Central Section Meeting: New Mexico Bureau of Geology and Mineral Resources Open-File Report 454B, p. I57–I66.
- Koning, D.J., Connell, S.D., Pazzaglia, F.J., and McIntosh, W.C., 2002, Redefinition of the Ancha Formation and Pliocene–Pleistocene deposition in the Santa Fe embayment, north-central New Mexico: New Mexico Geology, v. 24, p. 75–87.
- Koning, D.J., Grauch, V.J.S., Connell, S.D., Ferguson, J., McIntosh, W., Slate, J.L., Wan, E., and Baldridge, W.S., 2013, this volume, Structure and tectonic evolution of the eastern Española Basin, Rio Grande rift, north-central New Mexico, in Hudson, M.R., and Grauch, V.J.S., eds., New Perspectives on Rio Grande Rift Basins: From Tectonics to Groundwater: Geological Society of America Special Paper 494, doi:10.1130/2013.2494(08).
- Lambert, P.W., 1968, Quaternary Stratigraphy of the Albuquerque Area, New Mexico [Ph.D. thesis]: Albuquerque, University of New Mexico, 329 p.
- Lambiase, J.J., and Bosworth, W., 1995, Structural controls on sedimentation in continental rifts, in Lambiase, J.J., ed., Hydrocarbon Habitat in Rift Basins: Geological Society of London Special Publication 80, p. 117–144.
- Lanphere, M.A., Champion, D.E., Christiansen, R.L., Izett, G.A., and Obradovich, J.D., 2002, Revised ages for tuffs of the Yellowstone Plateau volcanic field: Assignment of the Huckleberry Ridge Tuff to a new geomagnetic polarity event: Geological Society of America Bulletin, v. 114, p. 559–568, doi:10.1130/0016-7606(2002)114<0559:RAFTOT>2.0.CO;2.
- Leeder, M.R., and Gawthorpe, R.L., 1987, Sedimentary models for extensional tilt block/half-graben basins, in Coward, M.P., Dewey, J.F., and Hancock, P.L., eds., Continental Extensional Tectonics: Geological Society of London Special Publication 28, p. 139–152.
- Leeder, M.R., and Jackson, J.A., 1993, The interaction between normal faulting and drainage in active extensional basins, with examples from the western United States and central Greece: Basin Research, v. 5, p. 79–102, doi:10.1111/j.1365-2117.1993.tb00059.x.
- Leeder, M.R., and Mack, G.H., 2001, Lateral erosion (“toe cutting”) of alluvial fans by axial rivers: Implications for basin analysis and architecture: Journal of the Geological Society of London, v. 158, p. 885–893, doi:10.1144/0016-760000-198.
- Leeder, M.R., and Mack, G.H., 2007, Basin-fill incision, Rio Grande and Gulf of Corinth rifts: Convergent response to climatic and tectonic drivers, in Nicholls, G., Williams, E., and Paola, C., eds., Sedimentary Processes, Environments and Basins: A Tribute to Peter Friend: International Association of Sedimentologists Special Publication 38, p. 9–28.
- Leeder, M.R., Mack, G.H., and Salyards, S.L., 1996, Axial-transverse fluvial interactions in half-graben: Plio-Pleistocene Palomas Basin, southern Rio Grande rift, New Mexico, USA: Basin Research, v. 8, p. 225–241, doi:10.1046/j.1365-2117.1996.00192.x.
- Lindsay, E.H., Johnson, N.M., Opdyke, N.D., and Butler, R.F., 1987, Mammalian chronology and the magnetic polarity time scale, in Woodburne, M.O., ed., Cenozoic Mammals of North America, Geochronology and Biostratigraphy: Berkeley, University of California Press, p. 269–284.
- Love, D.W., and Connell, S.D., 2005, Late Neogene drainage developments on the southeastern Colorado Plateau, New Mexico, in Lucas, S.G., Morgan, G.S., and Ziegler, K.E., eds., New Mexico’s Ice Ages: New Mexico Museum of Natural History and Science Bulletin 28, p. 151–169.
- Love, D.W., Maldonado, F., Hallett, B., Panter, K., Reynolds, C., McIntosh, W., and Dunbar, N., 1998, Geology of the Dailies 7.5-Minute Quadrangle: New Mexico Bureau of Geology and Mineral Resources Open-File Geologic Map 21, scale 1:24,000.
- Love, D.W., Connell, S.D., Chamberlin, R.M., Cather, S.M., McIntosh, W.C., Dunbar, N., Smith, G.A., and Lucas, S.G., 2001a, Constraints on the age of extensive fluvial facies of the upper Santa Fe Group, Albuquerque and Socorro basins, central New Mexico: Geological Society of America Abstracts with Programs, v. 33, no. 5, p. A-48.
- Love, D.W., Connell, S.D., Lucas, S.G., Morgan, G.S., Derrick, N.N., Jackson-Paul, P.B., and Chamberlin, R., 2001b, Third-day, Belen sub-basin: Belen, Sevilleta National Wildlife Refuge, and northern Socorro Basin, in Connell, S.D., Love, D.W., Lucas, S.G., Koning, D.J., Derrick, N.N., Maynard, S.R., Morgan, G.S., Jackson-Paul, P.B., and Chamberlin, R., trip leaders, Stratigraphy and Tectonic Development of the Albuquerque Basin, Central Rio Grande Rift, Field-Trip Guidebook: Albuquerque, New Mexico, Geological Society of America, Rocky Mountain–South-Central Section Meeting: New Mexico Bureau of Geology and Mineral Resources Open-File Report 454A, p. 27–53.
- Love, D.W., Connell, S.D., Lucas, S.G., Morgan, G.S., Derrick, N.N., Jackson-Paul, P.B., and Chamberlin, R., 2001c, Third-day road log: Geology of Los Lunas volcano, in Connell, S.D., Love, D.W., Sorrell, J.D., and Harrison, J.B.J., trip leaders, Plio-Pleistocene Stratigraphy and Geomorphology of the Central Part of the Albuquerque Basin: New Mexico Bureau of Geology and Mineral Resources Open-File Report 454C, p. 3-1–3-13.
- Lozinsky, R.P., 1994, Cenozoic stratigraphy, sandstone petrology, and depositional history of the Albuquerque basin, central New Mexico, in Keller, G.R., and Cather, S.M., eds., Basins of the Rio Grande Rift: Structure, Stratigraphy, and Tectonic Setting: Geological Society of America Special Paper 291, p. 73–82.
- Lozinsky, R.P., and Tedford, R.H., 1991, Geology and Paleontology of the Santa Fe Group, Southwestern Albuquerque Basin, Valencia County, New Mexico: New Mexico Bureau of Mines and Mineral Resources Bulletin 132, 35 p.
- Lucas, S.G., Williamson, T.E., and Sobus, J., 1993, Plio-Pleistocene stratigraphy, paleoecology, and mammalian biochronology, Tijeras Arroyo, Albuquerque area, New Mexico: New Mexico Geology, v. 15, p. 1–8.
- Machette, M.N., 1978, Geologic Map of the San Acacia Quadrangle, Socorro County, New Mexico: U.S. Geological Survey Geologic Quadrangle Map GQ-1415, scale 1:24,000.
- Machette, M.N., 1985, Calcic soils of the southwestern United States, in Weide, D.L., ed., Soils and Quaternary Geology of the Southwestern United States: Geological Society of America Special Paper 203, p. 1–42.
- Machette, M.N., Personius, S.F., Kelson, K.I., Haller, K.M., and Dart, R.L., 1998, Map and Data for Quaternary Faults and Folds in New Mexico: U.S. Geological Survey Open-File Report 98-821, 443 p., 1 plate.
- Machette, M.N., Marchetti, D.W., and Thompson, R., 2007, Ancient Lake Alamosa and the Pliocene to middle Pleistocene evolution of the Rio Grande, in Machette, M.N., Coates, M.M., and Johnson, M.L., eds., 2007 Rocky Mountain Section Friends of the Pleistocene Field Trip—Quaternary Geology of the San Luis Basin of Colorado and New Mexico, September 7–9, 2007: U.S. Geological Survey Open-File Report 2007-1193, p. 157–167.
- Machette, M.N., Thompson, R.A., Marchetti, D.W., and Smith, R.S.U., 2013, this volume, Evolution of ancient Lake Alamosa and integration of the Rio Grande during the Pliocene and Pleistocene, in Hudson, M.R., and Grauch, V.J.S., eds., New Perspectives on Rio Grande Rift Basins: From Tectonics to Groundwater: Geological Society of America Special Paper 494, doi:10.1130/2013.2494(01).
- Mack, G.H., and Seager, W.R., 1990, Tectonic controls on facies distribution of the Camp Rice and Palomas Formations (Pliocene–Pleistocene) in the southern Rio Grande rift: Geological Society of America Bulletin, v. 102, p. 45–53, doi:10.1130/0016-7606(1990)102<0045:TCOFDO>2.3.CO;2.
- Mack, G.H., Salyards, S.L., and James, W.C., 1993, Magnetostratigraphy of the Plio-Pleistocene Camp Rice and Palomas Formations in the Rio Grande rift of southern New Mexico: American Journal of Science, v. 293, p. 49–77, doi:10.2475/ajs.293.1.49.
- Mack, G.H., Cole, D.R., James, W.C., Giordano, T.H., and Salyards, S.L., 1994, Stable oxygen and carbon isotopes of pedogenic carbonate as indicators of Plio-Pleistocene paleoclimate in the southern Rio Grande rift, south-central New Mexico: American Journal of Science, v. 294, p. 621–640, doi:10.2475/ajs.294.5.621.
- Mack, G.H., McIntosh, W.C., Leeder, M.R., and Monger, H.C., 1996, Plio-Pleistocene pumice floods in the ancestral Rio Grande, southern Rio Grande rift, New Mexico, USA: Sedimentary Geology, v. 103, p. 1–8.
- Mack, G.H., Leeder, M., and Salyards, S.L., 2002, Temporal and spatial variability of alluvial-fan and axial-fluvial sedimentation in the Plio-Pleistocene Palomas half graben, southern Rio Grande rift, New Mexico, USA, in Renaut, R.W., and Ashley, G.M., eds., Sedimentation in Continental Rifts: SEPM (Society for Sedimentary Geology) Special Publication 73, p. 165–177.
- Mack, G.H., Seager, W.R., Leeder, M.R., Pareja-Arlucea, M., and Salyards, S.L., 2006, Pliocene and Quaternary history of the Rio Grande, the axial river of the southern Rio Grande rift, New Mexico, USA: Earth-Science Reviews, v. 79, p. 141–162, doi:10.1016/j.earscirev.2006.07.002.
- Maldonado, F., Connell, S.D., Love, D.W., Grauch, V.J.S., Slate, J.L., McIntosh, W.C., Jackson-Paul, P.B., and Byers, F.M., Jr., 1999, Neogene geology of

- the Isleta Reservation and vicinity, Albuquerque Basin, New Mexico, in Pazzaglia, F.J., and Lucas, S.G., eds., *Albuquerque Geology: New Mexico Geological Society Guidebook 50*, p. 175–188.
- Maldonado, F., Budahn, J.R., Peters, L., and Unruh, D.M., 2006, Geology, geochronology, and geochemistry of basaltic flows of the Cat Hills, Cat Mesa, Wind Mesa, Cerro Verde, and Mesita Negra, central New Mexico: *Canadian Journal of Earth Sciences*, v. 43, p. 1251–1268, doi:10.1139/e06-018.
- Maldonado, F., Slate, J.L., Love, D.W., Connell, S.D., Cole, J.C., and Karlstrom, K.E., 2007, Geologic Map of the Pueblo of Isleta Tribal Lands and Vicinity, Bernalillo, Torrance, and Valencia Counties, Central New Mexico: U.S. Geological Survey Scientific Investigations Map 2913, 35 p., 1 plate, scale 1:50,000.
- Marr, J.G., Swenson, J.B., Paola, C., and Voller, V.R., 2000, A two-dimensional model of fluvial stratigraphy in closed depositional basins: *Basin Research*, v. 12, p. 381–398, doi:10.1046/j.1365-2117.2000.00134.x.
- May, J.S., Kelley, S.A., and Russell, L.R., 1994, Footwall unloading and rift shoulder uplifts in the Albuquerque Basin: Their relation to syn-rift fanglomerates and apatite fission-track ages, in Keller, G.R., and Cather, S.M., eds., *Basins of the Rio Grande Rift: Structure, Stratigraphy, and Tectonic Setting*: Geological Society of America Special Paper 291, p. 125–134.
- McAda, D.P., and Carroll, P., 2002, Simulation of Ground-Water Flow in the Middle Rio Grande Basin between Cochiti and San Acacia, New Mexico: U.S. Geological Survey Water-Resources Investigations Report 02-4200, 81 p.
- McIntosh, W.C., and Quade, J., 1995, $^{40}\text{Ar}/^{39}\text{Ar}$ geochronology of tephra layers in the Santa Fe Group, Española Basin, New Mexico, in Bauer, P.W., Kues, B.S., Dunbar, N.W., Karlstrom, K.E., and Harrison, B., eds., *Geology of the Santa Fe Region: New Mexico Geological Society Guidebook 46*, p. 279–287.
- Molnar, P., 2004, Late Cenozoic increase in accumulation rates of terrestrial sediment: How might climate change have affected erosion rates?: *Annual Review of Earth and Planetary Sciences*, v. 32, p. 67–89, doi:10.1146/annurev.earth.32.091003.143456.
- Morgan, G.S., and Lucas, S.G., 2003, Mammalian biochronology of Blancan and Irvingtonian (Pliocene and early Pleistocene) faunas from New Mexico: *American Museum of Natural History Bulletin*, v. 279, p. 269–320, doi:10.1206/0003-0090(2003)279<0269:C>2.0.CO;2.
- NOAA (National Oceanic and Atmospheric Administration) Geophysical Data Center, 2005, Geomagnetism: <http://www.ngdc.noaa.gov/geomag> (accessed May 2008).
- Olsen, P.E., 1997, Stratigraphic record of the early Mesozoic breakup of Pangea in the Laurasia-Gondwana rift system: *Annual Review of Earth and Planetary Sciences*, v. 25, p. 337–401, doi:10.1146/annurev.earth.25.1.337.
- Opdyke, N.D., Lindsay, E.H., Johnson, N.M., and Downs, T., 1977, The paleomagnetism and magnetic polarity stratigraphy of the mammal-bearing section of Anza Borrego State Park, California: *Quaternary Research*, v. 7, p. 316–329, doi:10.1016/0033-5894(77)90024-2.
- Paola, C., 2000, Quantitative models of sedimentary basin filling: *Sedimentology*, v. 47, suppl. 1, p. 121–178, doi:10.1046/j.1365-3091.2000.00006.x.
- Paola, C., Heller, P.L., and Angevine, C.L., 1992, The large-scale dynamics of grain-size variation in alluvial basins, 1: Theory: *Basin Research*, v. 4, p. 73–90, doi:10.1111/j.1365-2117.1992.tb00145.x.
- Pazzaglia, F.J., Pederson, J.L., Garcia, A.F., Koning, D.J., Formento-Trigilio, M.L., and Toya, C., 1998, Geology of the Jemez Pueblo 7.5-Minute Quadrangle: New Mexico Bureau of Mines and Mineral Resources Open-File Geologic Map 14, scale 1:24,000.
- Peakall, J., 1998, Axial river evolution in response to half-graben faulting, Carson River, Nevada: *Journal of Sedimentary Research*, v. 68, p. 788–799, doi:10.2110/jsr.68.788.
- Peakall, J., Leeder, M., Best, J., and Ashworth, P., 2000, River responses to lateral ground tilting: A synthesis and some important implications for the modeling of alluvial architecture in extensional basins: *Basin Research*, v. 12, p. 413–424, doi:10.1046/j.1365-2117.2000.00128.x.
- Phillips, E.H., Goff, F., Kyle, P.R., McIntosh, W.C., Dunbar, N.W., and Gardner, J.N., 2007, The $^{40}\text{Ar}/^{39}\text{Ar}$ age constraints on the duration of resurgence at the Valles caldera, New Mexico: *Journal of Geophysical Research*, v. 112, B08201, doi:10.1029/2006JB004511.
- Reheis, M.C., Sarna-Wojcicki, A.M., Burbank, D.M., and Meyer, C.E., 1991, The late Cenozoic section at Willow Wash, west-central California: A tephrochronological Rosetta Stone, in Reheis, M.C., Slate, J.L., Sawyer, T.L., Sarna-Wojcicki, A.M., Harden, J.W., Pendall, E.G., Gillespie, A.R., and Burbank, D.M., eds., *Pacific Cell, Friends of the Pleistocene Guidebook for Field Trip to Fish Lake Valley, California–Nevada: U.S. Geological Survey Open-File Report 91-290*, p. 46–66.
- Reneau, S.L., and Dethier, D.P., 1996, Late Pleistocene landslide-dammed lakes of the Rio Grande, White Rock Canyon, New Mexico: *Geological Society of America Bulletin*, v. 108, p. 1492–1507, doi:10.1130/0016-7606(1996)108<1492:LPLDLA>2.3.CO;2.
- Renne, P.R., Swisher, C.C., Deino, W.D., Karner, D.B., Owens, T.L., and DePaolo, D.J., 1998, Intercalibration of standards, absolute ages and uncertainties in $^{40}\text{Ar}/^{39}\text{Ar}$ dating: *Chemical Geology*, v. 145, p. 117–152, doi:10.1016/S0009-2541(97)00159-9.
- Russell, L.R., and Snelson, S., 1994, Structure and tectonic of the Albuquerque Basin segment of the Rio Grande rift: Insights from reflection seismic data, in Keller, G.R., and Cather, S.M., eds., *Basins of the Rio Grande Rift: Structure, Stratigraphy, and Tectonic Setting: Geological Society of America Special Paper 291*, p. 83–112.
- Sadler, P.M., 1981, Sediment accumulation rates and the completeness of stratigraphic sections: *The Journal of Geology*, v. 89, p. 569–584, doi:10.1086/628623.
- Samson, S.D., and Alexander, E.C., Jr., 1987, Calibration of the interlaboratory $^{40}\text{Ar}/^{39}\text{Ar}$ dating standard, Mmhb1: *Chemical Geology*, v. 66, p. 27–34.
- Sarna-Wojcicki, A.M., Lajoie, K.R., Meyer, C.E., and Adam, D.P., 1991, Tephrochronologic correlation of upper Neogene sediments along the Pacific margin, conterminous United States, in Morrison, R.B., ed., *Quaternary Nonglacial Geology, Conterminous U.S.: Boulder, Colorado, Geological Society of America, Geology of North America*, v. K-2, p. 117–140.
- Schlische, R.W., 1991, Half-graben basin filling models: New constraints on continental extensional basin development: *Basin Research*, v. 3, p. 123–141, doi:10.1111/j.1365-2117.1991.tb00123.x.
- Schlische, R.W., 1995, Geometry and origin of fault-related folds in extensional settings: *American Association of Petroleum Geologists Bulletin*, v. 79, p. 1661–1678.
- Shanley, K.W., and McCabe, P.J., 1994, Perspectives on the sequence stratigraphy of continental strata: *American Association of Petroleum Geologists Bulletin*, v. 78, p. 544–568.
- Smith, G.A., 1994, Climatic influences on continental deposition during late-stage filling of an extensional basin, southeastern Arizona: *Geological Society of America Bulletin*, v. 106, p. 1212–1228, doi:10.1130/0016-7606(1994)106<1212:CIOCDD>2.3.CO;2.
- Smith, G.A., 2001, Development of a pyroclastic apron adjacent to rhyolite domes in a subsiding basin: Upper Miocene Peralta Tuff, Jemez Mountains, New Mexico, in Crumpler, L.S., and Lucas, S.G., eds., *Volcanology in New Mexico: New Mexico Museum of Natural History and Science Bulletin 18*, p. 85–96.
- Smith, G.A., and Lavine, A., 1996, What is the Cochiti Formation? in Goff, F., Kues, B.S., Rogers, M.A., McFadden, L.D., and Gardner, J.N., eds., *The Jemez Mountains Region: New Mexico Geological Society Guidebook 47*, p. 219–224.
- Smith, G.A., Wang, Y., Cerling, T.E., and Geissman, J.W., 1993, Comparison of a paleosol-carbonate isotope record to other records of Pliocene–early Pleistocene climate in the western United States: *Geology*, v. 21, p. 691–694, doi:10.1130/0091-7613(1993)021<0691:COAPCI>2.3.CO;2.
- Smith, G.A., McIntosh, W.C., and Kuhle, A.J., 2001, Sedimentologic and geomorphic evidence for sea-saw subsidence of the Santo Domingo accommodation-zone basin, Rio Grande rift, New Mexico: *Geological Society of America Bulletin*, v. 113, p. 561–574, doi:10.1130/0016-7606(2001)113<0561:SAGEFS>2.0.CO;2.
- Smith, R.L., Bailey, R.A., and Ross, C.S., 1970, Geologic Map of the Jemez Mountains, New Mexico: U.S. Geological Survey Miscellaneous Geological Investigations I-571, scale 1:125,000.
- Spell, T.L., Harrison, T.M., and Wolff, J.A., 1990, $^{40}\text{Ar}/^{39}\text{Ar}$ dating of the Bandelier Tuff and San Diego Canyon ignimbrites, Jemez Mountains, New Mexico: *Journal of Geophysical Research*, v. 98, p. 8031–8051.
- Spell, T.L., McDougall, I., and Doulgeris, A.P., 1996, Cerro Toledo rhyolite, Jemez Volcanic Field, New Mexico: $^{40}\text{Ar}/^{39}\text{Ar}$ geochronology of eruptions between two caldera-forming events: *Geological Society of America Bulletin*, v. 108, p. 1549–1566, doi:10.1130/0016-7606(1996)108<1549:CTRJVF>2.3.CO;2.
- Spiegel, Z., and Baldwin, B., 1963, Geology and Water Resources of the Santa Fe Area, New Mexico: U.S. Geological Survey Water-Supply Paper 1525, 258 p., 7 plates.

- Stearns, C.E., 1953, Tertiary geology of the Galisteo-Tonque area, New Mexico: Geological Society of America Bulletin, v. 64, p. 459–508, doi:10.1130/0016-7606(1953)64[459:TGOTGA]2.0.CO;2.
- Stearns, C.E., 1979, New K-Ar dates and the late Pliocene to Holocene geomorphic history of the central Rio Grande region, New Mexico: Geological Society of America Bulletin, v. 90, p. 799–800, doi:10.1130/0016-7606(1979)90<799:NKDATL>2.0.CO;2.
- Steiger, R.H., and Jäger, E., 1977, Subcommission on geochronology—Convention on the use of decay constants in geo- and cosmo-chronology: Earth and Planetary Science Letters, v. 36, p. 359–362, doi:10.1016/0012-821X(77)90060-7.
- Stone, B.D., Allen, B.D., Mikolas, M., Hawley, J.W., Haneberg, W.C., Johnson, P.S., Allred, B., and Thorn, C.R., 1998, Preliminary Lithostratigraphy, Interpreted Geophysical Logs, and Hydrogeologic Characteristics of the 98th Street Core Hole, Albuquerque, New Mexico: U.S. Geological Survey Open-File Report 98-0210, 82 p.
- Sun, W.W., and Kodama, K.P., 1992, Magnetic anisotropy, scanning electron microscopy, and X-ray pole figure goniometry study of inclination shallowing in a compacting clay-rich sediment: Journal of Geophysical Research, v. 97, p. 19,599–19,615, doi:10.1029/92JB01589.
- Tedford, R.H., and Barghoorn, S., 1999, Santa Fe Group (Neogene), Ceja del Rio Puerco, northwestern Albuquerque Basin, Sandoval County, New Mexico, in Pazzaglia, F.J., and Lucas, S.G., eds., Albuquerque Geology: New Mexico Geological Society Guidebook 50, p. 327–335.
- Tedford, R.H., Albright, L.B., III, Barnosky, A.D., Ferrusquia-Villafranca, I., Hunt, R.M., Jr., Storer, J.E., Swisher, C.C., III, Voorhies, M.R., Webb, S.D., and Whistler, D.P., 2004, Mammalian biochronology of the Arikareean through Hemphillian interval (late Oligocene through early Pleistocene epochs), in Woodburne, M.O., ed., Late Cretaceous and Cenozoic Mammals of North America: Biostratigraphy and Geochronology: New York, Columbia University Press, p. 169–231.
- Thorn, C.R., McAda, D.P., and Kernodle, J.M., 1993, Geohydrologic Framework and Hydrologic Conditions in the Albuquerque Basin, Central New Mexico: U.S. Geological Survey Water-Resources Investigations Report 93-4149, 106 p.
- Travis, C.J., and Nunn, J.A., 1994, Stratigraphic architecture of extensional basins: Insights from a numerical model of sedimentation in evolving half grabens: Journal of Geophysical Research, v. 99, p. 15,653–15,666, doi:10.1029/94JB00470.
- Van Hinte, J.E., 1978, Geohistory analysis—Application of micropaleontology in exploration geology: American Association of Petroleum Geologists Bulletin, v. 62, p. 201–222.
- Webb, S.D., and Opdyke, N.D., 1995, Global climatic influences on Cenozoic land mammal faunas, in Stanley, S.M., chairperson, Effects of Past Global Change on Life: Washington, D.C., National Academy Press, p. 184–208.
- Wells, S.G., Kelson, K.I., and Menges, C.M., 1987, Quaternary evolution of fluvial systems in the northern Rio Grande rift, New Mexico and Colorado: Implications for entrenchment and integration of drainage systems, in Menges, C.M., Enzel, Y., and Harrison, J.B.J., eds., Quaternary Tectonics, Landform Evolution, Soil Chronologies, and Glacial Deposits: Northern Rio Grande Rift of New Mexico: Albuquerque, New Mexico, Friends of the Pleistocene-Rocky Mountain Cell Guidebook, p. 55–69.
- Williams, P.L., and Cole, J.C., 2007, Geologic Map of the Albuquerque 30' × 60' Quadrangle, North-Central New Mexico: U.S. Geological Survey Scientific Investigations Map 2946, 31 p., scale 1:100,000.
- Wright, H.E., 1946, Tertiary and Quaternary geology of the lower Rio Puerco area, New Mexico: Geological Society of America Bulletin, v. 57, p. 383–456, doi:10.1130/0016-7606(1946)57[383:TAQGOT]2.0.CO;2.
- Xiao, H., and Suppe, J., 1992, Origin of rollover: American Association of Petroleum Geologists Bulletin, v. 76, p. 509–529.
- Zachos, J., Pagani, M., Sloan, L., Thomas, E., and Billups, K., 2001, Trends, rhythms, and aberrations in global climate 65 Ma to present: Science, v. 292, p. 686–693, doi:10.1126/science.1059412.
- Zhang, P., Molnar, P., and Downs, W.R., 2001, Increased sedimentation rates and grain sizes 2–4 Myr ago due to the influence of climate change on erosion rates: Nature, v. 410, p. 891–897, doi:10.1038/35073504.

MANUSCRIPT ACCEPTED BY THE SOCIETY 20 JULY 2012

Printed in the USA

